The Henryk Niewodniczański
INSTITUTE OF NUCLEAR PHYSICS
Polish Academy of Sciences
ul. Radzikowskiego 152, 31-342 Kraków, Poland
www.ifj.edu.pl/badania/publikacje
Kraków, 2019

Heat Transfer in High Field Superconducting Accelerator Magnets

Dariusz Bocian

Habilitation Thesis

Wydano nakładem Instytutu Fizyki Jądrowej im. Henryka Niewodniczańskiego
Polskiej Akademii Nauk
Kraków 2019

Recenzent: prof. dr hab. Piotr Malecki (IFJ PAN)

ISBN 978-83-63542-13-9

ABSTRACT

This monograph comprehensively describes the problem of heat transfer in superconducting accelerator magnets, which generate high magnetic fields and are cooled with superfluid helium at temperature of 1.9 K or normal fluid helium at a temperature of 4.2 K. The main objective of the research presented in the monography was to optimize the heat transfer in superconducting magnets in terms of their operation in accelerators. The magnets are affected by the shower of secondary particles generated by the particles lost from the beam or particle debris from experiments. The optimization of heat transfer in the superconducting magnets is essential for accelerator efficiency during the collection of the data for physics analyses. The quench of magnets stops accelerator operation and affects the integrated luminosity

The superconductors are characterized by the critical surface determined by three parameters: the critical temperature (T_c), the critical current density (J_c) and the critical magnetic field (B_c). The particles lost from the beams or coming from the collision debris are hitting the vacuum pipe and generating a shower of secondary particles, which deposits energy in the magnets coils causing increase of the conductor temperature above a critical one and in consequence provokes the quench of magnets. A quench is the transition of a conductor from the superconducting to the normal conducting state which occurs irreversibly in the superconducting magnets if one of the three parameters: the magnetic field, the current density or the temperature exceeds a critical value. In the research described in this monography the studied critical parameter is the temperature and the figure of merit is the energy deposited in the conductor volume at which the quench occurs.

This monograph contains the historical background and the overview of existing methods of solving of the heat transfer problem in multilayer systems, for example in the superconducting magnets. An essential part of the monography is the presentation of the original approach to the problem of optimizing the heat flow in superconducting magnets, designed and developed by the author of this monography and the experimental validation of this method carried out in the form of mini-experiments, planned and executed by the author at CERN.

In the monograph the details of calculations and measurements for the superconducting magnets currently installed and operating in the LHC are described as well as the status and analysis of superconducting magnets developed for the LHC upgrade in ~2025. The monograph focuses on the heat transfer from the superconductor to the heat exchanger through a multilayer structure made of solid elements and channels occupied by the normal fluid or the superfluid helium.

This monography summarizes many years of the author's work and experience in this field and includes: the description of the model, the summary of the results obtained for the superconducting magnets installed in the LHC, the results of mini-experiments carried out at CERN and FERMILAB and a description of applications of the developed model in the process of design of a new superconducting magnets for the LHC upgrade. The examples of alternative numeric calculations and measurements are briefly discussed and extended bibliography is presented.

Keywords: Superconductivity, superconducting magnets, quench, particle accelerators, LHC, heat transfer, cryogenics, superfluidity.

S T R E S Z C Z E N I E

Niniejsza rozprawa habilitacyjna stanowi całościowe, monograficzne przedstawienie problemu transportu ciepła w akceleratorowych elektromagnesach nadprzewodnikowych, wytwarzających wysokie pole magnetyczne i chłodzonych nadciekłym helem o temperaturze 1.9 K lub helem ciekłym o temperaturze 4.2 K. Przedstawione w monografii wyniki badań mają na celu zoptymalizowanie transportu ciepła w elektromagnesach nadprzewodnikowych w warunkach akceleratorowych, czyli poddanych działaniu strumieni cząstek wtórnych wygenerowanych przez cząstki pierwotne utracone z wiązki lub przez pozostałości cząstek pierwotnych ze zderzeń w eksperymentach. Optymalizacja transportu ciepła przez elementy elektromagnesów nadprzewodnikowych ma decydujące znaczenie dla wydajnej pracy akceleratora podczas gromadzenia danych dla analiz fizycznych.

Elektromagnesy nadprzewodnikowe charakteryzowane są przez powierzchnię krytyczną, wyznaczoną przez trzy parametry: temperaturę, indukcję magnetyczną oraz gęstość prądu. Cząstki pierwotne z wiązki lub ich pozostałości z eksperymentów uderzając w ścianki rury próżniowej akceleratora generują strumienie cząstek wtórnych, które deponują energię w cewkach elektromagnesów nadprzewodnikowych powodując wzrost ich temperatury a w konsekwencji *quench*. *Quench* jest zjawiskiem fizycznym podczas którego w elektromagnesach akceleratorowych pracujących w warunkach kriogenicznych nieodwracalnie przekracza się wartość krytyczną jednego z trzech parametrów wyznaczających powierzchnię krytyczną skutkującą przejściem nadprzewodnika do stanu rezystywnego. W przypadku opisywanych w tej publikacji badań parametrem krytycznym jest temperatura, zaś wielkością wyznaczaną jest wartość energii przy której następuje zjawisko *quench*-u.

Publikacja zawiera rys historyczny tego zagadnienia, przegląd istniejących technik oraz wypracowane sposoby rozwiązywania problemów transportu ciepła w układach wielowarstwowych, jakimi niewątpliwie są elektromagnesy nadprzewodnikowe. Zasadniczą częścią monografii jest przedstawienie oryginalnego podejścia do problemu optymalizacji przepływu ciepła w elektromagnesach nadprzewodnikowych, opracowanego i rozwiniętego przez autora monografii oraz weryfikacji eksperymentalnej tej metody przeprowadzonej w formie mini-eksperymentów, zaplanowanych i przeprowadzonych przez autora w CERN. W monografii szczegółowo opisane zostały obliczenia i pomiary dla elektromagnesów nadprzewodnikowych obecnie zainstalowanych i działających w LHC jak również status i analizy elektromagnesów nadprzewodnikowych rozwijanych w celu unowocześnienia LHC około 2025 roku. Monografia koncentruje się na technikach transportu ciepła z nadprzewodnika do wymiennika ciepła odbywającego się poprzez struktury wielowarstwowe złożone z elementów stałych oraz kanałów dla ciekłego lub nadciekłego helu. Monografia stanowi podsumowanie wieloletnich doświadczeń autora w tej dziedzinie i zawiera: opis modelu, podsumowanie wyników obliczeń uzyskanych dla elektromagnesów zainstalowanych w LHC, wyniki mini-eksperymentów przeprowadzonych w CERN i FERMILAB oraz opis zastosowań rozwiniętego modelu w procesie projektowania nowych elektromagnesów nadprzewodnikowych dla LHC. Przykłady alternatywnych obliczeń numerycznych oraz pomiarów zostały omówione skrótowo i opatrzone bogatym materiałem bibliograficznym.

Słowa kluczowe: Nadprzewodnictwo, elektromagnesy nadprzewodnikowe, quench, akceleratory cząstek, LHC, transport ciepła, kriogenika, nadciekłość.

STATEMENT OF AUTHOR'S CONTRIBUTION

This monograph presents the study of heat transfer in high-field accelerator superconducting magnets and includes both its modeling and experimental validation as well as the implementations of the developed models to optimize heat transfer in newly designed superconducting accelerator magnets. The presented simulation and experimental work at CERN, the validation of the results of simulation and measurements as well as the implementation of the model to design of new magnets are the original author's contribution. The introduction, historical overview, discussion of simulation methods and results obtained by other scientists were presented on the base of an extensive bibliographic review performed by the author of this monograph.

Since 2005 the author has been conducting a detailed study of heat transfer in high-field superconducting magnets developed or under development for Large Hadron Collider [1]-[6]. Four types of main LHC superconducting magnets were selected to be studied both by theoretical modeling and experimental validation of simulation results: the main arc dipoles (MB) operating at 1.9 K, the lattice quadrupoles (MQ) at 1.9 K, the long straight section insertion quadrupoles (MQM) part of them operating at 1.9 K and part at 4.5 K and the long straight section wide aperture insertion quadrupoles (MQY) operating at 4.5 K. All of these magnets were designed with the Nb-Ti conductor.

During these studies the author developed a unique simulation tool, called the *Network Model* which was based on the analogy of thermal and electrical networks. Also the author designed and build a dedicated experimental hardware called the Inner Heating Apparatus (IHA) in order to reproduce the heating of the magnet by the particles lost from the beam [4]. The results obtained from simulations with the *Network Model* and their validation with the use of magnets quench heaters (QH) and the Inner Heating Apparatus are the baseline of this monography. An extension of this study by the *Network Model* implementation to different LHC optics, both for ion beams [6] and the proton ones [7] or to ideas of enhancement of heat transfer in magnets by using a modern insulating scheme [8]-[9] are discussed.

Later, in 2008 the author implemented a *Network Model* to study the heat transfer in prototypes of the Nb_3Sn superconducting magnets developed for the upgrade of the LHC interaction region in ~2025, so called the inner triplet upgrade [10]-[12]. These magnets are developed to withstand large heat loads expected at the High Luminosity LHC (HL-LHC) which is an upgrade of the present LHC. The three families of the superconducting accelerator magnets prototypes were studied: the Technological Quadrupole (TQ), the Long Quadrupole (LQ) and the High-gradient Quadrupole (HQ). The next generation of LHC magnets developed for this upgrade are based on the Nb_3Sn conductor and the author was involved in these studies during his work for the USA LHC Accelerator Research Program (US LARP) as a Toohig Fellow at FERMILAB. During the Toohig fellowship the author was involved in three tasks: (1) the implementation of the *Network Model* to optimize the heat transfer in the TQ, LQ and HQ magnets [13]; (2) the characterization of the Nb_3SN conductor by studying strands behavior during the reaction [14], (3) the investigation of the coil production process to find the problem between the TQ and HQ coils performances after reaction [15].

All of the author's work presented in this monograph was organized in the way of complete mini-projects. First a theoretical model (the *Network Model*) was developed. As an initial step, the model of the MB based on its geometry and materials used for the MB construction was prepared. The model included the full thermal path of the MB magnet, namely from the

superconducting magnets coil, through the electrical insulation of the superconducting cables to the heat reservoir. The simulated conditions were corresponding to the operating conditions of the particle accelerator, in this case the LHC at CERN. An extensive study of the thermal properties of materials used to build the superconducting magnet as well as the coolant distribution in the magnet structure were performed.

At the initial phase of this work the results were validated with measurements performed by the author with one quench heater of the magnet connected to the current source. Successful validation of the MB model triggered further modeling work and models of the MQ, MQM and MQY magnets were prepared and validated with measurements. After that the second method of experimental validation of simulated results was developed. The author designed and built the Inner Heating Apparatus. This heating system was installed inside the magnet in order to simulate the heating of the magnet coil by the accelerated beam.

The outcome of these studies allowed to determine the limits for the thermal stability of the magnets for the LHC and its future upgrades. The author developed the heat transfer model and the measurement setups to validate and quantitatively explain the experimental results of the LHC and the HL-LHC magnet quench. The heat extraction mechanisms were identified and studied in details, especially the cooling efficiency of the micro-channels occupied by normal fluid or superfluid helium.

The author also supervised summer students at FERMILAB, who were involved in collecting available material thermal properties data in all kind of databases and publications, and to prepare the software which interfaced the *Network Model* with FLUKA and MARS data [16]-[17].

To conclude, the author of the monography used the *Network Model* to study the thermal stability of the LHC and the HL-LHC magnets and to estimate their quench limits for expected beam loss profiles given by FLUKA and MARS. The results of this work were one of the vital components which allowed for a safe initial operation of the LHC accelerator superconducting magnets.

Contents

Chapter I

Introduction

The superconducting magnets are an essential part of large particle accelerators. The operation of such superconducting devices require careful control of both electric power and cryogenic systems [18]-[20]. The main challenge of the accelerators and the storage rings operating with the superconducting magnets is their protection against the energy deposits to the coils from the particles lost from the beam. A relatively small fraction of the accelerated particles lost from the beam can provoke a superconducting magnets quench. For this reason a number of magnets and accelerator protection systems were developed. The protection systems require the determination of the level of values at which they are triggered. In case of accelerator superconducting magnets the crucial value is called the quench level i.e. the amount of energy deposited in the superconductor which causes an irreversible transition of the superconductor in the magnet coil from superconducting to a normal conducting state. All studies presented in this monography are leading to the determination of quench levels of all families of magnets installed in the LHC or developed for the LHC upgrade at different steady-state operational conditions.

I.1 Organization of the document

This monograph describes the complex modeling of heat transfer in superconducting accelerator magnets, the model validation with measurements and the implementation of the model to optimize the heat transfer in superconducting magnets designed for the LHC upgrade.

Chapter I provides a short introduction to the motivation of writing of this monograph, the list of discussed topics and information which issues will not be discussed. Chapter II presents some general information about superconductivity. Superconductors exhibit a unique set of properties, which are summarized in this chapter. Here, only basic information is given as well as the bibliography for better theoretical understanding of the phenomena of superconductivity. Chapter III gives a short introduction of current development of superconducting accelerator magnets and a compact historical overview with rich bibliographic references, followed by some details about superconducting magnet technology. Chapter IV discusses the heat transfer at cryogenic temperatures with the focus on multilayer structures and smoothly goes to a complex multilayer system of superconducting magnets including: the conductor, the electrical insulation, the helium and heat exchangers with particular attention to heat flow barriers resulting from a technological solution used during magnet design. There are always two challenges of design of superconducting magnets: electrical and thermal. The electrical challenge is wanting to increase thickness of the insulation to electrically protect the magnet and the thermal challenge is wanting to decrease the thickness of the insulation to provide

efficient cooling. Always the compromise between these to design issues have to be found in development of superconducting magnets. Chapters V to VII cover the description of the main achievement of the author and include the heat transfer modeling with the *Network Model*, the validation of model results with the dedicated tooling developed by the author and the implementations of the *Network Model* in the design process of new superconducting magnets. Chapter VIII covers a summary and description of plans of further development of the model and validation methods in view of the LHC upgrade around 2025 and possible implementation to the Future Circular Collider thermal studies.

I.2 Motivation and tasks

The modern design of the superconducting accelerator magnets requires an advanced thermal analysis in terms of the heat transfer optimization at cryogenics conditions. The higher energy of particles reached in the accelerators causes that only a small fraction of the particles lost from the beam can deposit sufficient energy in the coils of the superconducting magnets to provoke their quench. The quench is a transition of a conductor from the superconducting to the normal conducting state, which occurs irreversibly in accelerator magnets if one of the three parameters: the temperature, the magnetic field or the current density, exceeds its critical value. The heat transfer paths in the superconducting magnets are the complex multilayer system, which starts from the beam vacuum chamber through the cooling channels occupied by helium in parallel with the solid part of the magnet and ending at the heat exchanger pipe.

This monograph summarizes complex studies both theoretical and experimental, which lead to the determination of the quench level of the superconducting magnets for a steady-state operation of the accelerators. The transient operation is only mentioned in the monograph and it will be a subject of further development of the model and its experimental validation.

The following tasks were performed in order to reach the objectives described in this monography:

- The geometry of magnets.

  For all thermodynamic studies the geometry of the investigated object is crucial. The technical drawings were studied in detail as well as the distribution and amount of cooling medium inside the magnet coil. Dedicated measurements were performed in order to calculate the amount of helium inside the superconducting cables (see: Appendix 2).

- The materials properties at cryogenic temperatures.

  The superconducting magnets are a complex system consisting of different materials, among others the metals, the polyimide, the epoxy or the liquids. All of them behave differently in terms of the coefficient of the heat transfer, the coefficient of the thermal expansion or the Young modulus. At cryogenic conditions the Kapitza resistance is one of the key parameters.

- The temperature margin of the superconductor.

  The superconducting magnets operating with a temperature margin determined from the short sample measurements of the conductor, typically the load line of the magnet is set to 80-85% of the short sample critical surface (J_c, B_c, T_c). Due to the power dissipation by the particles lost from the beam, the conductor is heated up locally and it affects the difference between the transport current and the critical current. In most critical cases it can lead to the exceeding of the temperature margin of the superconductor and to the quench of the superconducting magnet. The temperature margin of each conductor was calculated with ROXIE software (a partial contribution of author – first studied magnets and partial contribution of other people at CERN and FERMILAB – magnets studied later during the course of work).

- The sources of the heat load to the superconductor.

  The protons lost from the beam, impacting the beam vacuum chamber, create a shower of secondary particles which deposes their energy in the magnet coils. The energy deposited in the magnet coils could cause a temperature increase and provoke the superconductor to quench, so heat has to be evacuated from the coil to the helium bath and finally to be compensated by the cryogenic system (the heat exchanger efficiency). This phenomena is really important in the case of impregnated cables, where cables are poorly cooled. The implemented heat load distributions were calculated with FLUKA or MARS software (a contribution of other people).

- The modeling of heat transfer.

  A heat transfer model was developed to determine the magnet quench levels for the steady-state heat loads. The model includes the material parameters and geometry details for a selected family of magnets. The model allows for the implementation of different heat load sources. The model described in this monograph was fully developed by the author based on the thermal and electrical analogy and it was called the *Network Model*.

- The experimental validation of the *Network Model*.

  The results of the simulation by means of the *Network Model* were validated with measurements performed at the normal fluid and the superfluid helium temperatures at the magnet test facility at CERN. Initially, the heat was loaded to the magnet with the use one of the magnet quench heater. In this case the coil was heated from its top. Later a dedicated apparatus, called the Inner Heating Apparatus (IHA) was designed and build by the author of monography. The IHA was installed inside the cold bore and provided the heat source from the inner part of magnet. Both heating scheme was introduced in the *Network Model* and the results of the simulation were successfully validated with the measurements. The current of magnet coil quenching was predicted with expected accuracy. The sources of discrepancy between the results of the simulations and measurements were identified and the increasing of accuracy is possible mainly due to dedicated measurements of thermal properties of materials used in the construction of superconducting magnets.

- The *Network Model* implementation.

  The successful validation of the *Network Model* with dedicated measurements allowed for the implementation of the model to study of the thermal behavior of the newly developed enhanced insulation and newly designed Nb_3Sn magnets. The *Network Model* was used to study the heat evacuation scheme and to determine the initial geometry of the helium cooling channels for the expected heat load map simulated with FLUKA or MARS software for newly designed LHC luminosity upgrade optics. The optimization of the magnet cooling channels scheme i.e. the dimensions and location of the cooling channels in the coils pole regions and the thickness of the cooling channel between the cold bore and the coil for the LARP Nb_3Sn quadrupole magnet was performed.

- The future development of the model and experimental methods of model validation.

  The next step of the *Network Model* development is the development of a dedicated module which introduces the energy deposits according to the LHC beam pattern and in the transient mode. Currently, the model determines the most conservative values of the quench levels at steady-state conditions and it was successfully validated with the dedicated experiments. In reality the duration of the losses and its relation to the transient mode are important parameters and further work on the *Network Model* development is foreseen.

Chapter II

Superconductivity

Superconductivity is an extraordinary phenomenon demonstrated by certain materials, which cooled down to the cryogenic temperatures, become the perfect conductors of electricity. It was discovered in 1911 by Heike Kamerlingh Onnes [21]. He measured the electrical resistivity of mercury at low temperatures and observed it sudden drop to zero below 4.15K. This discovery was possible because three years earlier he had succeeded in liquefying helium.

The theory of superconductivity was developed over next 46 years. In 1957 Bardeen, Cooper and Schrieffer (BCS) [22] presented their theory of superconductivity. They received a Nobel Prize in Physics for this theory in 1972. This theory describes superconductivity as a microscopic effect which is caused by a condensation of Cooper pairs [23] into a boson-like state [24]. This theory is not complete and still requires further work in order to describe all phenomena's observed in the experiments. The superconducting state appears quite abruptly at a critical temperature (T_c). Table 2.1 shows selected elemental materials and their critical temperature T_c. In addition, the superconductors are characterized also by the critical magnetic field (B_c) and critical current density (J_c) [25]. Above these values superconductors revert from the superconducting state to the normal resistive state. All these main parameters, namely: T_c, J_c and B_c are related to each other by the critical surface in (T, B, J) space (see: Fig. 2.1), which is characteristic for each of the superconducting materials. The discovery of materials that remain superconductive up to high current densities and magnetic field initiated the successful application of these materials in the field of superconducting magnets [18], [26]-[28].

Table 2.1 Selected elements demonstrating superconducting properties: transition temperatures (T_c) and critical magnetic fields (B_c) for some typical elemental superconductors [29].

Elements	Transition temperature T_c (K)	Critical magnetic fields B_c (mT)	Type
Al	1 .17	9.9	I
Re	2.42	23.5	I
Tl	2.39	17.1	I
In	3.4	29.3	I
Sn	3 .72	30.5	I
Hg	4 .15	41.1	I
Ta	4.48	83.0	I
La	4.9	79.8	I
V	5.38	102.0	II
Pb	7 .20	80.3	I
Tc	7.77	141.0	II
Nb	9 .25	198.0	II

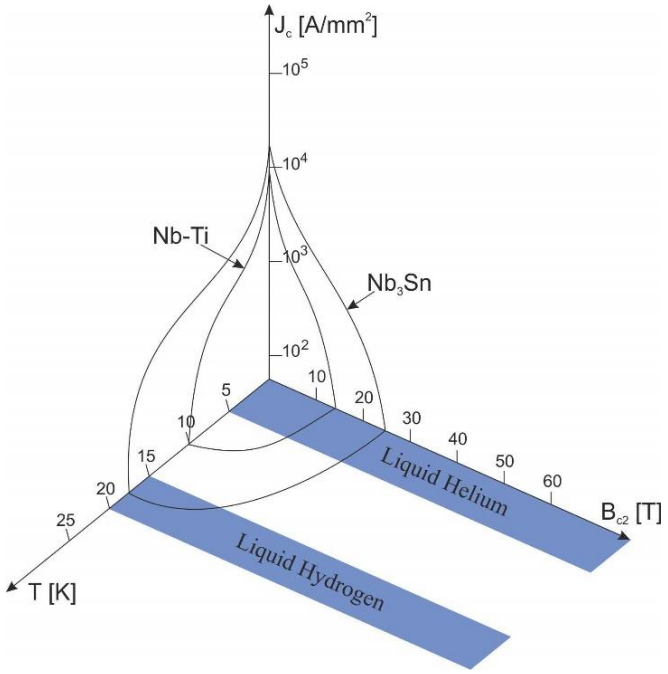

Fig. 2.1 The critical surface of Nb-Ti and Nb3Sn in (T,B,J) space.

With respect to response to a magnetic field superconductors can be classified as Type I or Type II (Fig. 2.2). A superconductor Type I has a single critical field (H_c) below which a Meissner effect is observed [31], namely magnetic field lines are completely expelled from the interior of the superconductor during its transition into the superconducting state and above which the superconducting state is lost (Fig. 2.3 a). A superconductor Type II has two critical fields (H_{c1} and H_{c2}). Below H_{c1} superconductor behaves as Type I and between H_{c1} and H_{c2} a partial penetration of magnetic field through isolated points (vortices) is allowed (Fig. 2.3 b). Type II superconductors is comprised of alloys and metallic compounds, except for niobium, technetium and vanadium. They operate at higher critical temperature that Type I superconductors. The theory of type II superconductor is not well developed, yet.

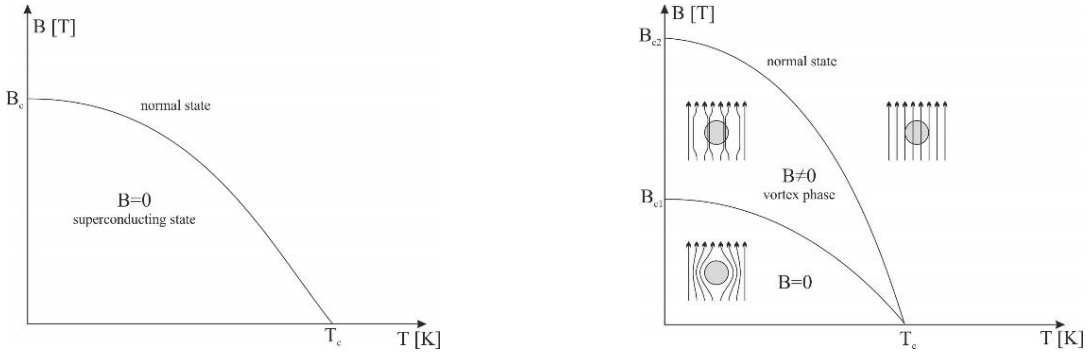

Fig. 2.2 Type I (left) and Type II (right) superconductor

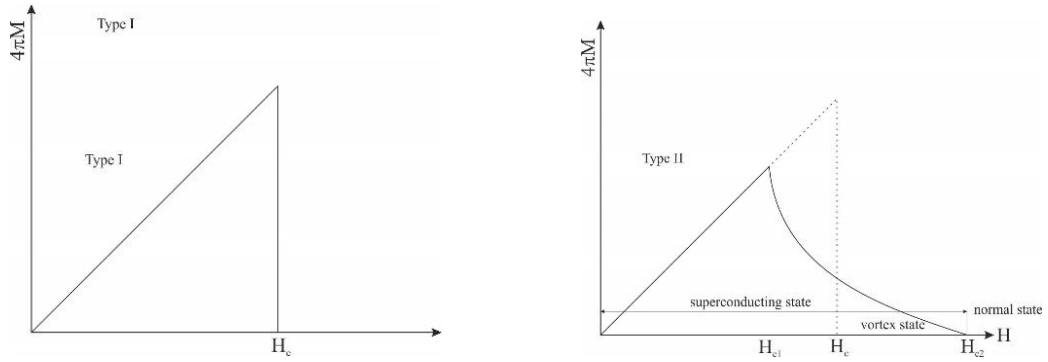

Fig. 2.3 Type I and Type II superconductor

Currently, in applied superconductivity the low temperature superconductors type II based on niobium (Nb, Nb-Ti, Nb_3Sn or NbN) are commonly used. Low temperature superconductors are the metals and alloys that become superconductive at liquid helium temperatures. Actually, Nb-Ti and Nb_3Sn are the only ones which currently are commercially available for large scale magnet production. The other superconductors from this family, namely Nb_3Ge (T_c=23.2K), Nb_3Al (T_c=18K), Nb_3Au (T_c=10.8K) or NbSe2 (T_c=7.2K) were not succeed in commercial production. Recently MgB_2 [32] became the third candidate for commercial use [33]. However these superconductors are different due to production process. The Nb-Ti alloy is produced by extrusion and drawing process only and the Nb 47 wt.% Ti is the most successful practical superconductor to date. For example the industrial production of Nb-Ti was run for Tevatron with requirements of filament diameter of 10 μm and J_c (5T, 4.2K)=1800A/mm^2 [34]. The Nb_3Sn precursor is produced by extrusion and drawing process (RRP: Restack Rod Process or PIT: Powder-In-Tube) and then reacted at high temperature (~650 °C) to obtain a superconductor. The Nb_3Sn is foreseen to be used in superconducting magnets at LHC upgrade. In case of MgB_2 the magnesium diboride powder is used in the process of the formation of a superconducting wire and this conductor is planned to be used in superconducting links at LHC upgrade.

Table 2.2 Selected properties of low temperature superconductors.

	Nb-Ti	Nb_3Sn
Critical temperature	10 K	18.3 K
Critical magnetic field	11 T	25 T
Critical Current density	3300 A/mm^2 (5T) 400 A/mm^2 (9.5T)	12000 A/mm^2 (5T) 3000 A/mm^2 (12T)
Ductility	Ductile, tough	Ductile, brittle after reaction
Typical strand diameter	0.4 – 2.0 mm	0.6 – 1.5 mm
Typical filament diameter	2.5 – 120 μm	2 – 6 μm
Typical filament number	1 – 40 000	3000 – 40 000

The Nb-Ti and Nb_3Sn superconductor limiting parameters are listed in Table 2.2. The Nb-Ti parameters are relatively low but it is ductile material which allow simple and effective manufacturing of strands, cables and coils. The Nb-Ti is widely used in magnets up to 6T at 4.2K and up to 9T at 1.9K (LHC). The Nb_3Sn is brittle and it cannot be drawn to thin filaments like Nb-Ti, The Nb_3Sn is very sensitive on a deformation of the superconductor under the influence of external compression forces and effects from the Lorenz force when the current flows. For this reason the fourth parameter, strain (ε), is included in the formula describing the critical parameters of conductor, namely B_c ,T_c, J_c, ε. This sensitivity to mechanical stress cause the reduction of current-carrying capacity. The manufacturing process of LHC upgrade magnets coils developed by US-LARP project require forming the final geometry of coil from precursors before the reaction and then proceed the high-temperature heat treatment, typically in three steps: 210°C, 400°C and 650°C, over 7 days for RRP strands. Also all voids have to be filled with epoxy or solder due to fact that bare strands and cables are sensitive to transverse stress in the pre-compressed coil. Filling gaps with epoxy or solder allow to evenly distribute applied pressure and avoid the local stress enhancement. However, filling the voids reduces the heat extraction capability from the coil interior, which is assumed as heat transfer barrier in case of studies presented in this monograph. The Nb_3Sn coils for accelerator magnets cannot be wound from fully reacted cable because of strong degradation due to coil bend in the coil head region. However, some types of magnets, so called pancake-like can be wound with fully reacted cables when the bending angle is large enough.

In 1986 Bednorz and Müller[1] announced the discovery of a *ceramic* oxide of lanthanum, barium and copper superconductor with a transition temperature of about T_c = 35K [35]. Following, the other high temperature superconductors (HTS) have been found, namely "1-2-3" compound $YBa_2Cu_3O_7$ with a transition temperature of T_c = 93K [36]-[37] as well as the "2-1-4" compound (e.g. $Ba_xLa_{2-x}CuO_{4-y}$) or $Tl_2Ba_2Ca_2Cu_3O_{10}$ with a remarkably high T_c = 127K [38]. The high-T_c materials are type II superconductor and in general have a very large upper critical field. This discovery is challenging in terms of theoretical understanding of high temperature superconductivity mechanism. These superconductors are called unconventional superconductors since they do not conform conventional BCS theory. The main question is what causes the ceramic copper oxide materials to be superconductors at temperatures well above 100 K. In conventional superconductors the electrons are paired into spherically symmetric wave functions (s-waves) due to exchange of virtual phonons. Actually, to produce such high critical temperature the lattice vibration cannot produce strong enough couplings. Some directions to explain this phenomena is given by research of hole conduction in parallel Cu-O planes. The discovery of high temperature superconductors which achieve superconducting state at liquid nitrogen temperatures started considerations of their applications in accelerator magnets.

[1] Bednorz and Müller were jointly awarded the Nobel Prize in Physics in 1987.

There are also other superconductors, the unconventional ones, which demonstrate remarkable properties. Presently, they have no practical use but they are interesting in terms of research of their properties. The representatives of such superconductors are the heavy-electron superconductors, as for example UBe_{13} (T_c = 0.85K) [39], $CeCu_2Si_2$ (T_c = 0.65K) [40], and UPt_3 (T_c = 0.54K) [41], which exhibits large specific heat at low temperature (even 3 orders of magnitude larger than in normal metals. In 2008, the iron-based family of high-temperature superconductors was discovered [42] which become superconducting at the range 55K – 80K. The H_3S (formed from H_2S under its decomposition under extremely high pressure of 150 GPa) exhibits superconductivity at 203K [43] which is up to now the highest temperature achieved by superconductor. In 2018 Massachusetts Institute of Technology announced another important discovery – the superconductivity of graphene [44] which could possibly find application in superconducting electronics. The above mentioned discoveries show that research on superconducting materials, their properties and possible applications is a dynamic and long-term activity.

Chapter III
Superconducting magnets

III.1 Introduction

The discovery of superconductivity immediately made scientists aware of the possible construction of high-field magnets and thus made a significant impact on both science and technology [45]. The construction of large magnets, which would be capable of generating very high fields with no power consumption opened a new era in research and development projects. Superconducting magnets have a number of advantages over normal conducting ones. The normal conducting, iron-core magnets are limited by iron saturation to the magnetic fields in order of 2 T. The superconducting magnets can generate a magnetic field even 10 times stronger. In addition superconducting magnets consume less power, they can be smaller, more stable, less noisy and thereby allowing more precise measurements in experiments. In order to present the full family of magnets, it is necessary to mention also non-superconducting high-field magnets, build from copper, operating both in room temperature and at a cryogenic one as well as hybrid magnets, which are combination of non-superconducting and superconducting ones, The hybrid magnets are in possession of the world magnetic field record of 45T (33.5T from normal-conducting insert and 11.5T outsert made from the superconductor) achieved at NHFML, Tallahassee, FL, USA [46].

There are five general types of superconducting magnets: (1) solenoids – cylindrical helices, the most widely used types; (2) dipoles – to generate a uniform transverse field with respect to its long axis and used to deflect trajectory of charged particles; (3) quadrupoles – to generate a linear gradient field transverse to its axis in its center and used to focus particles; (4) racetrack – a special type of magnet, wound in a plane with each turn consisting of two parallel sides and two semi-circles at each end, typically the pair is assembled to approximate the field of a dipole, used mainly in Maglev and motors; (5) toroid's – to generate a field in the azimuthal direction, used in particle physics experiments, tokamaks to confine hot plasma and also for superconducting magnetic energy storage devices (SMES).

The superconducting technology was successfully transferred to the industry and presently is widely used in NMR equipment, MRI machines (~80% of world Nb-Ti market), magnetic separation processes and mass spectrometers as well as in developing of superconducting transformers or superconducting electric motors,. But the main user of this technology still remains science and superconducting magnets continuously are used in new generations of particle accelerators (ISR, TEVATRON, RHIC, LHC) [20], [47]. Recently also the thermo-nuclear fusion infrastructures: Stellarator Wendelstein 7-X (W7-X) [48] and International Thermonuclear Experimental Reactor (ITER) [49]-[50] use superconducting magnets as well. The well-developed Nb-Ti technology is commonly used for the construction of accelerator magnets. For example the magnets

installed in LHC, which operate at 1.9 K or 4.5 K respectively and run up to 8.5 T as well as the ITER PF and CC coils use well developed Nb-Ti technology as well.

Superconducting magnet technology is interdisciplinary since it requires knowledge and training in many fields of engineering such as mechanical, electrical, cryogenic, materials and to deal with the design, manufacture and operation. The main issues in new high-field superconducting magnets are providing required cooling to low temperatures and the careful control of quench. Currently, the most challenging development work are the new magnets build with the Nb_3Sn superconductor for the upgrade of LHC, namely inner triplets for High Luminosity LHC and ITER central solenoid and toroid.

III.2 Historical overview

The idea of using superconductors to construct magnets which generate a magnetic field greater than the ones achieved with copper wires occurred immediately after the discovery of superconductivity. The use of superconducting materials for high-field magnet coils was very well understood already by H. Kamerlingh Onnes. In his paper presented at the 3rd International Congress of Refrigeration in 1913 in Chicago, USA, he proposed building a 10 T superconducting solenoid [51] based on the results which he obtained for the lead wire where he reached 500 A/mm^2. One year later he revised his idea due to the observation that pure-metal superconductors lose their superconductivity at a certain value of the magnetic field so called the critical magnetic field (H_c), which for lead was significantly less than 0.1 T. It was discovered that the magnetic field has an impact on the superconducting state and with all the superconducting materials known at that time it was impossible to build high field superconducting magnets. There were some trials on certain alloys like Pb-Bi in Leiden but unfortunately they abandoned research in this direction after few failures[2]. Then the First World War stopped research for several years. The work on superconductivity restarted in the 1920's with focus on metal alloys like lead-indium or lead thallium, leading to the observation of different behaviors of pure metals and metal alloys and in consequence to the discovery of two different types of superconductors: type I and type II. The scientists in Leiden, Toronto, Oxford and Kharkov had liquid helium and worked on superconductivity in metal alloys. They observed that the increase in the concentration of alloys caused the changing of the equilibrium of magnetic properties and they loosing superconductivity at higher critical field H_c. Then H_{c1} and H_{c2} for pure metals and alloys were introduced and intensive study of the thermodynamic properties of the new type of the superconducting state (type II) have been started, leading finally to the phenomenological theory of superconductivity [52]-[54]

The high magnetic field of order of 10 T was available starting from 1933 when Francis Bitter build a water cooled magnet, nowadays called the Bitter magnet or the Bitter solenoid [51], [55]. The Bitter magnet was used to create a strong magnetic field

[2] Today we know that they would succeed with right composition of this compound.

to be used in scientific research and in 2017 this type of magnet allowed the National High Magnetic Field Laboratory (NHMFL) at Florida State University in Tallahassee to achieve the strongest continuous magnetic field on earth of 41.5 T created by man [56]. The Bitter magnets are used when an extremely strong magnetic field is required. The normal conducting magnet generate enormous heat due to resistive heating by the large currents flowing through the Bitter plates. The cooling of such a device is one of the technological challenges, especially that heat dissipation increases with the square of the magnetic field strength. The first step to superconducting magnet technology was done in 1947 when Samuel Collins completed the large scale helium liquefier [57] which opened possibility of cooling superconductors, particularly superconducting magnets coils. Then the first operating superconducting magnet of 0.7 T at 4.2 K was built using Nb wires in1955 by G.B. Yntema [58]. He used Nb wires and winded them on iron core. His results were confirmed by other scientists.

Many important superconductors were discovered in the 1950's. The discovery of the niobium-tin compound which could support Jc >1kA/mm^2 in the magnetic field B_c = 8.8 T in the late 1950's by J.E Kunzler, E. Buehler, F.S.L. Hsu, and J.H. Wernick [59] opened a new era in superconducting magnet construction. Nb_3Sn is brittle material but its characteristics show that it is possible to build superconducting magnets generating magnetic field up to 20T. Extensive work in Bell Laboratories in those years allowed to make another important observation: the measurement of a short sample of wire in a transverse external magnetic field are indicative of their behavior in a solenoid so it is possible to predict the properties of solenoid from the short length of a wire [60]. In 1962 T.G. Berlincourt and R.R. Hake discovered the high ductile and easily fabricated superconductor - niobium-titanium alloy [61]. Currently Nb-Ti is the most widely used superconducting material, although used in magnets which are generating magnetic fields up to 10 T. Another important step in the superconducting magnet technology was the formulation in 1969 of the design principles of stability in cooled superconducting magnets by Z. J.J. Stekly, R. Thome and B.P. Strauss [62].

The next breaking point happen in 1986, when G. Bednorz and K. Müller publish the discovery of LaBaCuO, cuprate superconductors that could be possibly cooled by liquid nitrogen [35]. Starting from this year many cuprate superconductors (high temperature superconductors) were identified as YBCO with T_c = 93 K [36]-[37], BSCCO with T_c = 95-107 K [36],[63]-[64], TBCCO with T_c = 127 K [38] or HBCCO with T_c = 135 K at normal pressure [65] and T_c = 153 K at p = 150 kbar [66]. In 2007 the first world record of 26.8 T was achieved in NHMFL in Tallahassee, FL, USA by HTS magnet made from YBCO [67] and ten years later, in 2017 a new record of 32T [68] was achieved in the same laboratory. It is also worth mentioning the discovery in 2001 of MgB_2, a superconductor with a medium-range of critical temperature T_c = 32 K and demonstrating particular interesting properties [32]. Since 2007 it is intensively in terms of use it in superconducting magnets [69] and superconducting links[71] used to power LHC magnets [70]. In 2018 the scientists from LASA Milan announced that they had successfully completed the test of a superconducting coil winded with MgB_2 [71].

III.3 Accelerator superconducting magnets

The accelerator based sciences remain the main user of superconducting magnets and this is the mainspring to reaching new limits in the development of modern and innovative magnets in terms of technology and new superconductors. The discovery of Nb-Ti allowed to build in the late 1970's an accelerator superconducting magnet which was installed at CERN in the low-β insertion region of the Intersecting Storage Rings (ISR) in order to increase the luminosity of ISR [72]. The first large scale demonstration of using the superconducting magnets was the Tevatron [73] in the 1980's, where the magnets system composed of 774 dipoles and 240 quadrupoles was able to reach a record energy of the proton beam of 517 GeV and later 1 TeV of beam energy (2 TeV centre-of-mass energy). Next, two large projects were executed in the 1990's, namely the Hadron Electron Ring Accelerator (HERA) at DESY with superconducting magnets which guided the proton beam to collide with the electron beam [74] and Relativistic Heavy Ion Collider (RHIC) at BNL. Both projects strongly involved industry in building of superconducting magnets. After the successful construction, commissioning and starting operation of above mentioned accelerators a huge new project was launched: the Superconducting Super Collider (SSC). The plan was to build an 87 km tunnel with 7700 dipoles but unfortunately the SSC project was cancelled by the US Congress. The results of R&D did not disappear and they were used for the development of Large Hadron Collider (LHC). The 27 km tunnel available for LHC required pushing the Nb-Ti magnet technology to its extreme. The most important innovation developed in LHC was the two-in-one design, where the two channels are fully coupled both mechanically and magnetically (previously proposed by BNL). Another one was using superfluid helium to operate at 1.9K which boosts Nb-Ti performance and provides very good cooling in terms of heat transfer and heat capacity properties. Currently, the two-in-one design is a main driver for all magnets for future hadron colliders, even for those developed to operate with ion and proton beams, which is quite challenging given the difference in mass-to-charge ratio.

This monograph focuses on the LHC accelerator superconducting magnets, both dipoles and quadrupoles which are two-in-one designs. There are nine different main LHC magnets families identified at LHC [75]: the main dipole (MB) operating at 1.9 K, lattice quadrupole (MQ) also at 1.9 K, long straight section insertion quadrupole part operating at 1.9 K (MQM @1.9K) and at 4.5 K (MQM @4.5K), long straight section wide aperture insertion quadrupole (MQY) operating at 4.5 K, called low-β or inner triplet quadrupoles (MQXA and MQXB) operating at 1.9 K, separation dipole (MBR) operating at 1.9 K, long trim quadrupole (MQTL) operating at 1.9 K. The three prototype magnets for LHC upgrade developed by US LARP program [76], namely: the Technological Quadrupole (TQ), the Long Quadrupole (LQ) and the High-gradient Quadrupole (HQ) [77] were studied as well. Except MBR and MQTL, the rest of the listed above LHC superconducting magnets were studied in terms of their thermal sensitivity to operations of LHC.

Chapter IV
Heat transfer in multilayer structures

The multilayer structures subjected to thermal, mechanical or magnetic loads are typical feature in the design of scientific as well as industrial equipment. The heat transfer study in multilayer structures involve different branches of physics and engineering. The examples of such structures are: detectors, magnets, heat exchangers, power plants, submarine and aircraft technology and many other scientific and technological apparatuses. In general, the multilayer structures are characterized by different thermo-mechanical properties and different dimensions of each component. Each layer demonstrates different dependence on temperature as well as thermal contact resistance. The dependence of thermal conductivity on temperature for many materials can be found in literature [78]-[79], web databases [80]-[81] or articles presenting data measured in a dedicated experiment [82]-[85]. The contact thermal resistance is vital parameter and it depends on many factors as the thermo-mechanical properties of the contacting surfaces, quality (roughness) of the contacting surfaces, the load on the contacting surfaces, the temperature in the zone of contact or the value of the heat flux. A numerous physical phenomena appears at the connections between elements of structure. Also the thermo-mechanical properties of mediums occupying the space between considered surfaces have significant impact on the contact thermal resistance. The interlayer space can be occupied by substance (liquid, lubricant, etc.) that can undergo different changes as for example evaporation, phase transition, solidification and other physical-chemical transformations. This phenomena can lead to heat release or absorption affecting the surface of the layers by changing their temperature, increase or decrease their contact resistance aswell as or appear or disappear the contact resistance elements (for example: the effect of Kapitza resistance in superfluid helium). Also the contact resistance can cause temperature and heat flux discontinuities between the layers. The heat transfer through structures constructed from different materials both solid and liquid is a challenging issue in many areas, especially in experimental physics. One of the vital issue for multilayer structures is the cooling of developed equipment, both air-cooling, solid-cooling (cryogen free cooling, so called cryocoolers) and cooling with use of liquid (water, Nitrogen, fluid and superfluid Helium).

IV.1 Introduction

The laws of thermodynamics define fundamental physical quantities: heat Q [J], temperature T [K] and the entropy S. These quantities characterize the thermodynamic systems at thermal equilibrium. The heat transfer is the process of transfer of energy and entropy between two systems driven by temperature difference at both locations. There are three different mechanisms of heat propagation in the systems: heat conduction,

convection and heat radiation. Conduction is a transfer of energy and entropy in solids and fluids between adjacent molecules and in general there are atomic scale processes. Convection involves macroscopic movement of a fluid or gas between regions of different temperatures. Radiation is an energy transport by electromagnetic radiation from a heated surface to the surface which absorb the heat without support of any medium between them. Usually, the transfer of the heat involves all of these mechanisms. The details of heat transfer theory are available in many books (for example [78]-[79]) and only basic information is presented in this section. The basic laws for three basic modes of heat flow $\dot{Q}$ by an area A are:

- Fourier's law for conduction

$$\dot{Q} = -\kappa \cdot A \cdot \nabla T \qquad \text{Eq. 4. 1}$$

where:
κ - thermal conductivity $[\frac{W}{m \cdot K}]$,
A - area $[m^2]$,
T - absolute temperature in Kelvin [K], ∇T- temperature gradient,

- Newton law of cooling (General convection law both for free or forced flow)

$$\dot{Q} = h \cdot A \cdot (T_w - T_f) \qquad \text{Eq. 4. 2}$$

where:
h - heat exchange coefficient (coefficient of convective heat transfer) $[\frac{W}{m^2 \cdot K}]$,
T_w, T_f – temperature of wall and fluid respectively,

- Stefan-Bolzman's law for radiation

$$\dot{Q} = \sigma \cdot \varepsilon \cdot A \cdot \left(T_h^4 - T_c^4\right) \qquad \text{Eq. 4. 3}$$

where:
$\sigma = 5.6703 \cdot 10^{-8} \frac{W}{m^2 \cdot K^4}$ - Stefan-Bolzmann constant,
ε - emissivity of the surface, ($\varepsilon = 1$ for a black body),
A - area $[m^2]$,
T_h, T_c – temperature of hot and cold surface respectively,

The objective of this study is to describe how the rate of energy transfer is governed by the temperature difference and to identify the heat transfer barriers in the multilayer structures at cryogenics temperatures. In this monograph the investigated multilayer structures are composed of metals, polymers and liquids. Since liquid (fluid or superfluid

helium) occupies narrow channels the convection contribution to heat transfer is negligible while the thermal radiation component of heat transfer is skipped. Finally the only equation of heat transfer for conduction, known as Fourier law for conduction, is sufficient to describe the defined physics model of heat transfer.

IV.2 Solids at normal and cryogenics conditions

In defined physics models of multilayer structures the dominant volume is occupied by solids so the thermal conduction in metals, crystals and polymers is taken into account. In general the heat is carried out by electrons (dominates in metals), phonons (dominates in dielectrics) and molecular mechanism (dominates in liquids and gases). The highest heat transfer coefficient have pure metals where free electron conduction is the leading mechanism. Among the metals with the highest value of heat transfer coefficient are silver (κ = 419 W/ m·K). The copper (k=386 W/ m·K) is commonly used in superconducting magnets as stabilizer. In order to maximize the heat transfer coefficient, the purity of copper at cryogenic conditions must be kept on very high level and it depends on value of Residual Resistance Ratio[3] (RRR), typically values in superconducting cables are between 100 and 300. The dominant mechanism of heat transfer in metals is conduction electrons. Since thermal conductivity approximately tracks electrical conductivity according to the Wiedemann-Franz-Lorentz law:

$$\frac{\boldsymbol{\kappa_{th}}}{\boldsymbol{\kappa_{el}}} = \mathbf{C_{WFL}}\cdot\mathbf{T} \qquad \text{Eq. 4. 4}$$

$$\text{where: } C_{WFL} = \frac{\kappa_{th}}{\kappa_{el}\cdot T} = \frac{\pi^2}{3}\left(\frac{k_B}{e}\right)^2 = 2.44\cdot 10^{-8}\ W\Omega K^{-2}$$

This law states that the ratio of the electronic contribution of the thermal conductivity (κ_{th}) to the electrical conductivity (κ_{el}) of a metal is proportional to the temperature. The relationship is based upon the fact that both electrical and heat transport involve free electrons in the metal. In opposite to metals the dominant mechanism of heat transfer in insulators are atomic vibrations - phonons. The heat conduction in insulators involves the generation and propagation of atomic vibrations through the bounding that couple the atoms [78]-[79]. In absence of free electrons the strong covalent bonding between atoms allows for a very efficient heat transport. For polymers, due to weak Van-der-Waals bonding the thermal conductivity is very low, of order of 0.2 [W/m·K]. In case of diamond the heat transfer coefficient is more than 2 times higher than for metals (for example: Cu, Ag or Al) and of order 5000 times higher than for polymers [80]-[81]. Table 4.**1** show thermal conductivity for selected materials at 25°C. At cryogenic

[3] The residual resistivity ratio (RRR) of LHC superconducting strands is defined as the ratio of resistance at 293 K to the resistance at 10 K [86].

temperatures the thermal properties of solids change, especially the electrical insulation (see: Fig. 4.1 and Fig. 4.2). A limited number of publications present formulas for calculation of thermal conductivity at superfluid helium temperatures. The thermal conductivity of Copper at low temperatures depends on Residual Resistivity Ratio (RRR) so the purity of copper and annealing are important.

Table 4.1 Thermal conductivity of selected materials at reference temperature of 25°C

material	**type**	**κ_{th} [W/m·K]**
Copper[4]	Metal	390
Silver	Metal	420
aluminum	Metal	250
diamond	Insulator	1000
Polyimide[5]	Polymer	0.2
Fiberglass laminate[6]	Composite	0.3

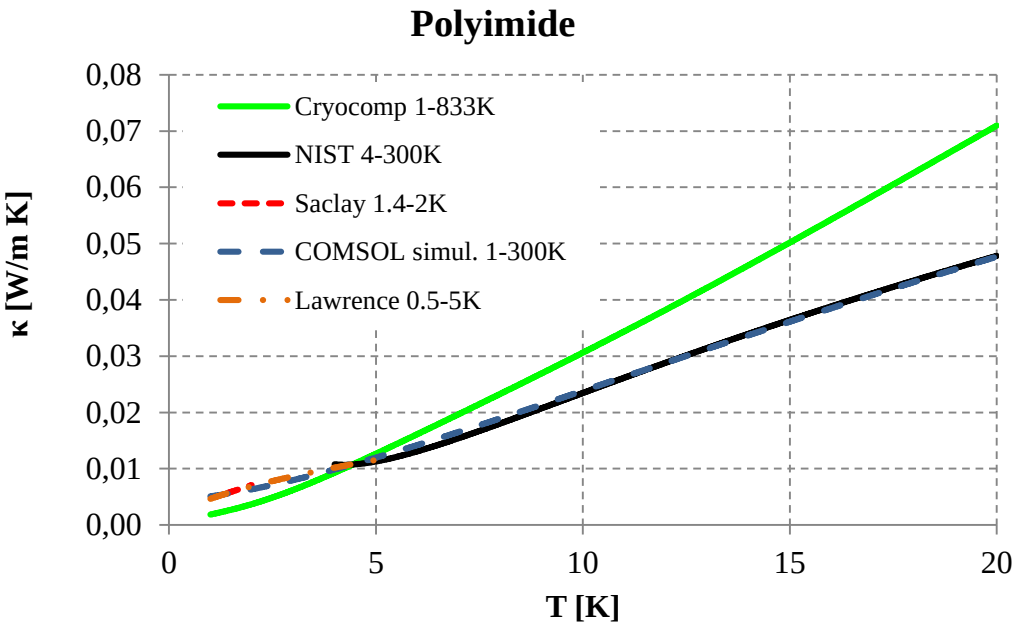

Fig. 4.1 The polyimide thermal conductivity

[4] Thermal conductivity of copper at cryogenics temperatures depends of residual resistivity ratio (RRR).
[5] The commercial names of polyimide insulation used in superconducting magnets are Kapton and Apical.
[6] The common names for high-pressure fiberglass laminate are G10 and G11.

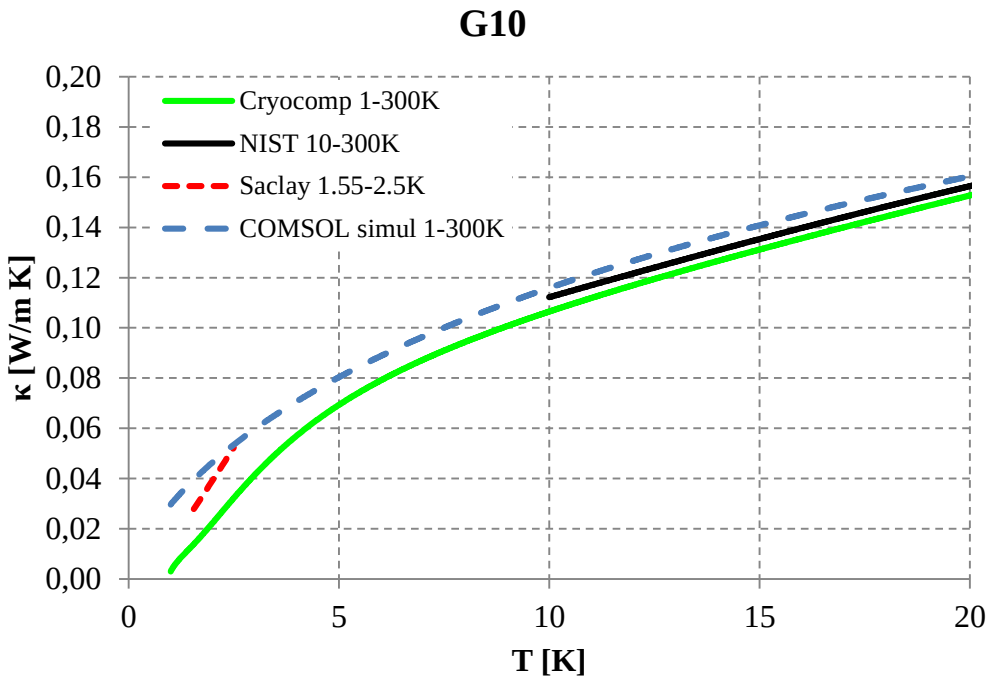

Fig. 4.2 The fiberglass laminate thermal conductivity

The formulas below show the measured data of polyimide and fiberglass laminate samples. They are compared with Cryosoft [80] database. The conclusion is that currently the spread of results of measurements is significant and dedicated measurements of thermal conductivity for each used insulating materials must be done in order to provide correct data for the thermal analysis of superconducting devices.

Kapton:	κ = 2.4E-3*T+2.28E-3	1.40 < T < 2.0 K [82]
	κ = 4.638E-3*$T^{0.5678}$	0.50 < T < 5.0 K [83]
	κ = 6.5E-3*T	0.20 < T < 5.0 K [84]
G10:	κ = 25.8E-3*T-12.2E-3	1.55 < T < 2.5 K [85]

IV.3 Cryogenic fluids

In general in scientific and industrial apparatuses the cryogenics liquids are used to obtain the cryogenics temperatures. The cryogenic temperatures are defined as temperatures below -180 °C (93.15 K) [81]. Due to the cryogenic liquids properties the different fluids are used for different temperatures ranges:

- 65-100 K – liquid Nitrogen (LN_2)
- 15-30 K – liquid Hydrogen (LH)
- 1-5 K – liquid Helium(LHe^4)

Also other cryogenic liquids are used in scientific and industrial applications, for example:

- liquid He^3
- liquid Neon (-27.1 K at atmospheric pressure) for cryogenic refrigerant in the range that helium is not needed
- liquid Deuterium (LD): bubble chambers
- liquid Argon (LAr): neutrino experiments, calorimetric detectors, cryosurgery (destroying tissue – cancer cells)
- liquid Methan (LCH_4): rocket fuel

In application discussed in this monography the liquid helium is used as a cryogenic temperatures source. In research instruments fluid helium is used at different working domains, among others: pressurized, saturated, subcooled or supercritical [30]. The Helium exists at liquid state at very low temperature, below 4.2 K at atmospheric pressure. In cryogenics the two-isotopes of helium, He^3 and He^4, are used. Both isotopes occur naturally but actually more than 99% of all available natural helium is He^4. Both isotopes demonstrate low boiling temperature. The He^4 boiling temperature at atmospheric pressure[7] is 4.23 K when He^3 boiling temperature atatmospheric pressure is 3.19 K. The critical points are: $T_{crit}(He^4)$ = 5.2 K at $p_{crit}(He^4)$ = 2.23 bar and $T_{crit}(He^3)$ = 3.35 K at $p_{crit}(He^3)$ = 1.16 bar. The helium exhibits properties which almost approximates that of an ideal fluid. One of the most important feature is superfluidity, the property that fluid demonstrates no viscosity and flows without loss of kinetic energy. The behavior of the helium is well described by classical models for gaseous and fluid phases and yet the superfluid phase requires use of quantum mechanics for description of its behavior [30]. The implementation of formulas describing liquid helium properties to and helium role as heat transfer media in multilayer structures are discussed in the next chapters.

IV.4 Thermal-electrical heat transfer equivalent

The heat conduction in a homogeneous material is described by the equation:

$$\frac{\partial^2 T}{\partial x^2} = \frac{c \cdot \rho}{\kappa} \cdot \frac{\partial T}{\partial t} \qquad \text{Eq. 4.5}$$

where: c – specific thermal capacitance,
ρ – density of the material,
κ – specific heat conductance,
T – temperature,
x – coordinates in the direction of heat transfer.

[7] $p_{atm}=1.01325 \cdot 10^5$ Pa

Assuming nodal approach for calculating the heat transfer due to heat conduction, the electrical analog is a transmission line.

$$\frac{\partial^2 U}{\partial x^2} = \boldsymbol{CL}\frac{\partial^2 U}{\partial t^2} + (\boldsymbol{CR} + \boldsymbol{GL})\frac{\partial U}{\partial t} + \boldsymbol{GRU} \qquad \text{Eq. 4.6}$$

where: C – capacitance per unit length,
L – inductance per unit length,
R – resistance per unit length,
G – transverse conductance per unit length.

Although the full description of transmission line is much more complex than Eq. 4.5 but a detailed analysis of equation allows for simplifications of Eq.4.6 and to get an equivalent to Eq.4.5. Equation Eq.4.5 describes a diffusion or compensation process. The transmission line equation Eq.4.6 as a wave equation, describes all the properties typical for a wave as for example standing waves or reflections. These are physical processes which have no at first view direct relationship. But, we observe that in the field of heat conduction in solid media the volume cannot cool itself. This means that the electrical term of inductance (L)[8] and the term of transverse conductance (G) are equal to zero. Then the equation of the equivalent transmission line obtain a reduced form presented in Eq.4.7 and it has the same structure as the heat equation form showed in Eq.4.5 [92].

$$\frac{\partial^2 U}{\partial x^2} = \boldsymbol{CR}\frac{\partial U}{\partial t} \qquad \text{Eq. 4.7}$$

where: C – capacitance per unit length,
R – resistance per unit length.

As long as we consider small temperature differences between the systems, the linearization of basic thermodynamic laws for the flow of heat permit to develop the analogy with an electrical circuit. This approach allow to describe a complex multilayer systems and to simplify them to qualitative evaluation. The analogy between heat diffusion and RC transmission line can be expressed in the following:

$$\nabla^2 T = R_{th} C_{th} \frac{\partial T}{\partial t} \qquad \Leftrightarrow \qquad \nabla^2 U = RC \frac{\partial U}{\partial t} \qquad \text{Eq. 4.8}$$

[8] It is worth to mentioned for further development of thermal modeling of devices immersed in large volume of helium that the equivalent of electrical inductance is the thermal inductance wherein a thermal change of an object surrounded by a fluid induces change in convection currents within that fluid, thus inducing a change in the kinetic energy of the fluid. The thermal inductance unit is thermal henry [H_{th}] (see Fick diffusion law).

$$R_{th} = \frac{\Delta x}{\kappa_{th} \cdot A} \qquad \text{Eq. 4.9}$$

$$C_{th} = c_p \cdot \rho \cdot \Delta x \cdot A \qquad \text{Eq. 4.10}$$

where: R_{th} - thermal resistance,
C_{th} - thermal capaticance,
κ_{th}- thermal conductivity (material dependent constant of proportionality),
ρ - material density,
c_p- specific heat at constant pressure,
Δx - length of component,
A - cross-sectional area.

Above the transient condition is described. In case of a steady-state condition the analogy between temperature rise and voltage difference can be expressed as equivalent of Fourier and Ohm laws.

$$\Delta T = qR_{th} \qquad \Leftrightarrow \qquad \Delta U = iR \qquad \text{Eq. 4.11}$$

Table 4.2 summarizes the equivalents of thermal and electrical circuits.

Table 4.2 The electrical analogy of the equivalent thermal circuit

Thermal circuit			**Electrical circuit**		
$\dot{Q}$, q	[W]	Heat transfer rate[9]	I	[A]	Current
ΔT	[K]	Temperature	ΔU	[V]	Bias (Voltage)
R_{th}	[K/W]	Thermal resistance	R	[V/A]	Resistance
κ_{th}	[W/Km]	Thermal conductivity	κ_{el}	[1/Ωm]	Electrical conductivity
Q	[J]	Heat	Q	[C]	Charge
C_{th}	[J/K]	Thermal Capacitance	C	[C/V]	Capacitance
L_{th}	[H_{th}]	Thermal Inductance	L	[H]	Electrical Inductance
		Heat reservoir	$\mathcal{E}$		EMF (Electromotive Force)
		Absolute zero			ground
		Heat generator			Current supply

[9] Heat transfer rate is amount of heat transferred per unit time.

Below, the examples of implementation of thermal-electrical analogy used in superconducting magnets modeling is presented. The thermal elements and base systems and their electrical equivalent are shown.

- Conduction of heat through basic element modeled as thermal resistance:

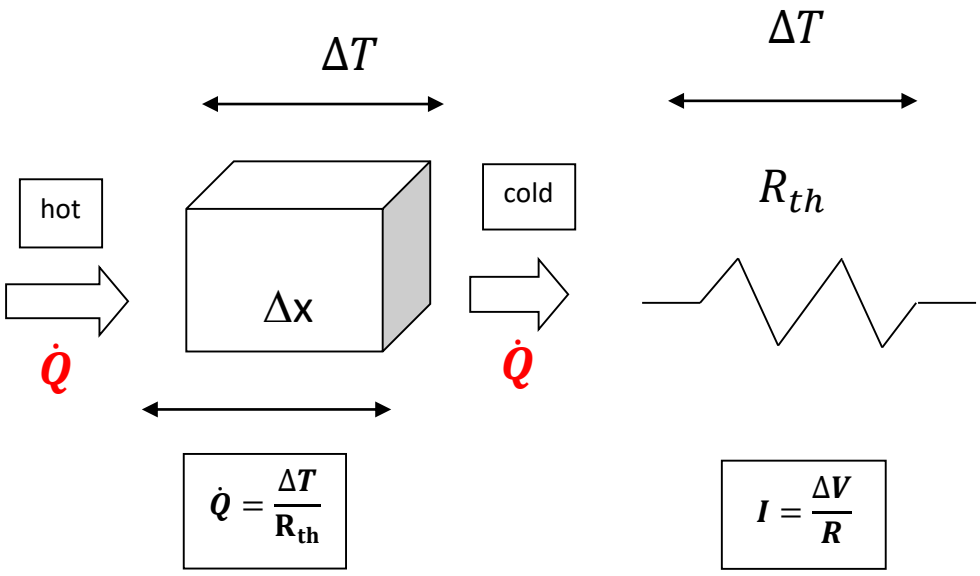

- Conduction between two heat reservoirs

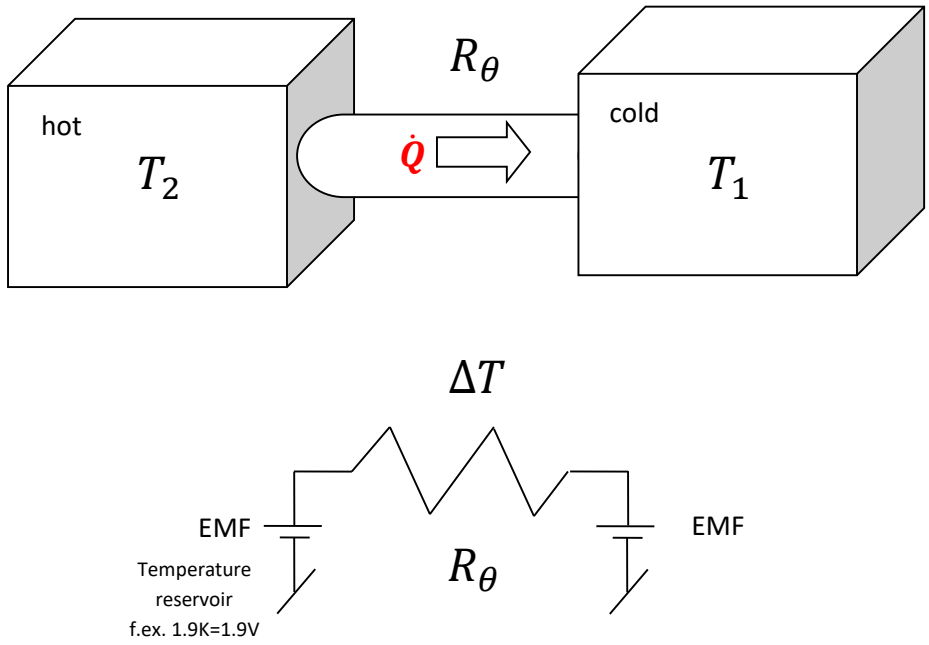

EMF (Electromotive Force)

$$\mathcal{E} = \frac{W}{q} = \frac{\frac{W}{t}}{\frac{q}{t}} = \frac{P}{I} \qquad \text{Eq. 4.12}$$

$$[\mathcal{E}] = [V] = \left[\frac{J}{C}\right] = \left[\frac{W}{A}\right] = \left[\frac{kg \cdot m^2}{A \cdot s^3}\right]$$

where: P – power dissipated in the circuit,
I – electrical current.

- Conduction from heat source to heat reservoir

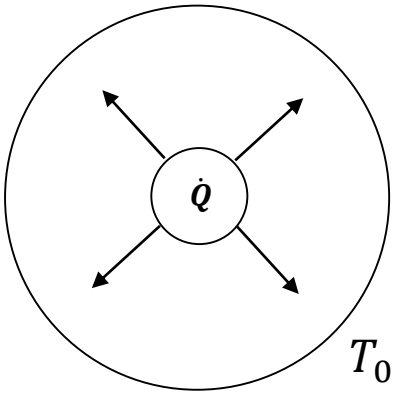

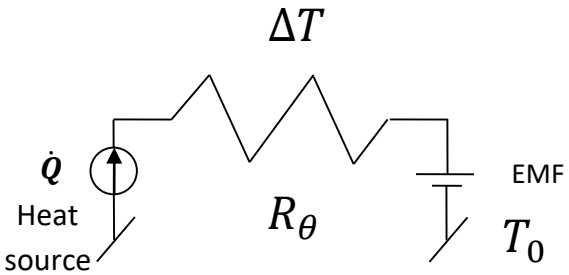

- Heating of element in time (transient case)

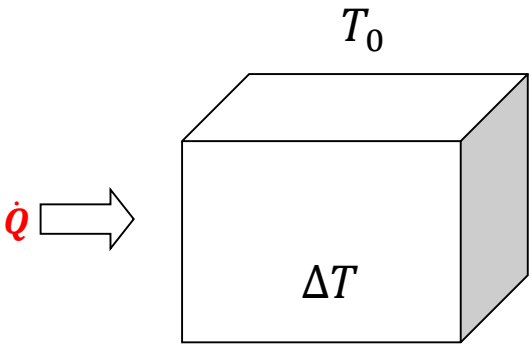

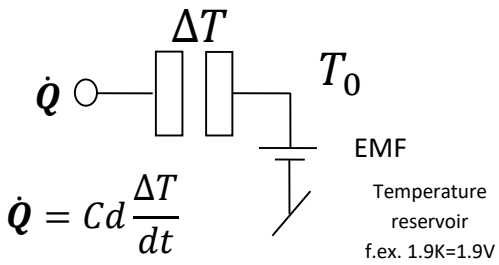

$$\dot{Q} = C_{th}\frac{\partial T}{\partial t}$$

$$I = C\frac{\partial V}{\partial t}$$

IV. 5 Multilayer structure in the superconducting magnets

Heat transfer through multilayer structures is a vital problem for equipment working at cryogenic temperatures. The high field superconducting accelerator magnets are the example of multilayer structure subjected to thermal, mechanical or magnetic loads. Superconducting magnets operating in an accelerator environment are affected by particles lost from the beam. To be more precise, the particles lost from the beam hitting beam screen and beam pipe generates the shower of secondary particles which deposits energy in superconducting magnet coil.

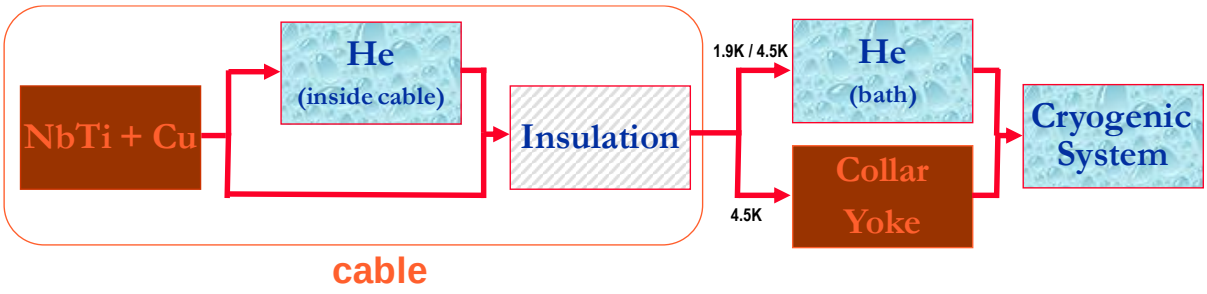

Fig. 4.3 The scheme of heat transfer path in accelerator superconducting magnet

Fig. 4.3 shows the heat propagation path from source to the heat reservoir through different layers of materials from which the superconducting magnet is constructed. The presented scheme consists of layers of superconductors with copper stabilizers, helium (fluid or superfluid), electric cable insulation, stainless steel (collar) and iron (yoke). For superconducting magnets the heat is generated inside the superconductor and the main cooling path is provided by helium until the heat exchanger (Fig. 4.4). Each material in the magnet demonstrates different dependence on temperature as well as thermal contact resistance. The simple comparison of thermal conductivity allow to identify that the electric insulation of magnet cables and coils is a barrier for the heat transfer from superconductor to heat exchanger. There are two requirements for electric insulation which are difficult to combine: (1) providing good electric insulation and (2) allowing for efficient heat extraction from the conductor to helium. The optimization of the magnet design with these two requirements is challenging. For a steady-state thermal analysis the whole multilayer structure can be represented as a system of serial connected thermal resistances made of different materials and their contacts between heat source and heat reservoir.

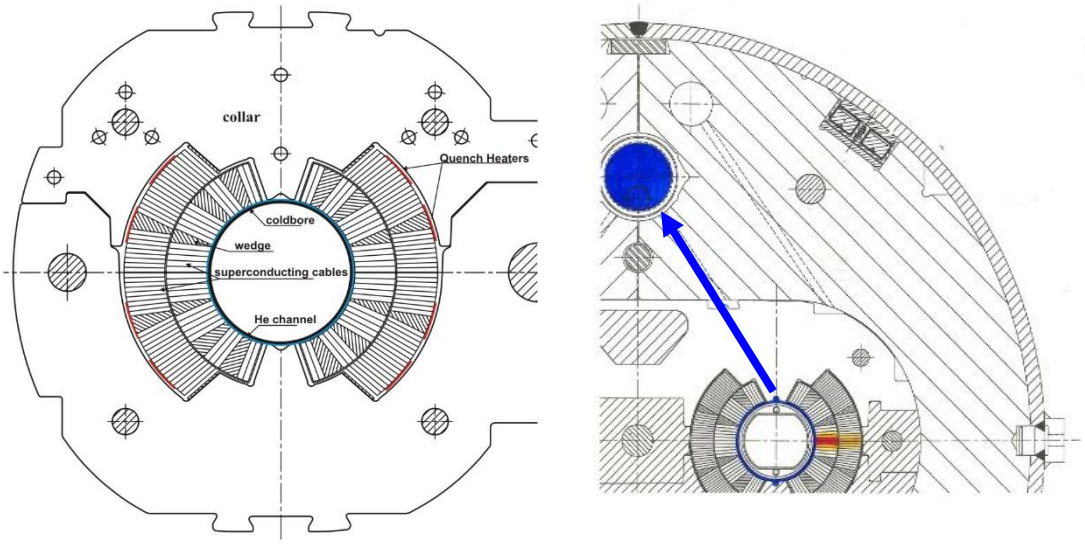

Fig. 4.4 The drawing of LHC main dipole magnet – helium path. Cold bore, helium around cold bore, coil and collar (left), cold bore, helium around cold bore, coil, collar, yoke and heat exchanger pipe (right)

In analysis of the multilayer structure of superconducting magnets also the contact thermal resistance between the solids parts and between the solids and liquid, so called Kapitza resistance, are taken onto account in calculations. The thermal contact resistance per unit area between two solids is defined as:

$$R_C = \frac{\Delta T}{\dot{Q} / A_C} \qquad \text{Eq. 4.13}$$

where: R_C - thermal contact resistance,
ΔT – temperature discontinuity,
$\dot{Q}$ – heat flow,
A_C – contact surface.

The contact resistance (R_c) between two solids, on which we observe temperature discontinuity, appears due to microscopic roughness and the contact surfaces touch each other only at certain number spot-like points. In addition, the phonon scattering occurs at the interface due to an acoustic mismatch between different materials. That is why, R_c depends strongly on the surface preparation and forces applied to the contact surfaces, which can increase number of contact points. There are methods to decrease contact resistance by applying appropriate fillers but it is not the case of superconducting magnets. In case of superconducting magnets it have to be mentioned that the contact thermal resistance changes due to plastic deformation of the local contact spots during cycling loading. At liquid helium temperatures contact conductance is proportional to T^n, where $1 < n < 2$ for metals and $n = 3$ for insulators [94].

The Kapitza resistance [86] plays vital role in flow of heat across the interface between liquid helium and a solid. The general equation is:

$$R_K = \frac{T_S - T_{He}}{\dot{Q}/A} \qquad \text{Eq. 4.14}$$

where: R_K - Kapitza resistance,
T_S – temperature of solid material,
T_{He} – temperature of helium,
$\dot{Q}/A$ – heat flow per unit area.

A common use equation relate the measured values of Kapitza coefficient with temperatures and Kapitza resistance and it has following form:

$$R_K = \frac{1}{\sigma_K}\left(T_S^2 + T_{He}^2\right)\cdot\left(T_S + T_{He}\right) \qquad \text{Eq. 4.15}$$

where: R_K – Kapitza resistance,
σ_K – Kapitza coefficient
T_S – temperature of solid material,
T_{He} – temperature of helium.

The measured values of Kapitza coefficient (σ_K) range from ~550 to ~1200 $Wm^{-2}K^4$ [82]- [90]. The following results, summarized in Table 4.3 and plotted in Fig. 4.5, were obtain in dedicated experiments for materials used in superconducting magnets:

Table 4.3 Kapitza resistance

Material - fluid	Formulas	References
Polyimide – He II	$R_K=10.54\cdot10^{-3}\cdot T^3$ Km^2W^{-1}	[82]
Polyimide – He II	$R_K=0.7\cdot10^{-3}\cdot T^3$ Km^2W^{-1}	[87]
G10- He II	$R_K=1462\cdot10^{-6}\cdot T^{-1.86}$ Km^2W^{-1}	[85]
Copper – He II	$R_K=550$, $R_K=900$, $R_K=1200$,	[88]-[90]

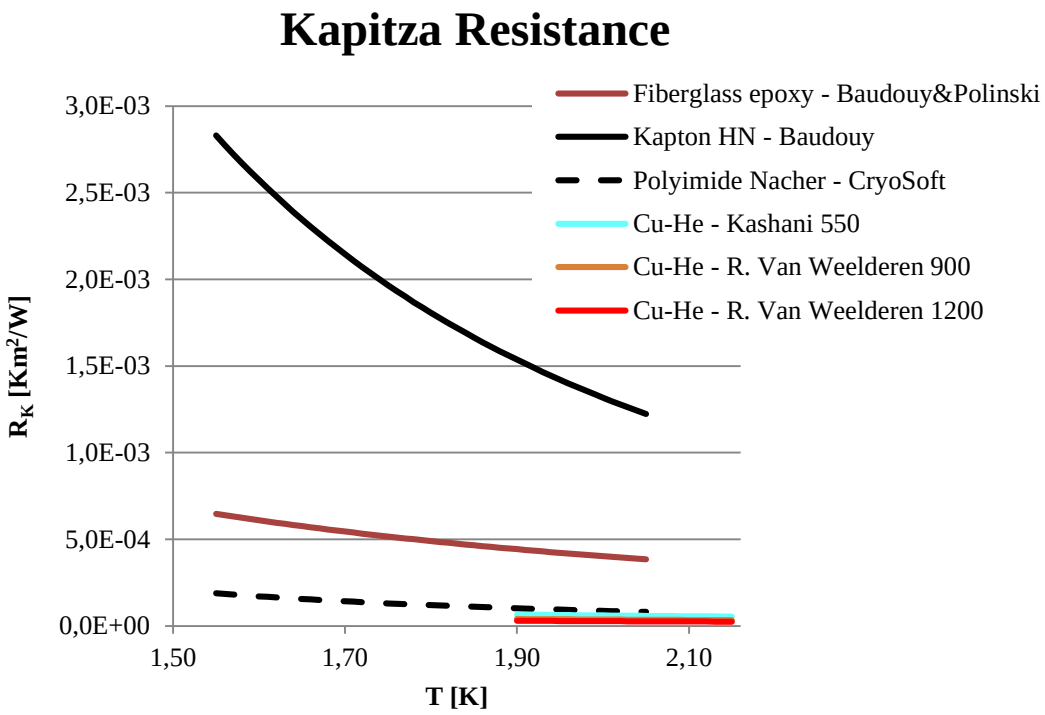

Fig. 4.5 Kapitza resistance measurements

Chapter V
Heat Transfer Modeling

The operation of accelerators and preservation of designed beam parameters require usage of different types of magnets. The main dipole magnets are used to bend the beam and in case of circular accelerators to keep the beam on designed orbit. The lattice quadrupole magnets are used to keep the particles together in the beam (FODO patterns). The interaction region quadrupoles, so-called inner triplet quadrupoles, are used to focus beam in the interaction point. The family of corrector magnets (dipoles, quadrupoles, sextupoles and octupoles) are used to preserve the beam quality and septum magnets are used in beam extraction systems. The most of LHC accelerator magnets are built with use of superconducting Nb-Ti technology. The proper work of the superconducting magnet requires that the operation temperature is maintained below the current sharing temperature (T_{cs}) of the conductor used to build the coil. The difference between the cooling system temperature (T_{bath}) and superconductor current sharing temperature is called the temperature margin ($T_{marg.}$) and it is the safety factor for magnet operation. Typically minimal T_{marg} value for accelerator magnets is of order from 1.4 K. The main operational challenge of superconducting accelerators is protection against quench[10], namely keeping conductor temperature within allowed range of changes determined by T_{marg}. Each quench induced by energy deposits from the beam reduces discovery potential of LHC and it can also lead to magnet damages caused by the thermal stresses, which can appear in superconducting magnet structure (for example break of filaments in strands used in coil cable). The main objective of heat transfer modeling in superconducting magnets is the determination of the energy amount from the beam which can be safely deposited in the magnet coil and which does not provoke the magnet to quench.

V.1 Heat transfer numerical simulations

The modeling of heat transfer in superconducting magnets involves different branches of physics and engineering, namely: superconductivity, material science (properties of materials at low temperatures), thermodynamics (heat transfer), accelerator physics (heat source, energy deposits to the coil), engineering design (superconducting magnet design). The main difficulties in calculating the heat flow in superconducting magnet structure is the fact that the solid and the fluid domain must be calculated simultaneously. This fact means that the numerical simulation is complex, especially in case of superfluid helium. Many scientific publications describe an original approach to optimize the heat transfer in superconducting magnets or propose a new cooling schemes, as for example [93], [95]-

[10] Quench is the transition of conductor from the superconducting to the normal conducting state which occurs irreversibly in the accelerator magnets if one of the three parameters: temperature, magnetic field or current density exceeds a critical value.

[104]. The complexity of the numerical simulation of superfluid helium shows the fact that its mathematical description requires six scalar equations with independent variables as temperature, density, pressure, first velocity and second sound velocity [93]. The detailed analysis of this description allowed to make the assumption that the thermo-mechanical and the Gorter-Mellink terms are the dominant ones in the superfluid component momentum equation [93]. The simplified description of superfluid helium is one with momentum and energy equations only [104].

The years of work in different laboratories on modeling of the heat transfer in superconducting magnets resulted in the development of many software tools or the implementation of existing commercial software to these studies. The numerical simulations of heat transfer carried out with use of commercially available software were performed with multiphysics software, ANSYS or COMSOL, which use the Finite Element Analysis (FEA) tools. The examples of numerical simulations with ANSYS are [104]-[106] and with COMSOL are [107]-[108]. The models build with ANSYS or COMSOL use magnet geometry to which beam loss related heat sources prepared with MARS or FLUKA simulation packages were implemented. Some initial work was done also with the Simulation Program with Integrated Circuit Emphasis (SPICE) in order to develop novel techniques to solve sets of coupled heat transfer differential equations [113]. In this monograph the SPICE based software (PSPICE) was selected as a tool for *Network Model* implementation and it is one of many software developed at CERN. Other examples are:

- The ROXIE (Routine for the Optimization of magnet X-sections, Inverse field calculation and End design), which is the software for the design and optimization of LHC superconducting magnets in 2D or 3D, and provides a magnet-level basic thermal network solver. The examples of numerical simulations with ROXIE are [109]-[110],
- The SPQR (Simulation Program for Quench Research), which is dedicated to Quench simulations for superconducting elements in the LHC accelerator [111],
- The THEA (Thermal, Hydraulic and Electric Analysis), which is a software dedicated to 1D/2D steady-state and transient multi-physics analysis of the superconducting cable by thermal and hydraulic networks [112],
- QP3 (Quench Protection), which is software based on a 1D thermal network. QP3 is dedicated to study the quench behavior over the longitudinally segmented conductor and allow to solve the coupled and highly non-linear problems [114],
- ZERODEE, which is software dedicated to the stability analysis of superconducting cables and allows extensive parametric study with respect to heat capacity, thermal contacts (solid-solid and solid-helium) and quick estimate of stability margin for long normal zone [115]-[116],
- Other software as for example quench simulation of superconducting coils with the Wilson's method [117].

V.2 The Network Model

The *Network Model* was developed to study the thermal behavior of the superconducting magnets and to determine the quench levels of the accelerator magnets for beam loss scenarios [118]-[120] occurring at steady-state conditions. Fig. 5.1 schematically shows the construction of *Network Model*. The idea of the *Network Model* is based on the nodal structure of thermal circuits. The essential part of the model are magnet technical drawings, which provide the details for the creation of the mesh of thermal elements. Other required information is: materials thermal properties at cryogenic temperatures [30], [80]-[90], coil cables temperature margin calculated from the magnetic field distribution obtained from ROXIE software [121]-[122] and beam loss profiles obtained from FLUKA software [123]-0. The non-beam loss induced heat source, as the eddy currents and magnetic hysteresis losses, were evaluated with use of [125]. The estimation of their contribution to the quench level value is of the order of 2% and they were neglected in further thermal study of superconducting accelerator magnets.

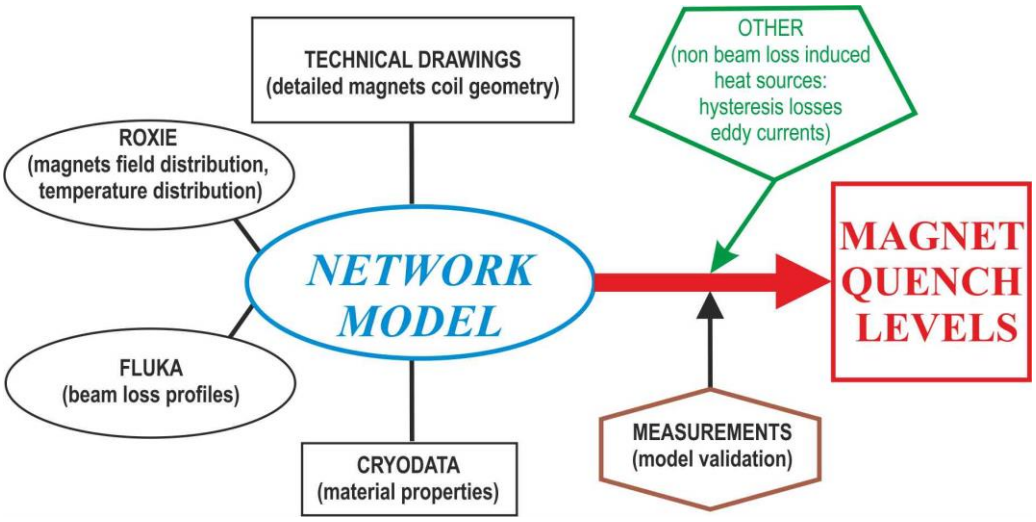

Fig. 5.1 Network Model construction overview

The fundamental unit of the *Network Model* is superconducting cable, which is used to wind the magnet coil. Fig. 5.2 shows the drawing of the Rutherford type cable and insulation scheme used in LHC superconducting magnets. The cable schematic cross-section with indication of all key elements is depicted in Fig. 5.3 whereas the process of preparation of the fundamental unit of the *Network Model* is presented in Fig. 5.4. The magnet coil is constructed from the cable unit and other elements, namely inter-layer insulation placed between the cable layers, ground insulation, cold bore and helium channel around the cold bore as well as collar and yoke. They were included in the model

with segmentation corresponding to the cable dimensions. The two-dimensional *Network Model* was normalized to one meter of magnet length which corresponds more or less to the longitudinal length of secondary particle cascade, which is developing after hitting the cold bore and magnet coil by particles lost from the beam. The steady-state *Network Model* is constructed from the following thermal elements: heat source, thermal resistance and heat reservoir, and reproduces the heat flow path in superconducting accelerator magnets. This path schematically is showed in Fig. 5.5 (see also Fig. 4.4).

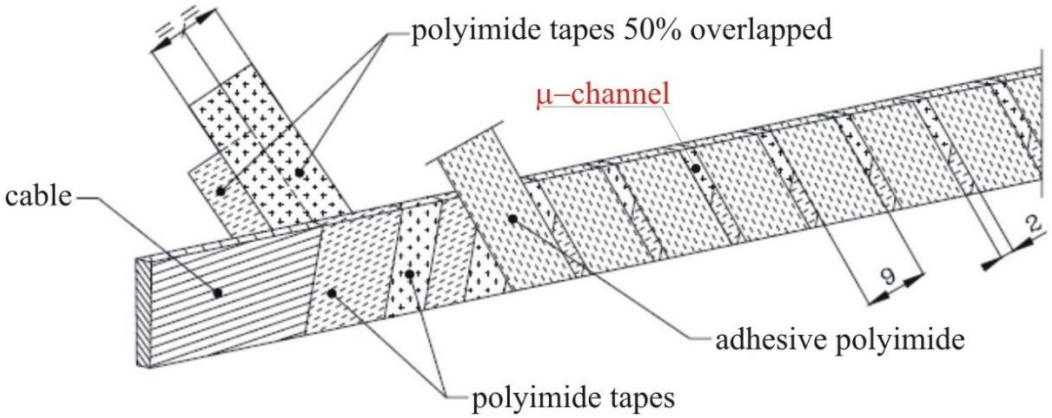

Fig. 5.2 The Rutherford type cable with insulation winding scheme for the LHC superconducting magnet coils. The metal part and insulation is indicated in the figure. The helium volume in the μ-channels indicated in the figure is a vital parameter in the calculation of the cable thermal stability.

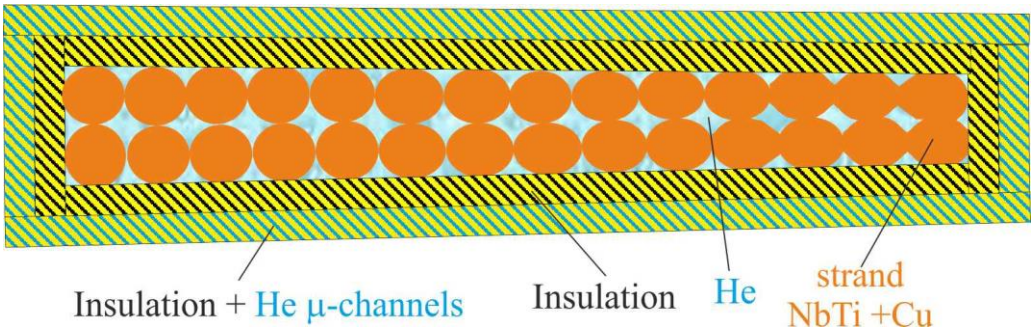

Fig. 5.3 Schematic cross-section of an insulated superconducting Rutherford type cable. The free void volume which could be occupied by helium is depicted between strands and between the strands and the cable insulation.

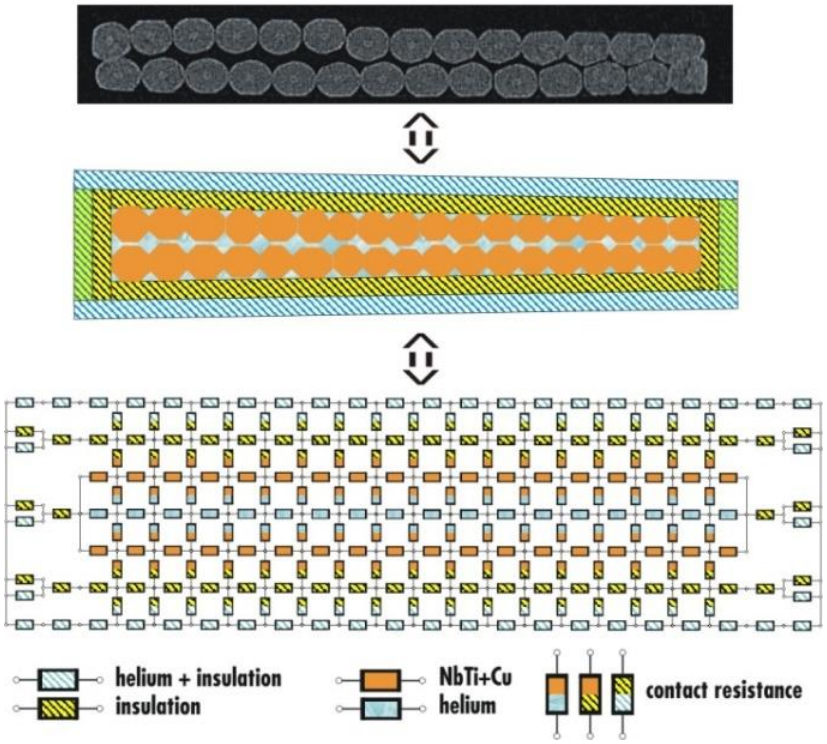

Fig. 5.4 The *Network Model* fundamental unit creation. The real photo of the superconducting cable cross-section, its physical model and the equivalent *Network Model*.

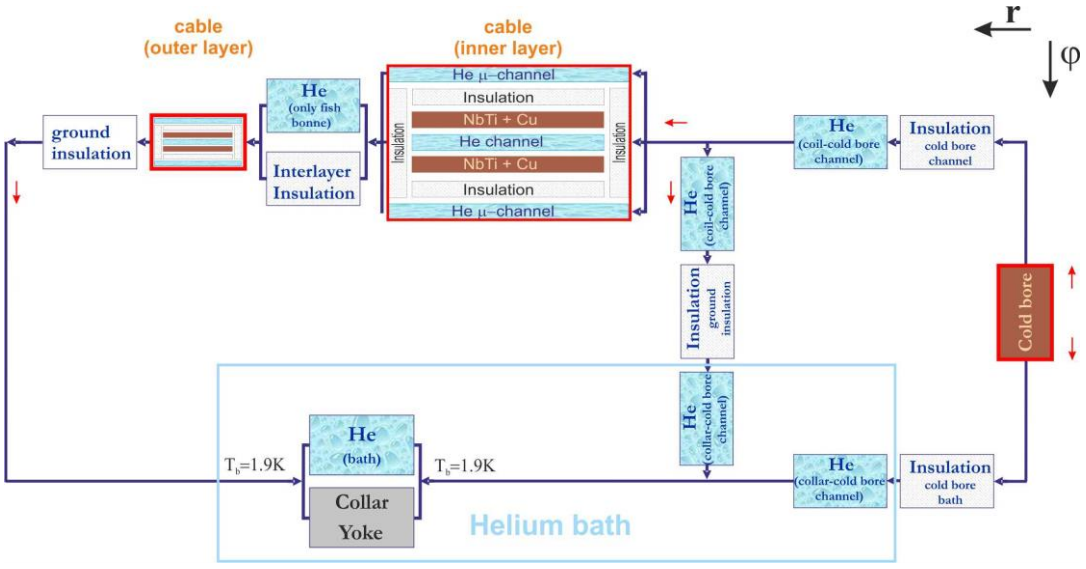

Fig. 5.5 The scheme of heat flow path in the LHC superconducting magnet (see also Fig. 4.4)

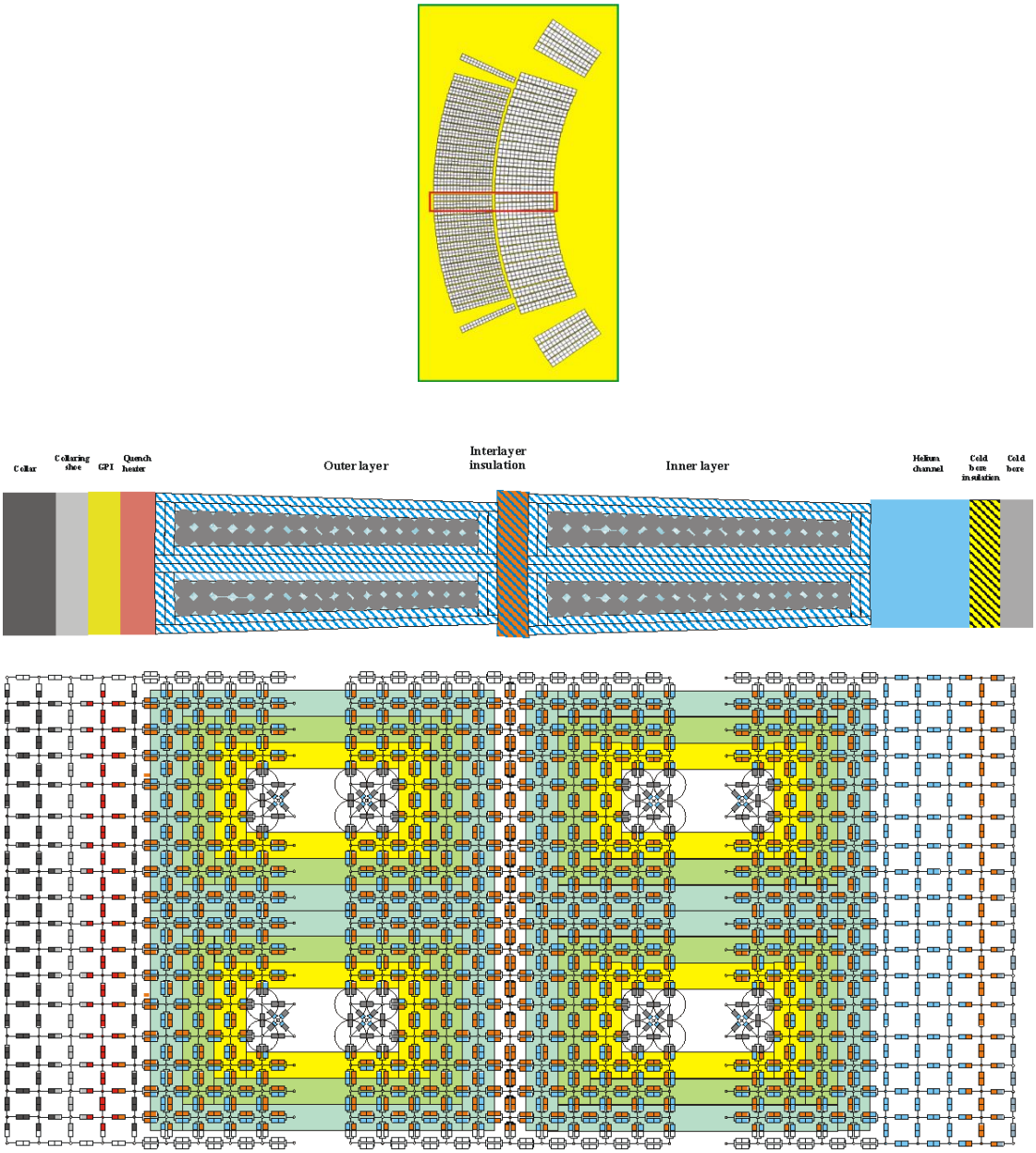

Fig. 5.6 The magnet coil cross-section (top) and its 2-dimensional *Network Model* (bottom) together with remaining superconducting magnet components: cold bore, collar, yoke, ground insulation

The values of the thermal conductivity of solid components of magnets (superconductor, electrical insulation, stainless steel, iron, Kapitza resistance) used to calculate the thermal resistances are taken from commercially available databases [80]-[81] and literature [30], [92]-[90]. The modeling of helium requires much more attention. The helium takes on an active role in carrying heat away from the superconducting cable strands. Due to the very high thermal conductivity and heat capacity of superfluid and supercritical helium heat can be evacuated very efficiently from the metal components of the cable. The seven different heat transfer mechanisms in helium were identified and implemented in the *Network Model* (Fig. 5.7): (1) the superfluid helium heat conductivity in narrow channels; (2) the superfluid helium heat

conductivity in wide channels; (3) the nucleate boiling in the normal liquid helium; (4) the heat conductivity of normal liquid helium; (5) the convection in normal liquid helium; (6) the heat conductivity of gaseous helium; (7) the convection in gaseous helium (see: [30], [96]-[97], [126]-[127]). The bold (red) rectangle blocks in Fig. 5.7 indicate the most conservative heat transfer mechanisms in helium. In the superconducting magnets the dominant mechanism of heat propagation is heat conduction. Due to narrow helium channels the contribution from convection is small. Also contribution from heat radiation is negligible.

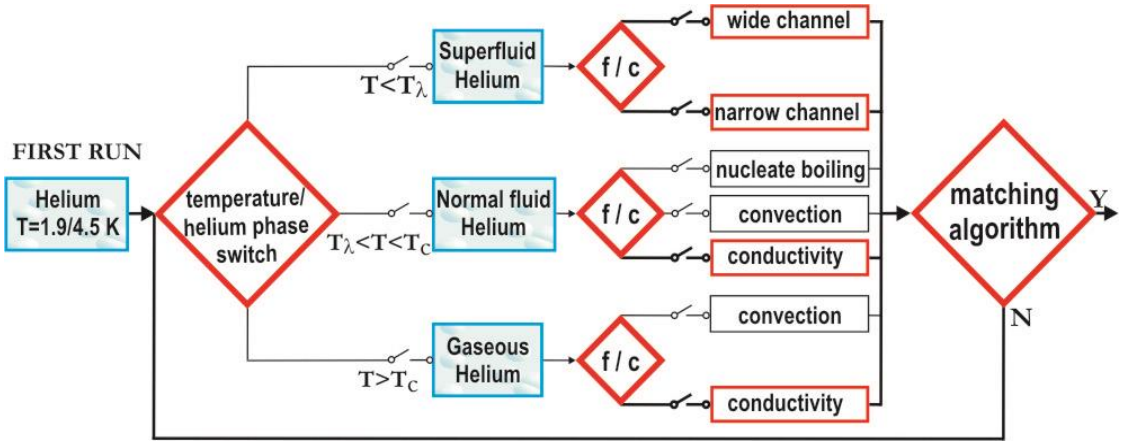

Fig. 5.7 The helium heat transfer mechanisms implemented in the *Network Model*. The bold (red) rectangular blocks indicate the most conservative heat evacuation path. The f/c mean flux/channel size switch. The recurrence model is used to iterate matching the helium thermal resistance values to the simulated temperature distribution in the coil or stack of cables.

The helium channels in the superconducting magnets are the main heat evacuation path so proper modeling of helium thermal properties in the *Network Model* is fundamental to understand the heat flow mechanism, especially in the magnets operating at superfluid helium temperatures. The superfluid helium heat transfer is calculated with the experimentally determined equation by Claudet et al. in [126]. This formula (Eq. 5.1) is in good agreement with 1-dimensional Gorter-Mellink equation [127].

$$\frac{\dot{Q}}{S} = \left[\frac{X(T_c) - X(T_h)}{l}\right]^{0.29}\left[\frac{W}{cm^2}\right]$$
$$X(T) = A\cdot\left[1 - exp(-[B\cdot(2.16 - T)]^{2.5})\right] \qquad \text{Eq. 5. 1}$$
$$A = 520,\ B = 3$$

where: S – helium channel cross-section in [cm^2],
l – helium channel length in [cm],
T_c – temperature of the colder channel end in [K],
T_h – temperature of the warmer channel end in [K].

The Eq. 5.1 was determined for cylindrical channels at atmospheric pressure. The *Network Model* use the 1-dimensional elements so the channel shape has no impact on heat transfer. In addition the equivalent helium channel cross-section in the cable is used to calculate the thermal resistivity. The normal fluid helium is modeled with the data from [30] and [80]. The gaseous phase inside the narrow channels is described in the *Network Model* by a constant heat transfer coefficient, which is in the order of 70 $W/m^2/K$ as extrapolated from [97]. The volumes inside the coil cables are semi-closed volumes with a very limited direct link to the helium bath, mainly due to insulation winding imperfection [98]. The amount of helium inside the cable is a vital parameter in the *Network Model*. The free void volume is defined as the space inside the insulated superconducting cable that can be occupied by helium. In order to determine the free void volume in all types of main LHC cables (see: Appendix 1), dedicated measurements were performed by the author of this monography. A detailed description of the measurement methodology and obtained results are presented in Appendix 2.

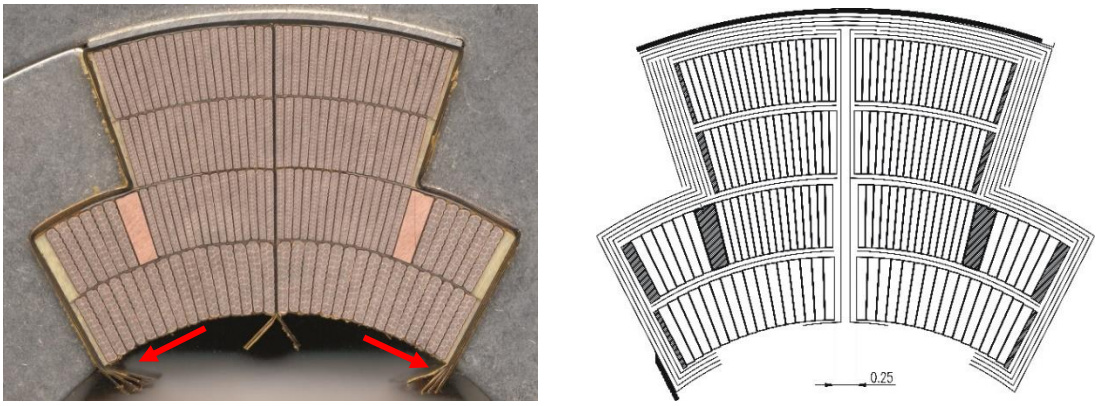

Fig. 5.8 MQY magnet photo and technical drawing. The ground insulation flaps indicate in the picture is one of heat transfer barrier because their segment.

The LHC magnets operate at 1.9 K in arc regions and at 4.5 K in the long straight section located just before low-β quadrupoles and experiments. The steady-state heat load to the semi-closed helium volumes may lead to the transition of helium from a liquid state to gas and thereby reducing the cooling capabilities of helium. The blocking of existing heat flow paths may lead in consequence to the quench of magnet. Since the superconducting magnets are composed of materials with different coefficients of thermal expansion, the temperature fluctuations may create mechanical stresses detrimental to thermal and electrical stability of magnets. The analytic thermal analysis show that the main barriers for the heat flow is the cable electrical insulation and the coil ground insulation extension (flaps) in the helium channel around the cold bore (see: Fig. 5.8).

V.3 The Network Model cross-check

The comparison of the results of simulation of simple coil geometry have been performed for the *Network Model* and COMSOL multiphysics software (Fig. 5.10). The whole cable model with ground insulation and helium bath was implemented in both software. The results of simulations show the difference of 1.6% maximum (Fig. 5.9). This result confirmed that the *Network Model* is exact tool for fast and effective steady-state heat transfer simulations.

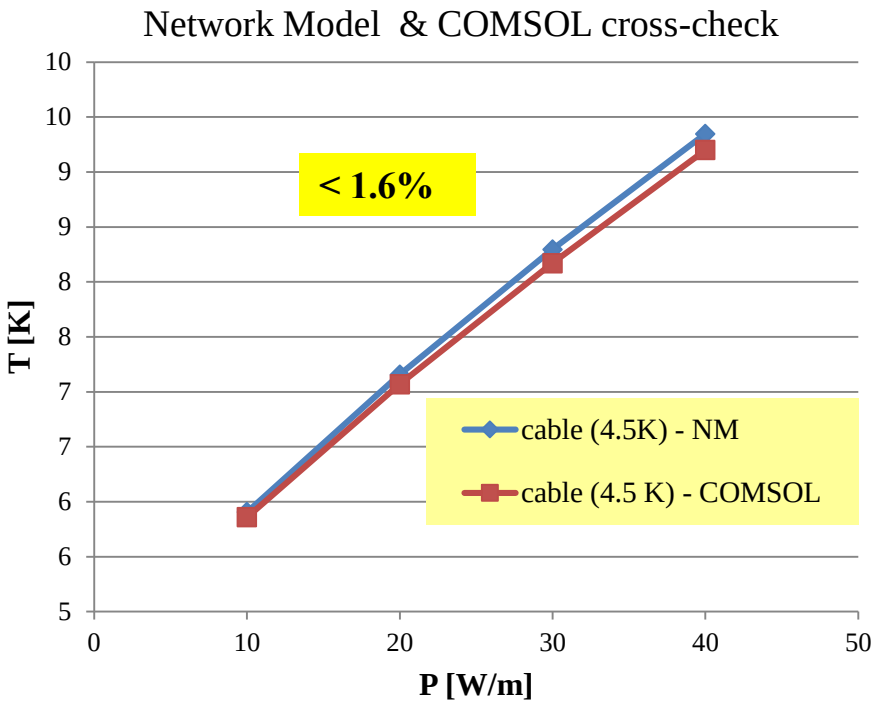

Fig. 5.9 The *Network Model* and COMSOL multiphysics comparison. The maximal difference between simulation is less than 1.6%.

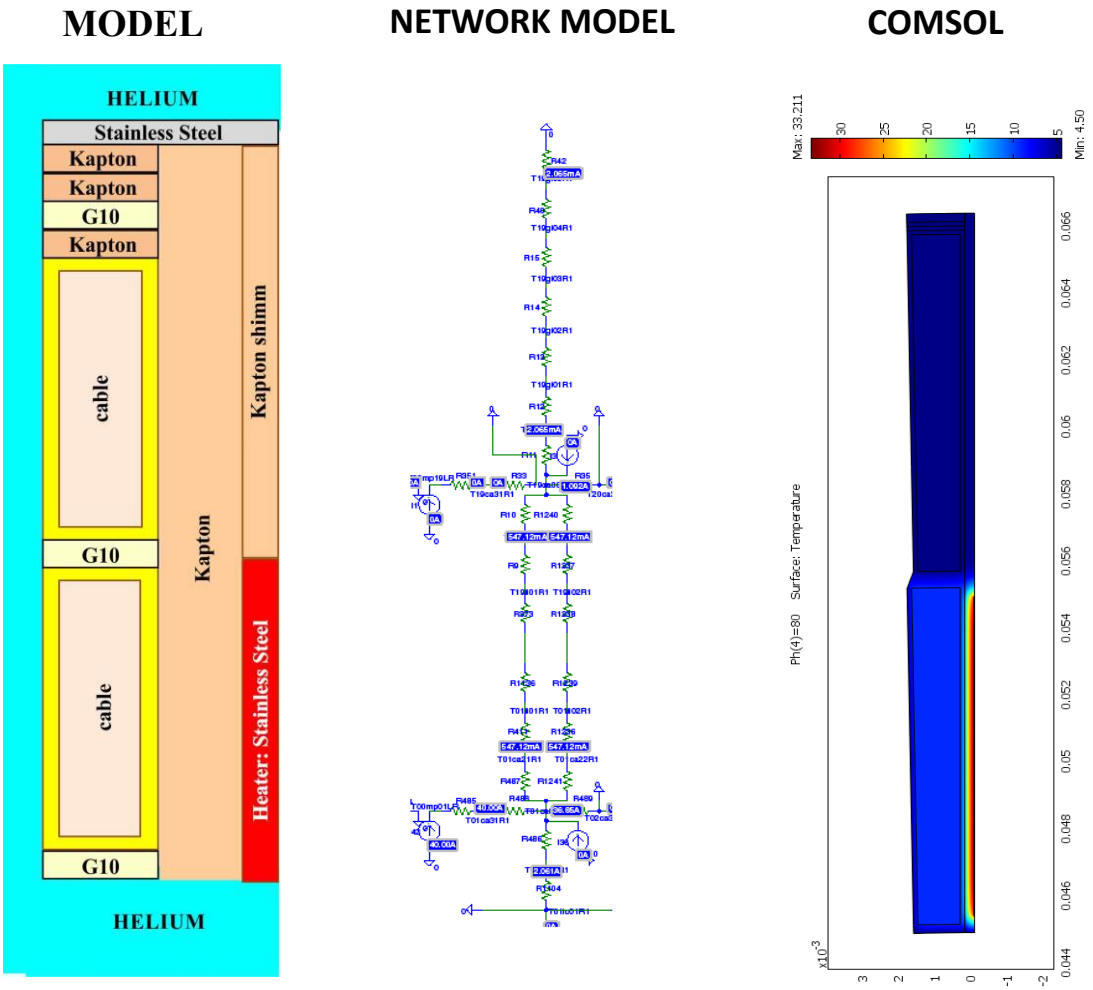

Fig. 5.10 The *Network Model* and COMSOL multiphysics comparison. From left: geometry implemented to the models, *Network Model*, COMSOL model (graphical representation of simulation).

Chapter VI
Models validation with experimental results

The results of the simulations with the *Network Model* were validated with the experimental results. The validation procedure is showed in Fig. 6.1. The *Network Model* was developed at CERN during serial tests of the LHC magnets and model validation measurements were performed on magnets which are currently installed in the LHC. The two measurement procedures were developed during this campaign. The first considered procedure was based on keeping the magnet current constant (I_{coil} =const) and ramp quench heater current (I_{QH}) with a step of 0.1 A. The maximal current for powering the quench heater was set to 2 A. This procedure was abandoned since the ramping of I_{QH} with a step of 0.1 A per second or even per minute could not assure a steady-state condition. The second procedure was based on keeping the quench heater current constant (I_{QH} =const.) over 300 seconds or more and then slowly ramping the current of the magnet (I_{coil}) with a step 20-50 A/s at a low current region, namely up to 1000A and then decreasing the ramp speed to 1A/s. This procedure assured a high precision of the magnet quench current measurements.

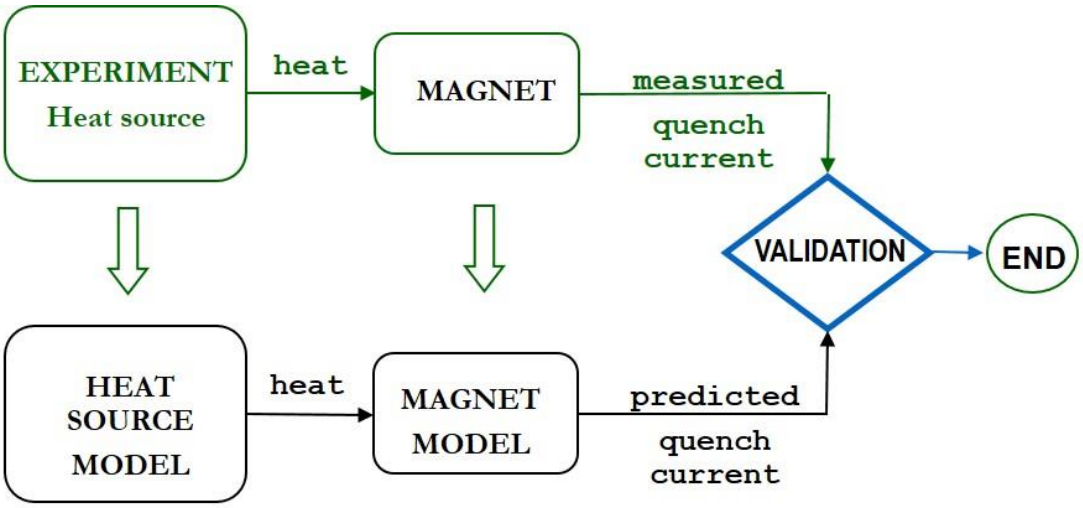

Fig. 6.1 The *Network Model* validation procedure.

VI.1 The Network Model validation with quench heaters

The superconducting magnets installed in the accelerators are protected by the quench protection system build-up with quench heaters [128]. Currently, the alternative methods of magnet protection are under development and testing at CERN, as for example the Coupling-Loss Induced Quench (CLIQ) [129]. The quench heaters protect superconducting magnets against the development of excessive voltage and overheating

after a transition to a resistive state. The heating strips are made of stainless steel partially plated with copper (Fig. 6.2). The strips are embedded between two polyimide foils. The copper plating pattern is adapted for the various types of magnets in order to keep the resistance of the heater circuit at the same value. This fact allows to power the quench heaters with only one type of power supply. The copper plating allows to control the strip resistance and thus for the connection of quench heaters in series. The quench heaters are powered by the capacitor banks, discharged after quench detection. The quench heater strips are positioned along the magnet between the coil and the collars. The positions of quench heaters in the measured magnets are shown in Fig. 6.4 and Fig. 6.5. The quench heaters installed in the LHC magnets are made of 25 μm thick and 15 mm or 21 mm wide stainless steel strips [128]. They are insulated with 100 μm thick polyimide film. The stainless steel strip thickness can vary within the range given by technical specifications. This implies the difference of measurements of the quench heaters resistance for each magnet. It is an important value for the quench limit experiments performed since the power dissipated to the magnet coil is an essential parameter calculated from the strip resistance and the DC current value of which the strip is powered.

The quench heaters build-in in the main LHC superconducting magnets are very favorable for the studies dedicated to the quench limits studies. The experimental setup is composed of built-in quench heaters and the DC power supply (Fig. 6.3). The quenches were provoked at different levels of the magnet current in function of the power dissipated to the selected quench heater. The experimental setup was implemented into the *Network Model* and the simulation results were compared with the measurement results. During a steady-state quench experiment the selected quench heater strip was powered in the DC mode from an external power supply, leaving the remaining quench heaters in magnet protection mode. The power dissipated to the quench heater strip was transferred through the polyimide insulation to the coil, heated the coil cables and provoked the quench of the magnet. Typically the quench started in one of the cables below the quench heater strip and the natural quench propagation drive the entire conductor into the normal conducting state.

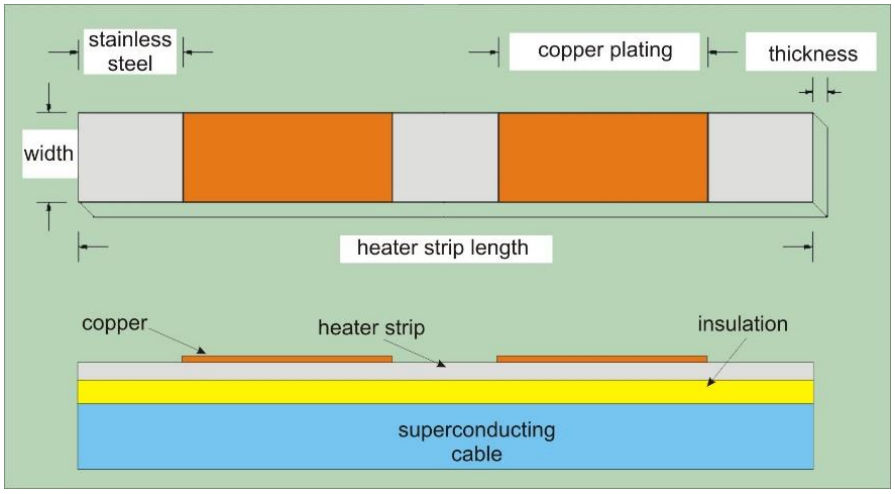

Fig. 6.2 The schematic view of copper plated quench heater stripe installed in the LHC magnets.

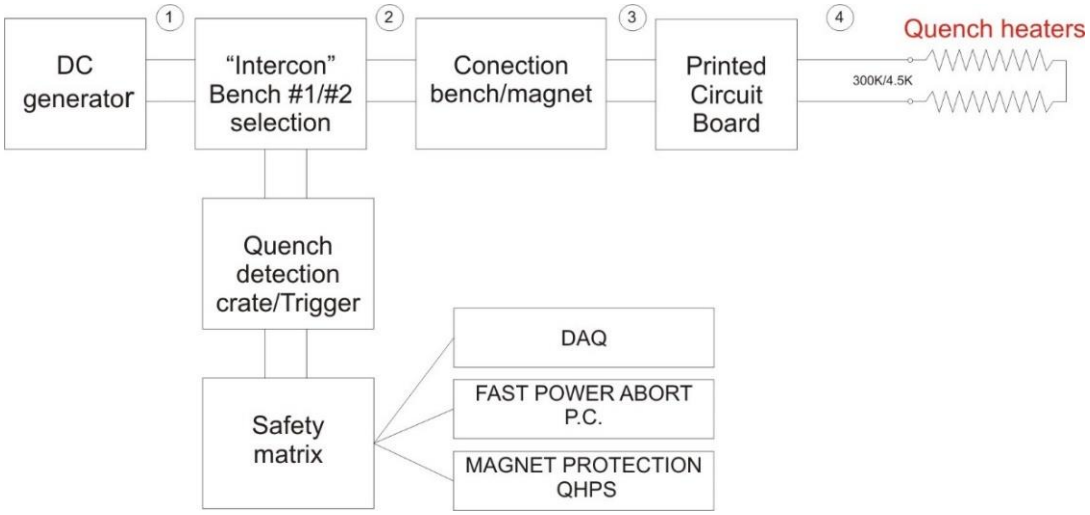

Fig. 6.3 The sketch of the experimental setup for the quench heater provoked quenches. The sketch shows the quench heaters connection during tests.1 - cabling between the quench heater patch panel and the "intercon", 2 - cabling between the racks and the test bench, 3 – the instrumentation cable of the magnet, 4 – the capillary cable 300K/4.5K.

The *Network Models* of four families of the LHC magnets were prepared: the main arc dipole (MB), the main arc quadrupole (MQ) and the Long Straight Section quadrupole magnets (MQM and MQY). The fundamental units of the models were prepared according to the cables characteristics shown in Appendix 1 and helium volumes calculated from dedicated measurements (Appendix 2) and technical drawings. The validation procedure shown in Fig. 6.1 was used to compare the results of simulation with measured values. The modeling of the magnet coil and implementation of the quench heater in the *Network Model* is shown in Fig. 5.6. The prepared magnet models allowed to simulate any measurement configuration based on quench heaters, namely any of quench heaters installed in magnet could be modeled as the heat source. In the model shown in Fig. 5.6 the power dissipated to the quench heater strip is transferred through the polyimide insulation to the coil, heating the coil cables and provoking the quench of the magnet.

The *Network Model* simulation resulting in the temperature map of the whole simulated system for the given power dissipated to quench heater. From magnet design we obtain the map of temperature margins for a selected operational value of magnet current. The magnet quench current (quench level) was determined by comparing these two temperature maps.

The simulation and measurements were performed on 7 different LHC magnets at temperature of T = 4.5 K: MQM 627, MQM 677, MQM 659, MQY 609, MQY 659, MQ 356 and MB 2624. The results of the numerical simulation and experimental validation are presented in Fig. 6.6 and Fig. 6.8-Fig. 6.13. For all measured magnets the largest difference between measurements and simulations was found to be of the order of 20%, whereas the majority of the differences did not exceed 10 %. For example the difference between the measured and simulated values for three measured magnets from the MQM family is shown in Fig. 6.7. It shows 8 % difference at maximum. The MQM magnet is a special one because it was optimized to operate both superfluid (1.9 K) and

normal fluid (4.5 K) helium temperatures. The main sources of discrepancy between simulation and measurements are the material properties used in simulation. In an ideal case the heat conductivity of materials used in magnet construction should be measured. In the simulation data from the available database was used [80]-[81] and compared with available measured data [82]-[86].

The model validation with precision up to 20 % at a temperature of 4.5 K was regarded as sufficient for the initial quench level knowledge. Further updates of input parameters, especially material properties, and the development of the *Network Model* allowed to significantly increase the precision of the simulation of the LHC magnet types working at 4.5 K as well as 1.9 K.

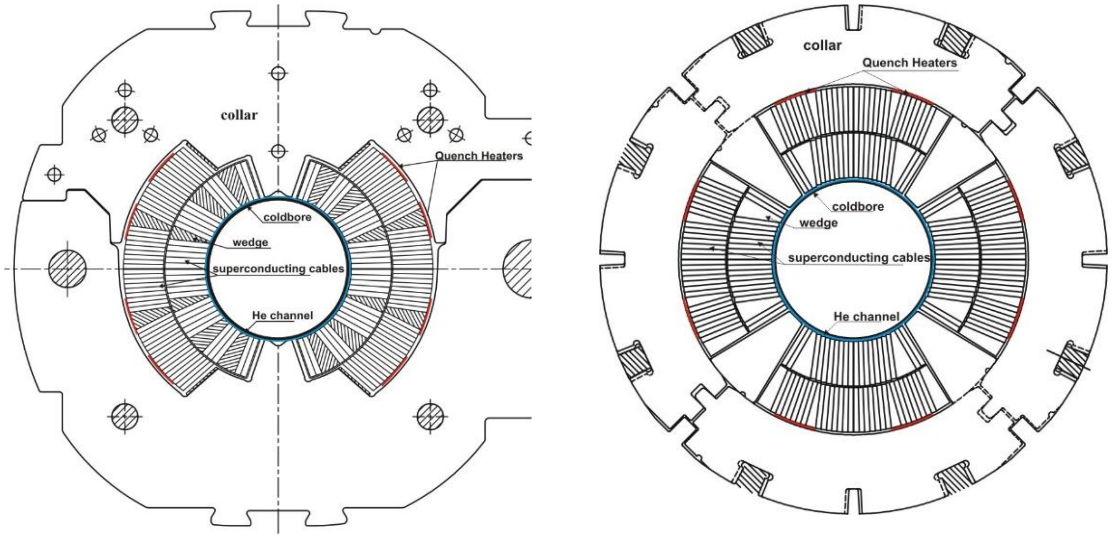

Fig. 6.4 The LHC arc magnets: the main dipole MB (left) and the main quadrupole MQ (right). The red lines on top of coils indicate the position of the quench heaters. MB and MQ coils are immersed in superfluid at T_b=1.9 K.

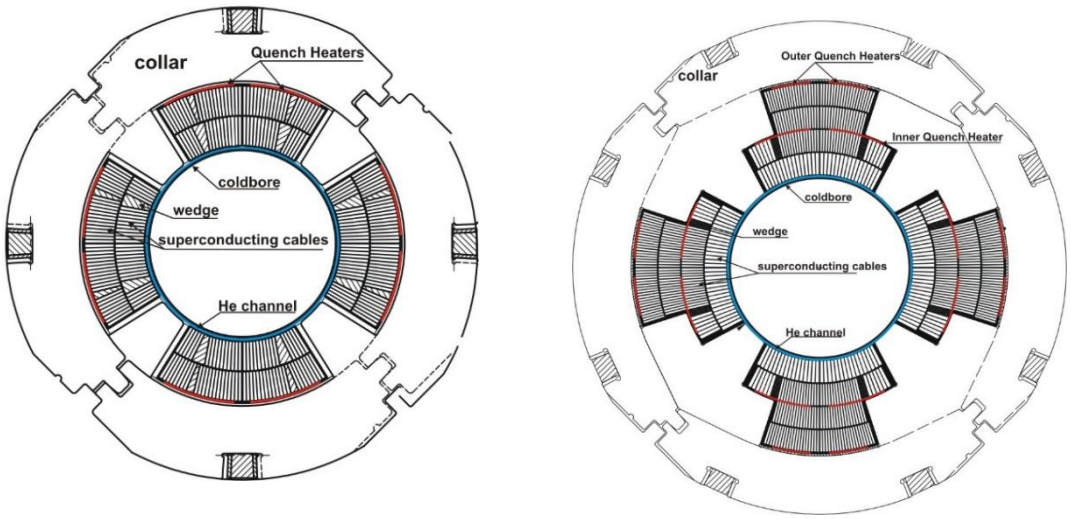

Fig. 6.5 The LHC Long Straight Section quadrupole magnets: MQM (left) and MQY (right). The red lines on top or in the middle of the coils indicate the position of the quench heaters. Selected MQM coils are immersed in superfluid T_b=1.9 K and rest of the MQM and MQY are immersed in normal fluid T_b=4.5 K.

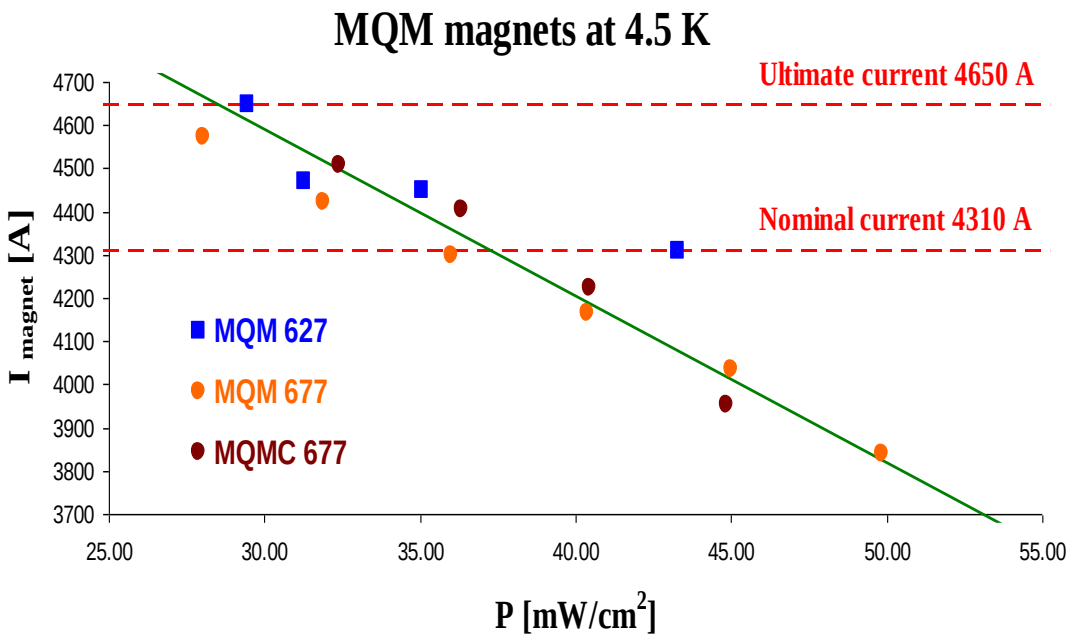

Fig. 6.6 The result of the simulation (solid line) and measurements with quench heater of MQM magnets.

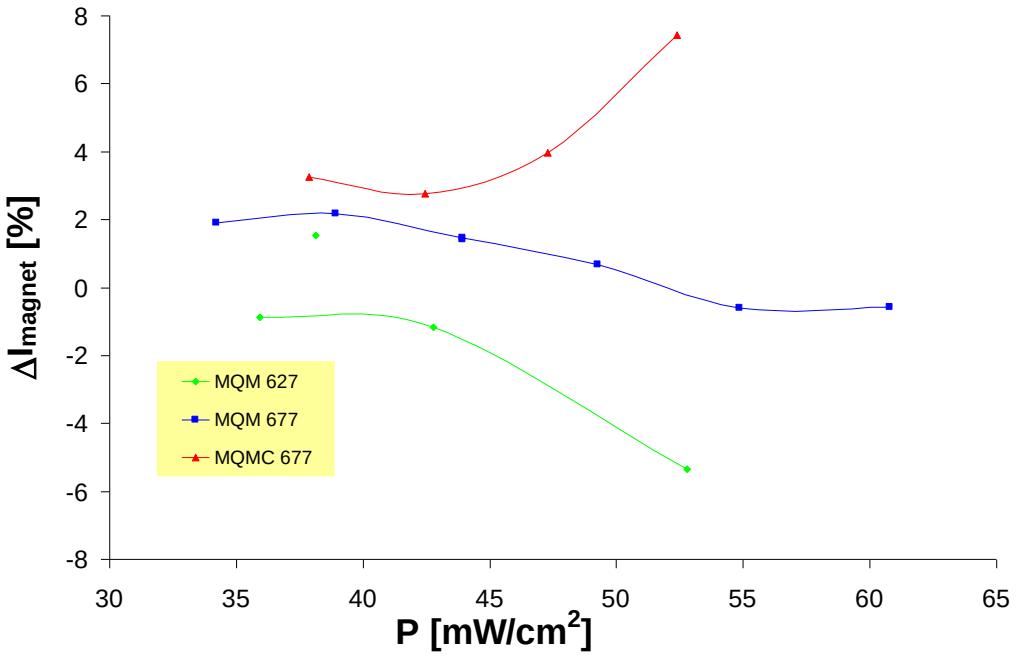

Fig. 6.7 The relative difference between simulations and measurements and for MQM magnets.

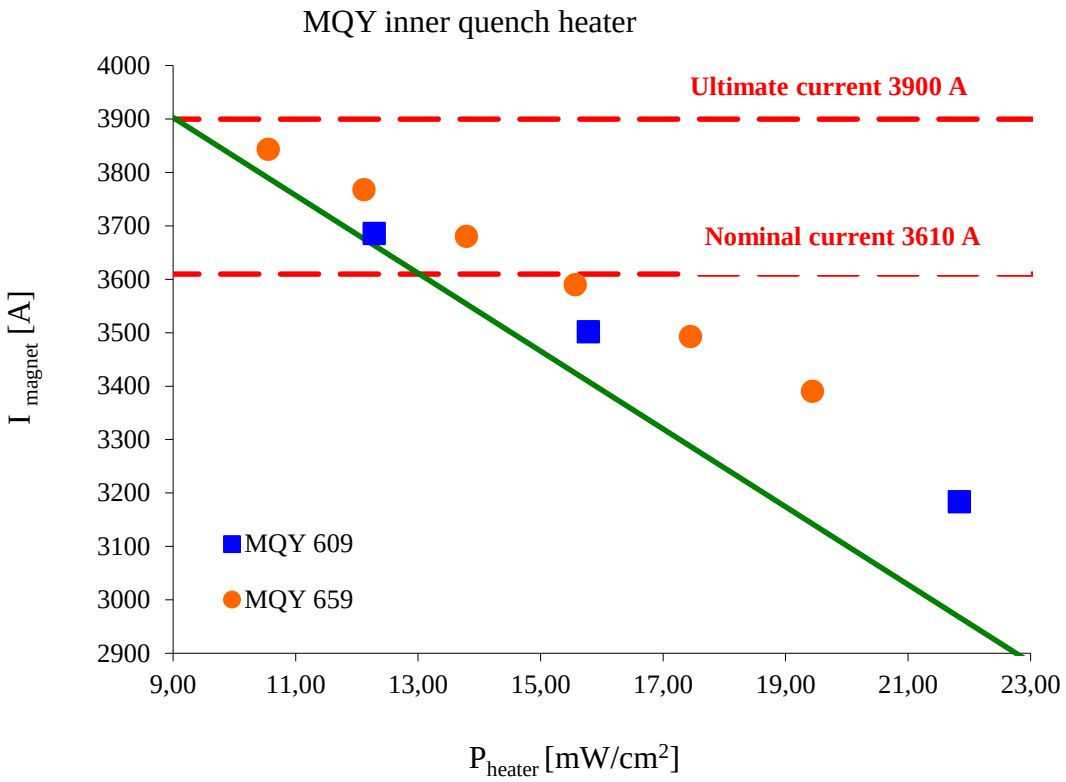

Fig. 6.8 The result of the simulation (solid line) and measurements of the MQY magnet inner heater.

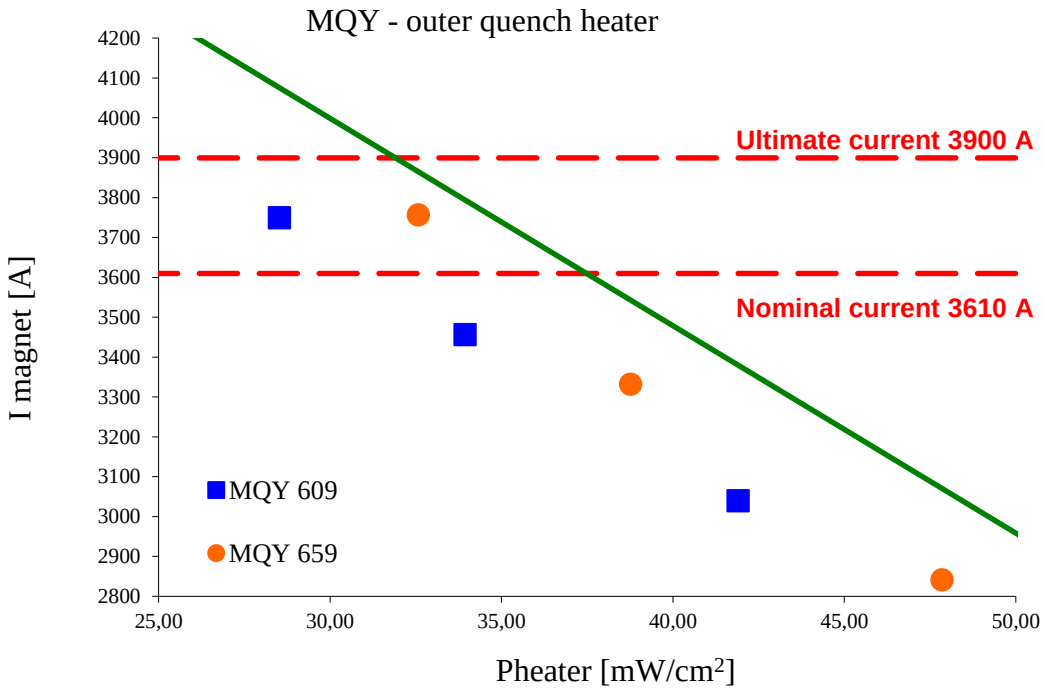

Fig. 6.9 The result of the simulation (solid line) and measurements of the MQY magnet outer heater.

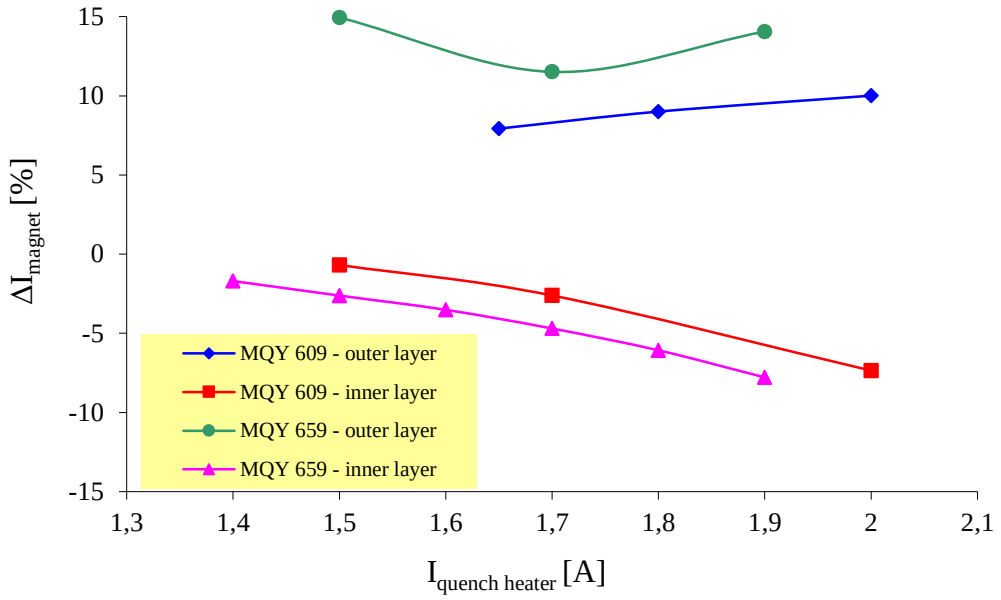

Fig. 6.10 The relative difference between simulations and measurements and for MQY magnets.

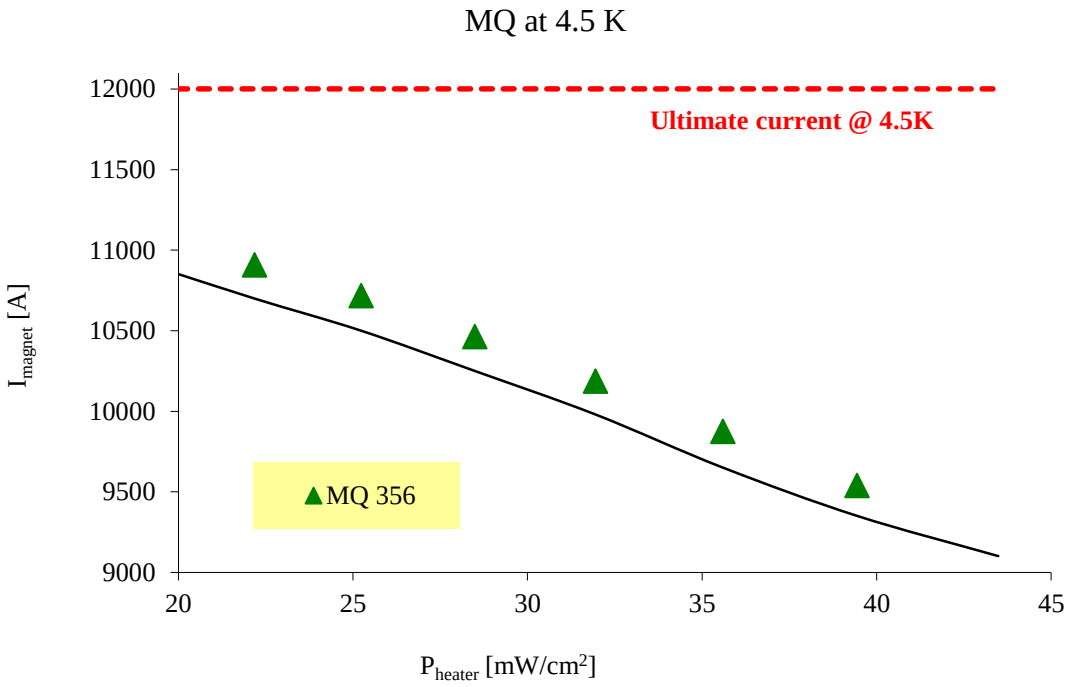

Fig. 6.11 The result of the simulation (solid line) and measurements of the MQ magnet.

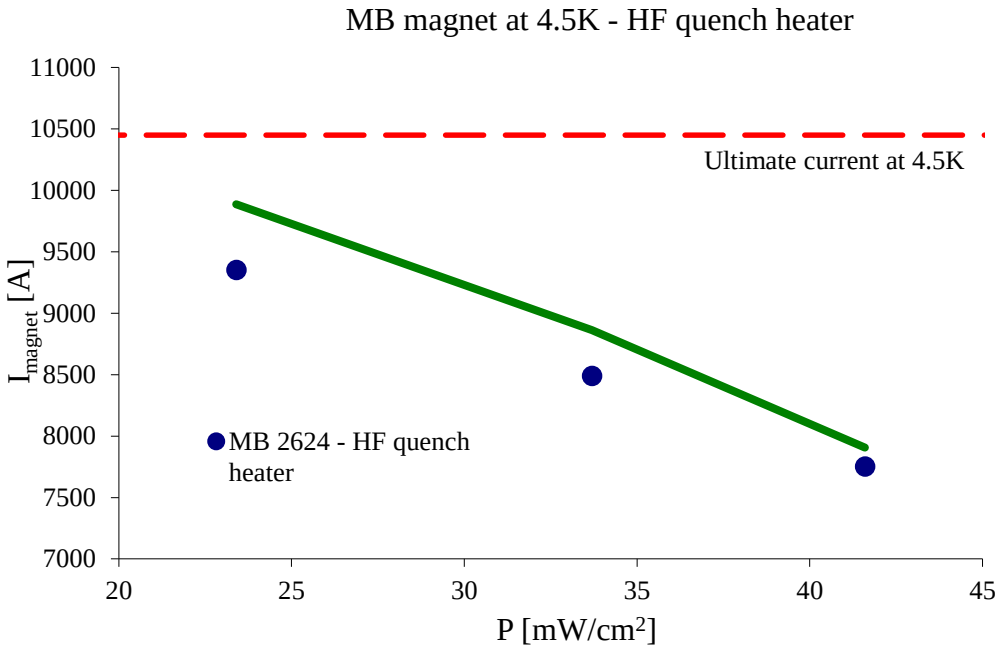

Fig. 6.12 The result of the simulation (solid line) and measurements of the MB magnet HF quench heater.

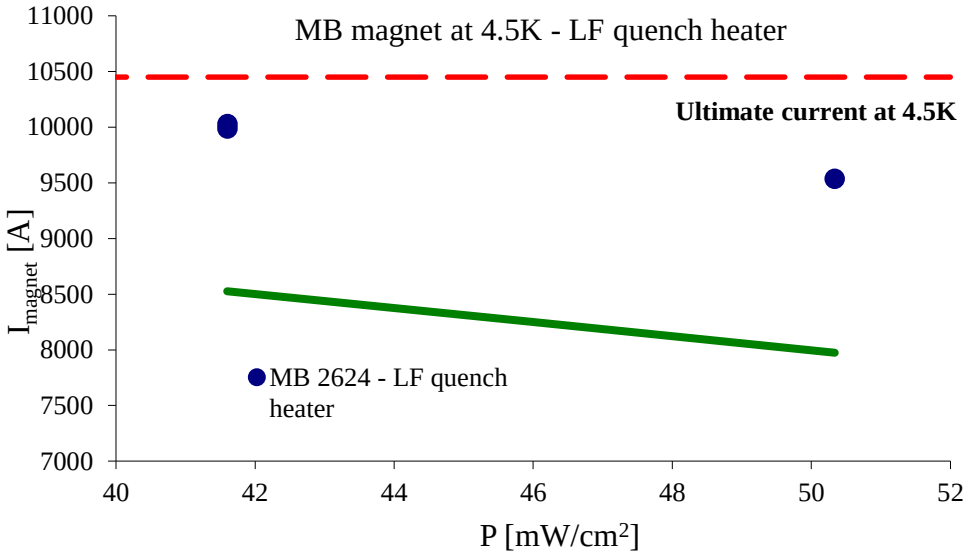

Fig. 6.13 The result of the simulation (solid line) and measurements of the MB magnet LF quench heater.

The proper set of the LHC magnet quench levels increases the operational efficiency of the LHC by setting appropriate initial threshold values for the beam loss monitor system. In 2008 the first results were obtained with the *Network Model*. For this simulation a conservative approach was always applied in the case of material properties since measured values were not available. The simulation with a typical Gaussian beam loss profile calculated with the FLUKA [123]-0 allowed to get first results of the quench level

for the MQM magnets family: 6 mW/cm^3 and 4 mW/cm^3 for nominal and ultimate currents respectively. The corresponding values for the MQY magnets family were 8 mW/cm^3 and 5 mW/cm^3. It has to be noted that these values were obtained for steady-state conditions and not for the real LHC beam pattern.

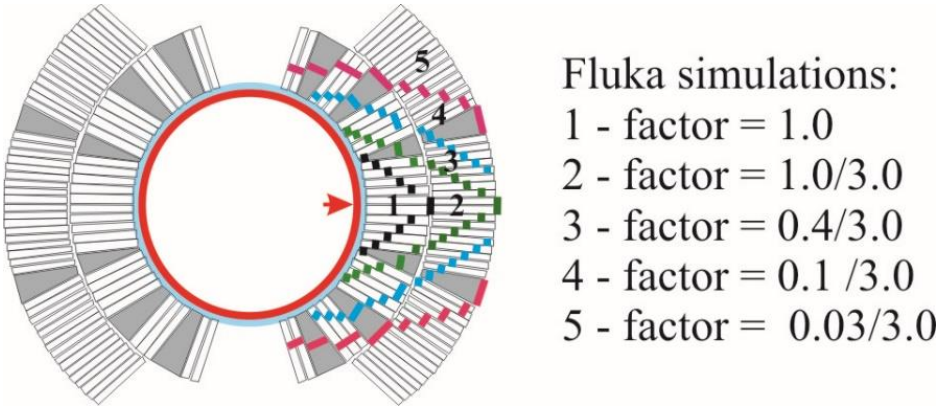

Fig. 6.14 The schematic diagram of the heat deposits in the magnet coil (left) and coefficients of the heat deposits in case of the Gaussian profile calculated by the FLUKA [123]-0 (right). The red arrow indicates impact region of particles lost from the beam [1].

VI.2 The Network Model validation with Internal Heating Apparatus

The successful validation of the *Network Model* with an experimental setup based on magnet quench heaters initiated the work on a more realistic reproduction of accelerator conditions and on designing a tool which would allow to heat the coil from the beam pipe and to validate the model. Some indication of a typical heating scheme was given [95] and its radial energy deposition is depicted in Fig. 6.15.

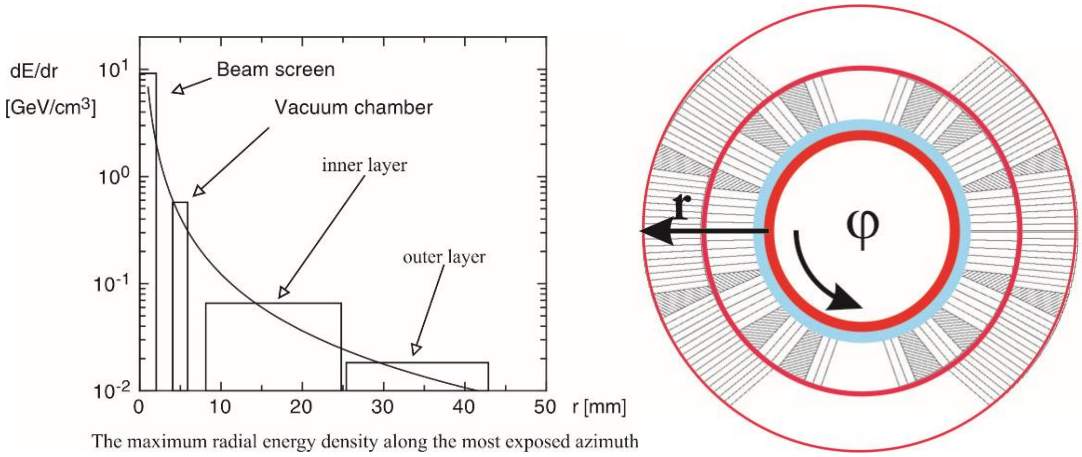

Fig. 6.15 The estimation of radial energy deposition scheme in superconducting magnets [95].

The tool, called the Internal Heating Apparatus (IHA), which allows to heat up the magnet coil from the inside of the cold bore was developed (Fig. 6.16). The IHA was constructed from a 1 m long and 0.5 mm thick stainless steel tube (Fig. 6.16) and the insulated heating strips were glued to this tube (Fig. 6.18). The heating strips installed on the support tube were made of 25 μm thick and 15 mm wide stainless steel and insulated with 100 μm thick polyimide film. Inside the support tube the expanding cone system was installed to press the heaters to the cold bore and to assure good thermal contact. Along the tube, the 3 mm gap was left in order to assure the flexibility of the support during the installation and during cone expansion. The four heating strips were installed on the support tube. Each strip was equipped with four wires to allow the precise measurements of the voltages and it was powered independently with one DC power supply. The temperature of the IHA was measured by two PT100 temperature probes installed in the middle and at the end of the support tube. The experimental setup consisting of IHA and DC power supplies allowed to generate the heat which was transferred throughout the heating strip insulation, the cold bore tube, the cold bore tube insulation and finally the helium channel around the cold bore to the magnet coil. The red lines in Fig. 6.19 and Fig. 6.20 show the position of heating strips. Also the positions of the temperature sensors are indicated. The heating strips are located under the high field region of the magnet which is located at the coil extremities as well as in the middle of the coil under the low field region. The experimental setup with the IHA allows to provoke magnet quenches in a large range of coil currents from few hundred amperes up to an ultimate magnet current (for example $I_{ultimate}$=12850 A for main dipole). Fig. 6.18 shows photos of the Internal Heating Apparatus and its installation inside the magnet.

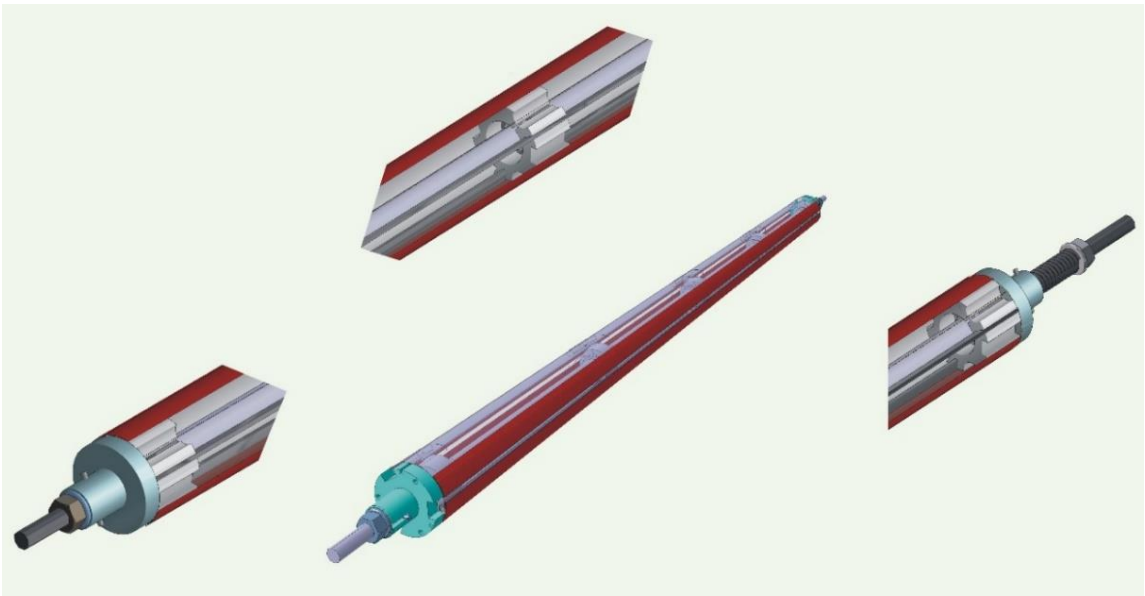

Fig. 6.16 View of Inner Heating Apparatus – CATIA model

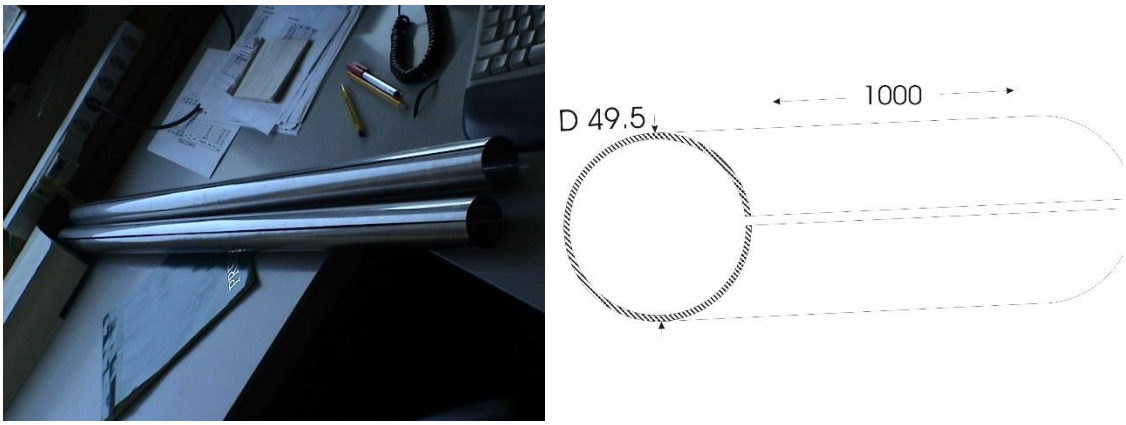

Fig. 6.17 The stainless steel support tube of the Internal Heating Apparatus

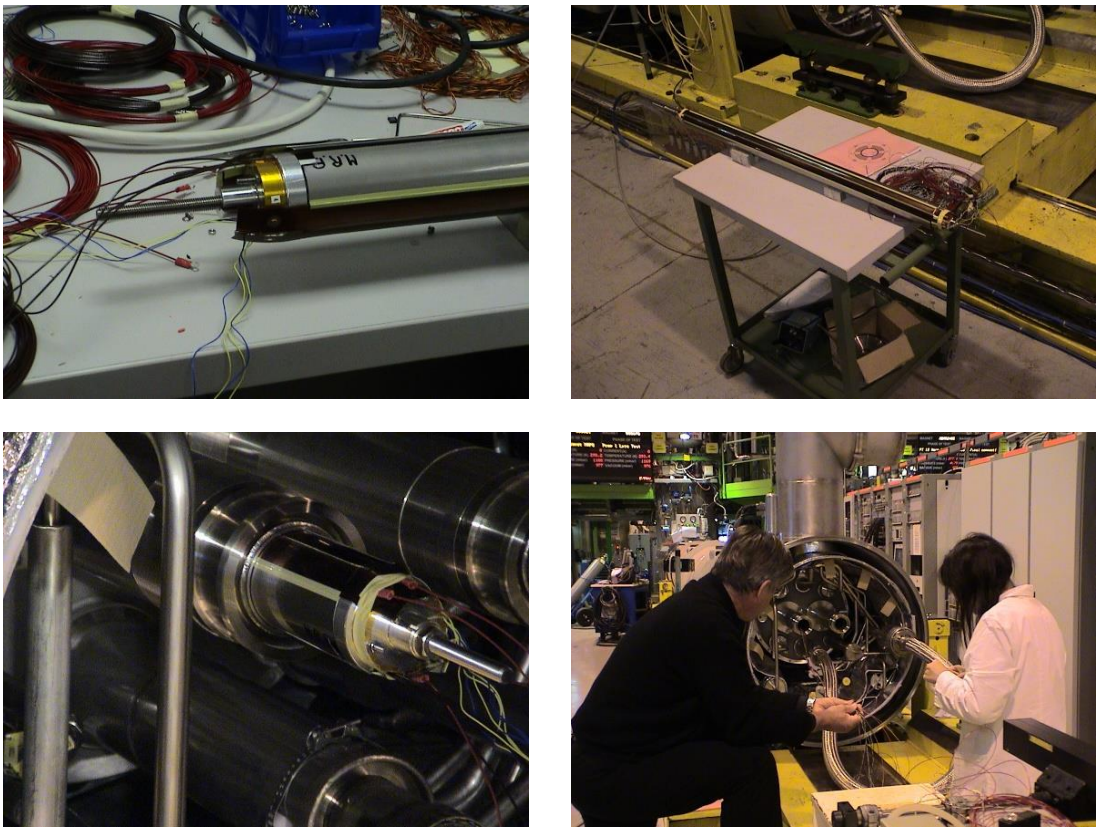

Fig. 6.18 Internal Heating Apparatus and its installation inside the magnet cold bore.

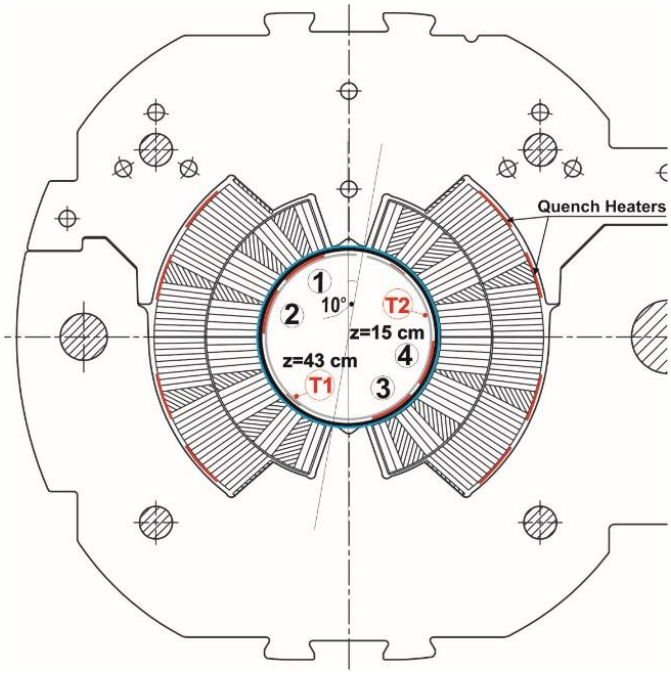

Fig. 6.19 The cross section of the main dipole magnet equipped with IHA. The heating strip and temperature probe azimuthal positions are shown.

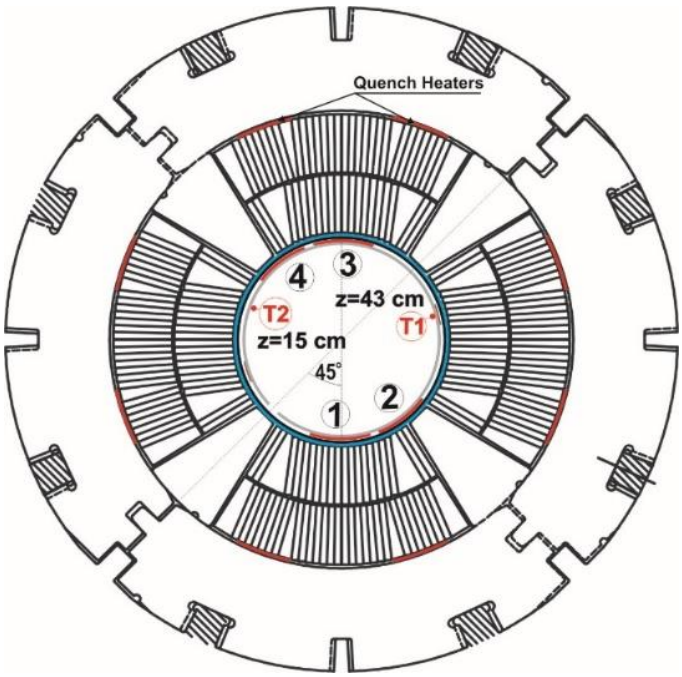

Fig. 6.20 The cross section of the main focusing quadrupole magnet equipped with IHA. The heating strip and temperature probe azimuthal positions are shown.

The *Network Models* of the LHC magnets prepared previously for simulations with the quench heater as a heat source were updated by adding the IHA as a heat source and used for quench simulations. The numerical simulation and comparison with the measured values obtained for the main dipole MB and lattice quadrupole MQ magnets are shown in Fig. 6.21 and Fig. 6.22 thus relative difference is showed in Fig. 6.23. The largest difference between measurements and simulations was found to be 70 % for the MB magnet's very low current (~2000 A), whereas the majority of the differences did not exceed 40 %. The discrepancy of the simulated and measured results originate from critical current parametrization which is non-linear and not optimized for a low current, yet. At a high current the difference is of order of 10 %.

The simulation with typical Gaussian beam loss profile calculated with the FLUKA [123]-0, depicted in Fig. 6.14 and radially homogeneous distribution [95] (Fig. 6.15) provides for main dipole MB 17 mW/cm^3 and 12 mW/cm^3 respectively and for MQ lattice quadrupole magnets are 23 mW/cm^3 and 17 mW/cm^3 respectively. The knowledge of the estimation of conservative quench levels of the main magnets will allow setting appropriate initial threshold values for the beam loss monitor system.

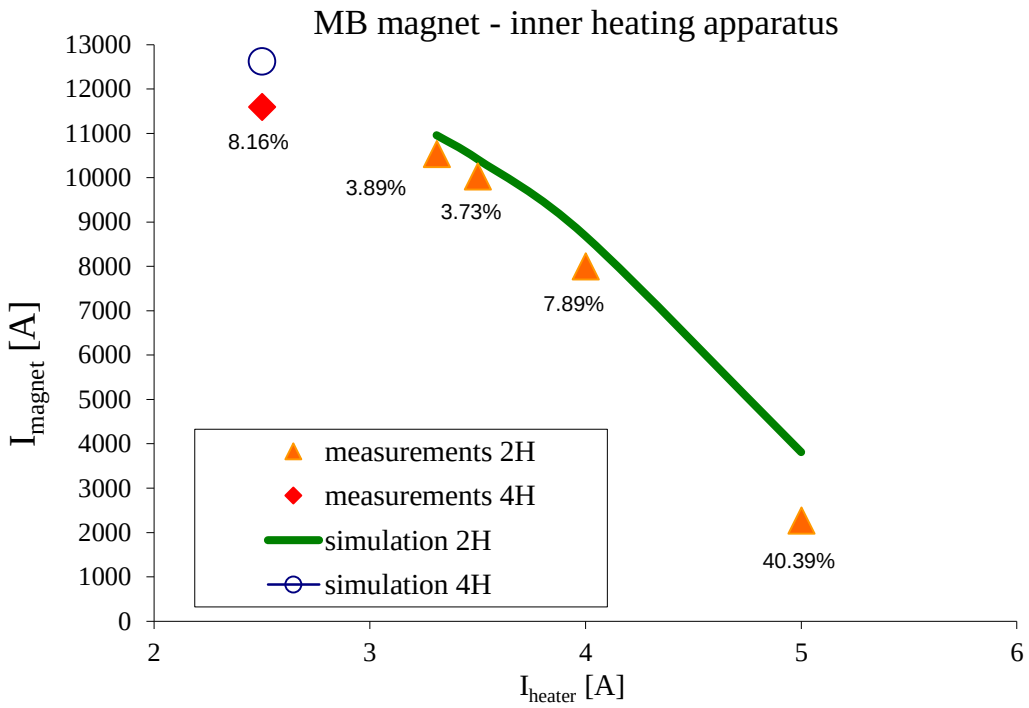

Fig. 6.21 The results of the simulation (solid line) and measurements (markers) for the MB magnet at 1.9 K. The power dissipated in the heating strips is shown on x-axis and corresponding magnet quench current is depicted on y-axis. The relative difference between simulated and measured values is shown in the figure.

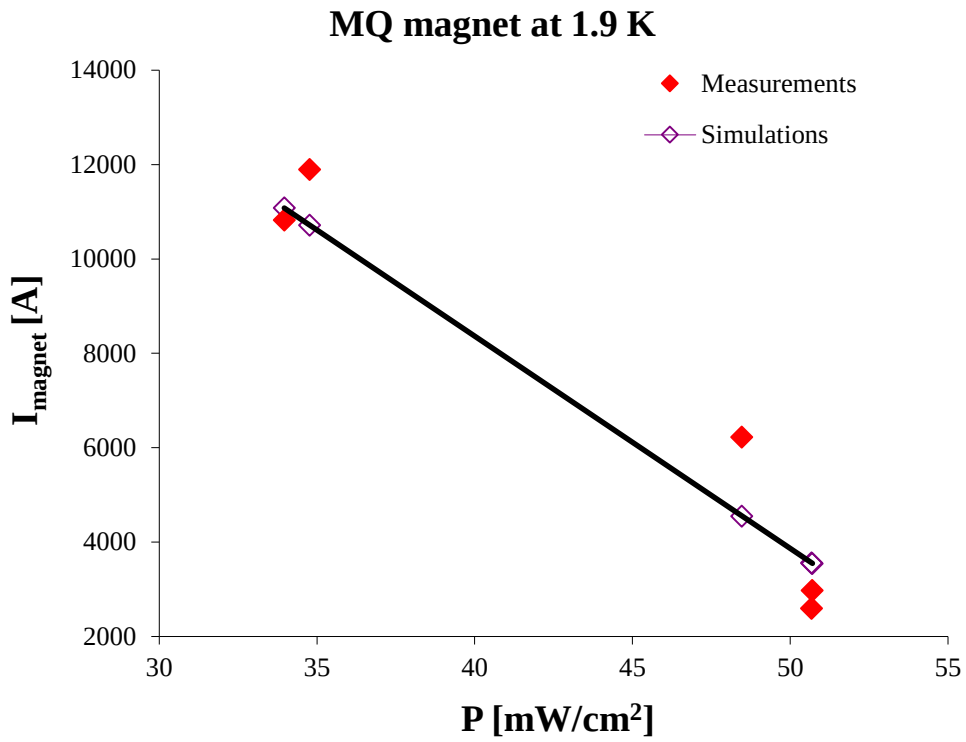

Fig. 6.22 The results of the simulation (solid line) and measurements (markers) of the MQ magnet at 1.9 K. The power dissipated in the heating strips is shown on x-axis and corresponding magnet quench current is depicted on y-axis.

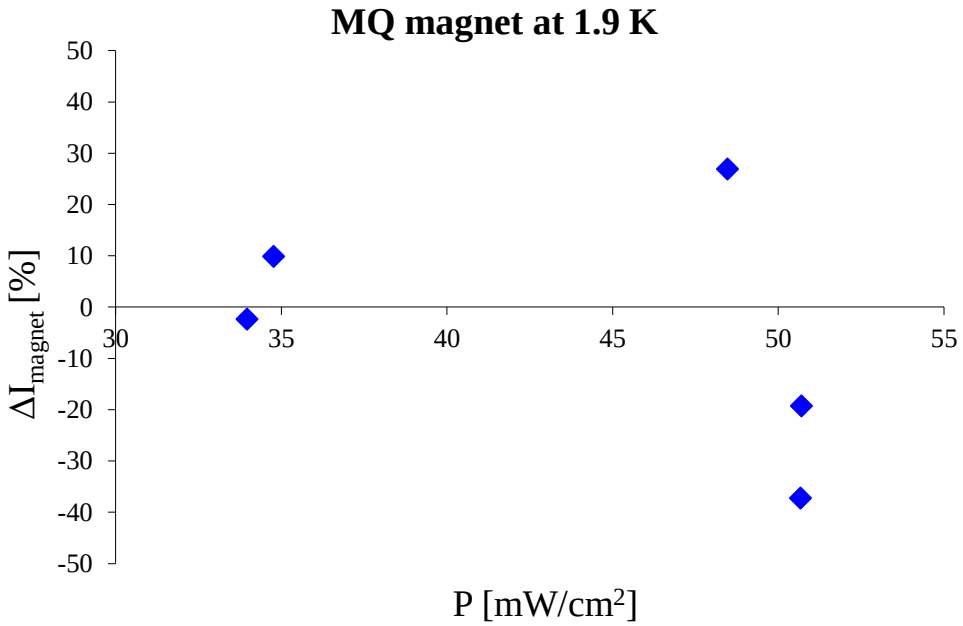

Fig. 6.23 The relative difference between simulations and measurements for MQ magnets.The power dissipated in the quench heaters is shown on x-axis and relative difference between measurements and simulations is depicted on y-axis.

Chapter VII
Network Model Implementation

The implementation of the *Network Model* to the study of the superconducting magnets thermal behavior requires a uniform modeling method. The assumptions for steady-state modeling are:

- the steady-state conditions reached in the magnet coils cables means that after heating with a heat source with a constant heat flux the temperature inside the cable does not change with time;
- the superconducting cables in the magnet coil are much longer than the length of the *Network Model* element so there is no heat transfer along the cable, which means no temperature gradient along the cable;
- the thermal conductivity of the cable is much greater than the thermal conductivity of electrical insulation. This assures us that cable at steady state is at uniform temperature;
- since the thermal conductivities change with temperatures, the recurrent procedure to establish the proper conductivity for the simulated element has to be implemented.

The main heat flow barrier in the superconducting magnets are cable and coil electrical insulations: polyimide and fiberglass laminates. The thermal conductivities from [80] were selected as basic ones for calculating the thermal resistances of each *Network Model* element. The data used for insulating materials is presented in Fig. 7.1.

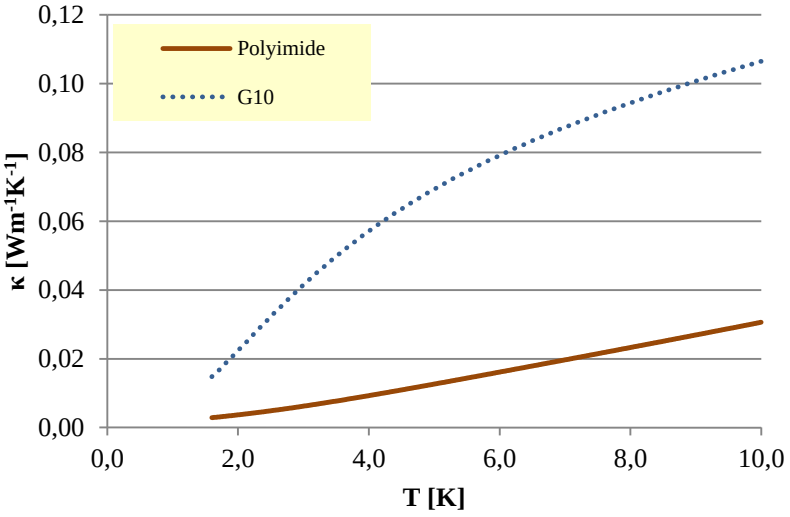

Fig. 7.1 The thermal conductivity of electrical insulation materials Polyimide and G10 [80] used in simulations of superconducting magnets.

VII.1 Enhanced Superconducting Cable Insulation

The main challenge during designing the accelerator superconducting magnets, which typically operate in a high radiation environment, is to develop the effective heat extraction paths from magnet coils to the heat reservoir. The insulation scheme used for the cables used to wind the coils of the magnets installed in the LHC (see: Appendix 2) is impermeable for helium and almost seals the superconducting cables. Thus the heat conduction of polyimide insulation determine the heat transfer from the cable to the helium bath. However some of the measurements of the heat transfer of the LHC cables insulation [98] suggesting existence of tiny channels, mainly due to the insulation imperfections, which may provide a link between the strands and the helium bath and which can increase the heat transfer through polyimide insulation.

Further investigations resulted in the proposition of a new insulation scheme for the Nb-Ti superconducting cables [99]-[100] to be used in magnets for the upgrade of the LHC. The proposed insulation scheme introducing the network of micro-channels inside the superconducting cables electrical insulation. These channels are occupied by liquid helium and provide a direct link between the strands and the helium bath. The two enhanced insulation schemes were proposed (Fig. 7.2). The schemes differences are the winding scheme of the 2nd insulation layer and the thickness of the 1st and 3rd insulation layer. The details of both enhanced insulation schemes, including the wrap angles, are summarized in Table 7. 1 and Table 7.2. The wrap angles define the length of the channels inside the insulation. From the electrical point of view the longer helium paths are positive since they mean a longer path for a potential electrical arc. From a thermal point of view the longer channels decrease heat transfer, especially for superfluid helium where the heat transfer is a function of channel length (see: Eq. 5.1).

The enhanced insulation schemes are challenging for modeling with the *Network Model* because they require a 3-dimensional heat flow model. The complexity of the helium paths in the enhanced cable insulation is showed in Fig. 7.3. The basic sample length corresponds to the LHC cable 01 transposition pitch of 115 mm. The analytic view of the heat transfer paths in the enhanced cable insulation is presented in Fig. 7.4 and its *Network Model* implementation is depicted in Fig. 7.5. The 3-dimensional model considers two main components: heat transfer perpendicular and parallel to the cable (Fig. 7.6) and the *Network Model* implementation of EI#1, showed in Fig. 7.7.

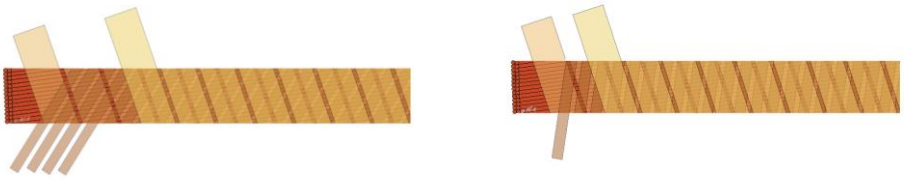

Fig. 7.2 The enhanced insulation scheme EI#1 (left) and EI#4 proposed in [99]-[100] scaled from real cable dimensions (LHC cable 01).

Table 7. 1 The parameters of enhanced insulation scheme EI#1 proposed in [99]

layer	layer 1	layer 2	layer 3
material	polyimide (Kapton, Apical)	polyimide (Kapton, Apical)	polyimide with adhesive coating (Kapton, Apical)
thickness	***25.4*** *μm*	***75*** *μm*	***55*** *μm thick,*
width	***9*** *mm*	***4 x 2.5*** *mm*	***9*** *mm*
gap between wrappings	***1*** *mm*	***4 x 1.5*** *mm*	***1*** *mm*
wrapping		cross wrapped with 1st and 3rd layers	50% overlap with 1st layer
wrap angle	α_1 ***=71.68 deg***	α_2 ***=62.16 deg***	α_3 ***=71.90 deg***

Table 7.2 The parameters of enhanced insulation scheme EI#4 proposed in [100] and used in MQXC prototype magnet.

layer	layer 1	layer 2	layer 3
material	polyimide (Kapton, Apical)	polyimide (Kapton, Apical)	polyimide with adhesive coating (Kapton, Apical)
thickness	***50*** *μm*	***75*** *μm*	***69*** *μm thick,*
width	***9*** *mm*	***3*** *mm*	***9*** *mm*
gap between wrappings	***1*** *mm*	***1.5*** *mm*	***1*** *mm*
wrapping		cross wrapped with 1st and 3rd layers	50% overlap with 1st layer
wrap angle	α_1 ***=71.68 deg***	α_2 ***=81.6 deg***	α_3 ***=72.00 deg***

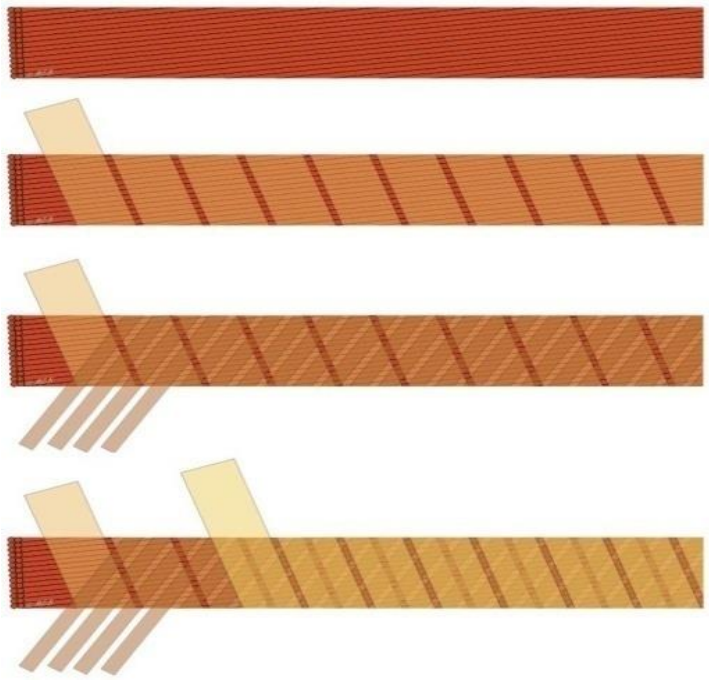

Fig. 7.3 The sketch of enhanced insulation EI#1. The channel system in each insulation layer is showed. The presented sample length correspond to the transposition pitch of the LHC cable1 of 115 mm.

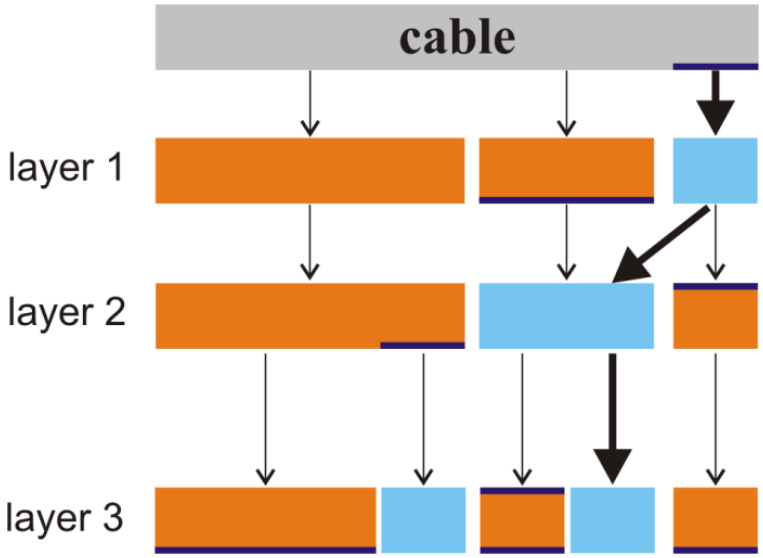

Fig. 7.4 The analytic view of heat transfer paths in enhanced insulation. Light (blue) elements represent helium channels, dark (brown) show insulation and dark (blue) lines depict the Kapitza resistance. The bold arrows in the sketch show the dominating heat transfer path. The heat flow scheme is: helium in 1st insulation layer, next heat flows along the cable with use of helium in 2nd insulation layer and finally the helium in 3rd insulation layer is connected with helium bath.

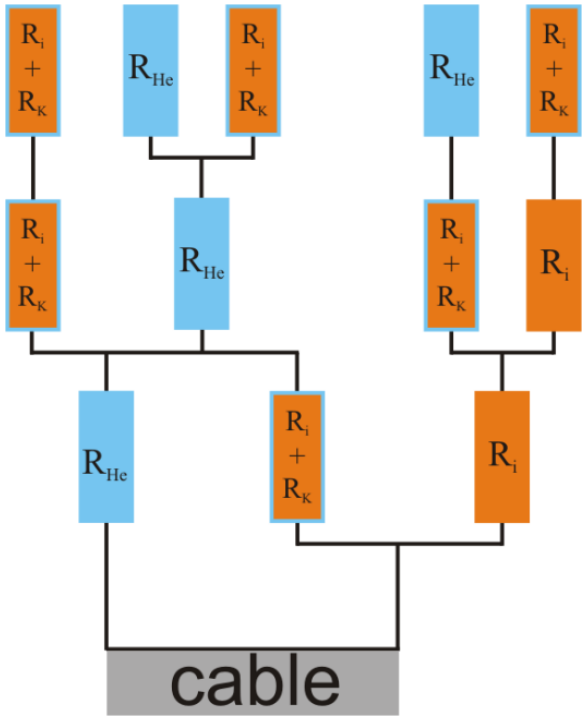

Fig. 7.5 The *Network Model* implementation of the schematic view of heat extraction paths in enhanced insulation. The thermal resistance of insulation is R_i, the Kapitza resistance - R_K, helium - R_{He}.

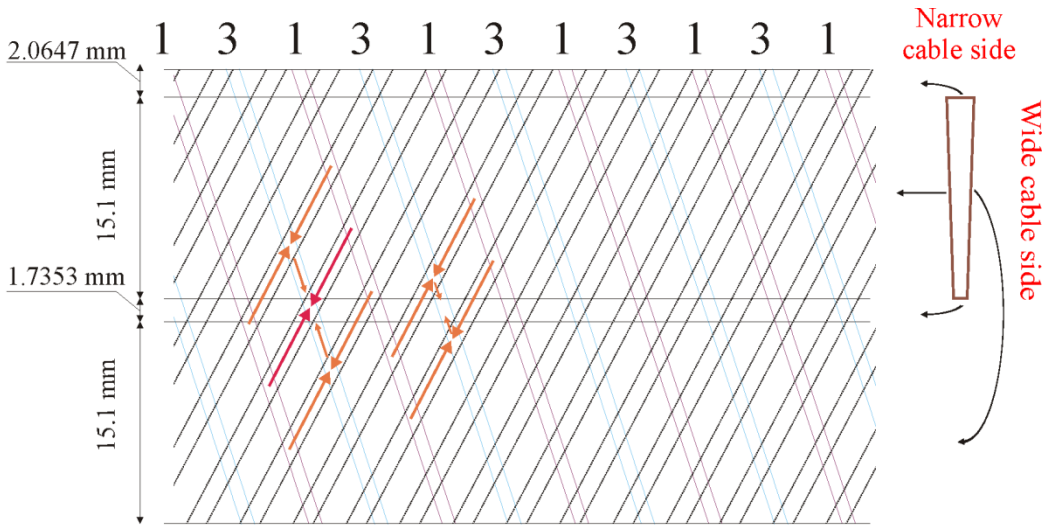

Fig. 7.6 A schematic view of helium path network for EI#1. The numbers 1 and 3 indicates the helium channels in insulation layer 1 and layer 3. The arrows indicate the heat extraction areas i.e. the areas that helium from the cable has direct contact with helium bath.

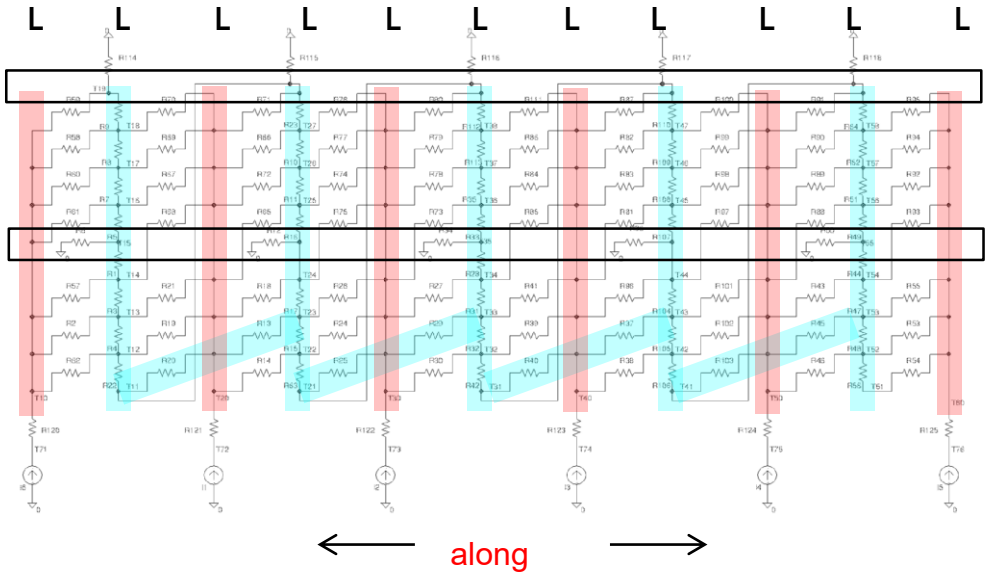

Fig. 7.7 The *Network Model* of helium channels in EI#1. The 3-dimensional problem is converted to 2-dimensional map. The light blue lines show helium channels.

A schematic view of the helium channels in the enhanced insulation EI#1 shown in Fig. 7.6 was used to build the EI #1 *Network Model* and the result is depicted in Fig. 7.7. In the experimental setup with a stack of cables [130], the heat from the cable is evacuated mainly through helium channels and at the end by the narrow sides of the cables, which are in contact with the helium bath (see: Fig. 7.8) [8]. The prepared *Network Model* was used for numerical simulation of the experimental setup described in [130] and to validate the simulation results with measurements.

The experimental setup described in [130] was built from the six dummy cables of 150 mm active part long and made of 28 resistive $CuNi_{10\ wt.\%}$ strands. The geometry of the cables was chosen to be the same as the LHC cable 01. The cables were insulated according to the EI#1 scheme (Fig. 7.3). The cables were superimposed alternatively with the thick or the thin edge to one side to form a rectangular stack. The sample was cured according to the standard bonding cycle of the LHC main superconducting magnets, consisting of a pressure cycle up to 80 MPa at a temperature of 190 °C. The measurements were performed under a pressure of 30 MPa, applied on the wide side of the cables. Fig. 7.8 show a schematically cross-section of the experimental setup described in [130]. The thermal conductivity of $CuNi_{10wt.\%}$ is shown in Fig. 7.9 and other parameters were taken from [80].

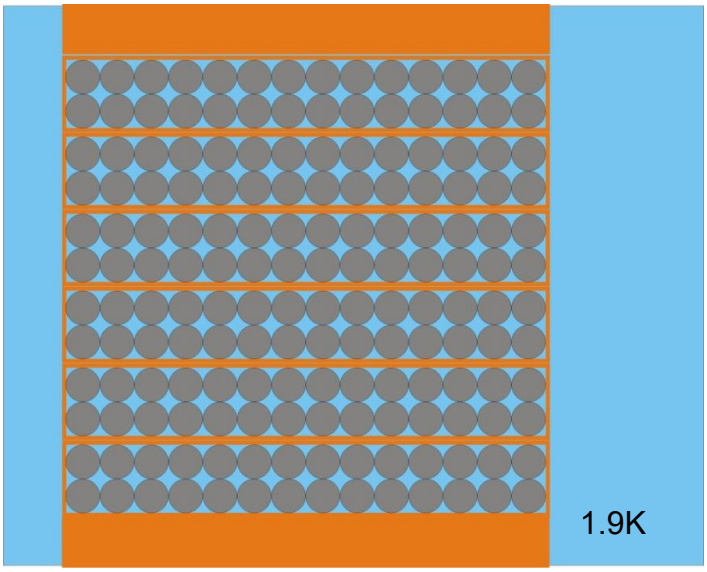

Fig. 7.8 A cross-section of experimental setup described in [130] implemented in the *Network Model*.

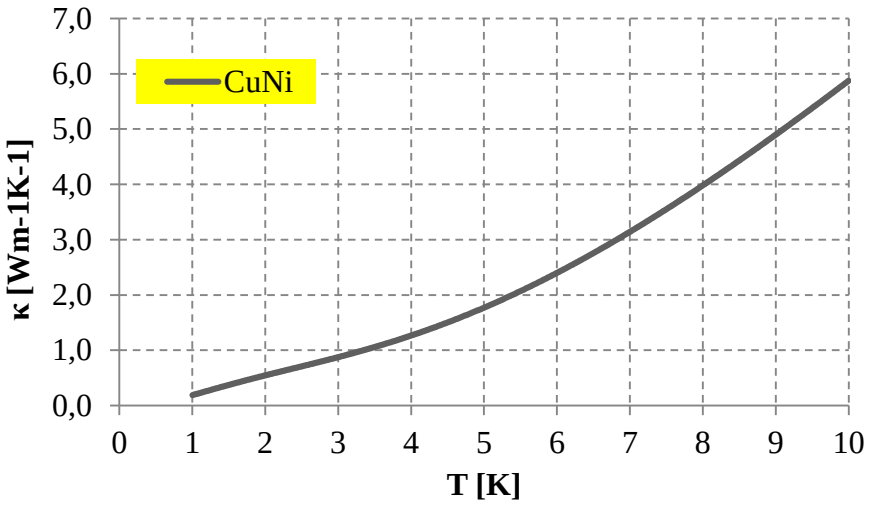

Fig. 7.9 The thermal conductivity of $CuNi_{10wt.\%}$

The initial numerical simulation of the EI#1 was performed with a model build by taking into consideration only the helium channels, i.e. neglecting the heat transfer through the solid insulation part. The contribution of the heat transfer through the solid parts ranges between 1 % for low heat fluxes up to 15 % for fluxes of order of 1 W/m (Fig. 7.13). For the superfluid helium part the Kapitza resistance [86] is the limiting factor for the heat transfer from the solid material to the superfluid helium. The measured values of the Kapitza coefficient (σ_K) range from ~550 to ~1200 $Wm^{-2}K^4$ [86]-[90]. The impact of the Kapitza resistance was studied and dedicated simulations were performed for three different values of the Kapitza coefficient, namely σ_K = 550, 900 and 1200 $Wm^{-2}K^4$ (Fig. 7.10-Fig. 7.12). A vital parameter of the Kapitza resistance calculation is the contact surface between the material and helium. The cable surface is not flat but it is determined by the structure of the cables which are built from the strands. Thus the real cable contact surface with helium is larger than the surface calculated from cable geometry. The most conservative approach is implemented when the strands are not deformed and they have an ideal cylindrical shape. That is why, in the simulation the contact surface calculated from the cable dimensions was increased by 50 % and it is noted as 150 % S in Fig. 7.10-Fig. 7.12. This analysis show a small impact of the contact surface on the final numerical calculation results. In summary the Kapitza resistance is relatively small with respect to the thermal resistance of the helium channels, and a dominant contribution to the heat transfer through helium coming from the thermal resistance of the helium channel in the second layer of the insulation. Subsequently, the model was improved by including the heat transfer path through the solid part of the cable insulation. The comparison of Fig. 7.11 and Fig. 7.12 shows that solid part contribution is not negligible for high heat fluxes and including this part in the model gives a very good agreement between simulation and measurements up to $\Delta T < 0.2$ K, what can be seen in Fig. 7.12.

The results of numerical simulations with *Network Model* for nominal helium channels dimensions calculated from the Enhanced Insulation specification showed disagreement with the measurement data presented in [130]. These comparison of the results is presented in Fig. 7.10. After a careful cross-check of all of the model parameters and a series of basic checks of the model itself, the idea of reducing the helium channels dimensions due to applied pressure was investigated. Indeed, a very good agreement with experimental results over the helium temperature increase range of $\Delta T < 0.05$ K (T_{bath}=1.9 K) was obtained by reducing the effective helium channels cross-section in the second layer of insulation (L2) by 5 0% (Fig. 7.11-Fig. 7.12). It worth mentioning here that the reduction of the effective helium channel cross-section is the only free parameter implemented in the *Network Model*. Further analysis and investigations showed that the reduction of the helium channel cross-section can be considered as a combination of several effects. The leading effect which may cause the helium channels cross-section decrease is the pressure applied to the measured sample. Other possible effects, which may contribute to the reduction of the helium channels cross-section are: the plastic deformation due to the local peak stress; the plastic deformation during curing, and the possible creep of insulation.

The results obtained from the *Network Model* simulations were so interesting that they triggered the ANSYS simulations of possibly reducing of the sizes of channels in the Enhanced Insulation due to applied pressure. These numerical simulations confirmed that applied pressure reduces helium channel cross-section significantly [9]. The *Network Model* simulation of the EI#1 suggest that the helium channels may have a reduced cross-section in operational conditions and a further study of this insulation scheme is needed. Still, the Enhanced Insulation provides a significantly better heat evacuation from the cable. But, better heat evacuation means that the protection of the magnet with quench heaters is much more difficult since more power is needed to dissipate in the quench heater strips to protect the magnet during quench. This means that new solutions for magnet protection are needed as for example CLIQ [129].

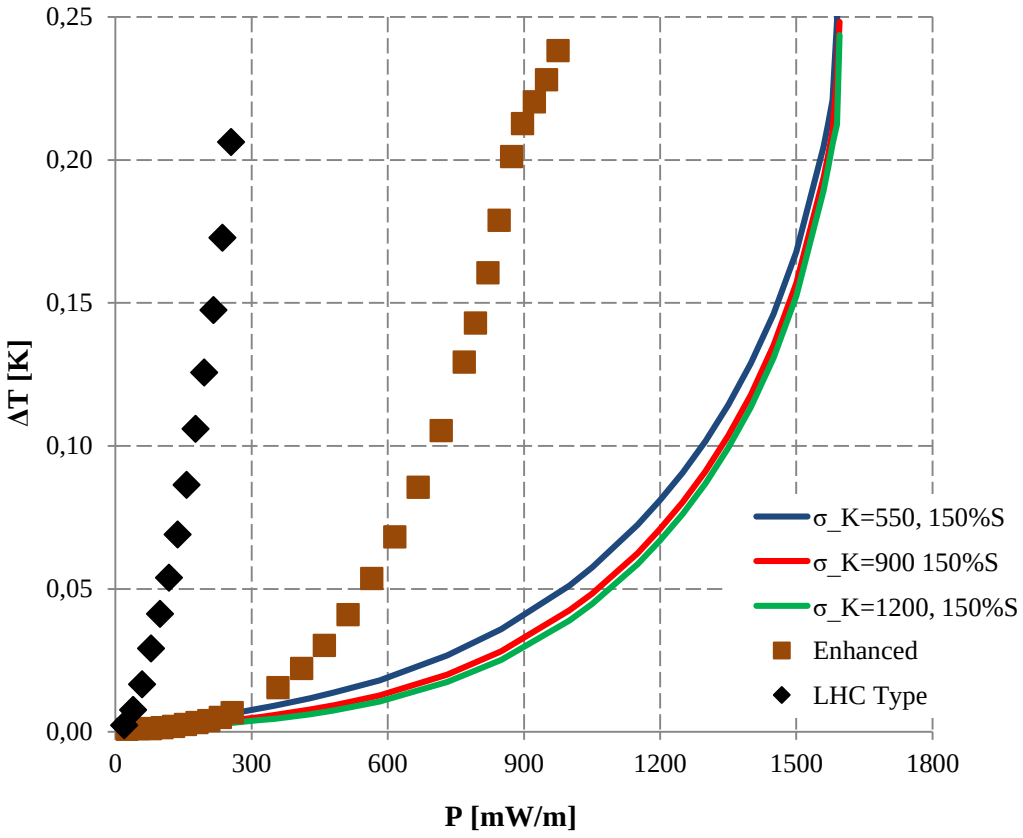

Fig. 7.10 Numerical calculation of heat flow in EI#1 with *Network Model* for heat transfer through helium only assuming that the helium channels are 100% open (nominal helium channels cross-section) and its comparison with experimental data published in [130]. The simulations were performed for three values of Kapitza coefficient and for contact surface equal 150 % of surface calculated from cable dimensions (150 % S).

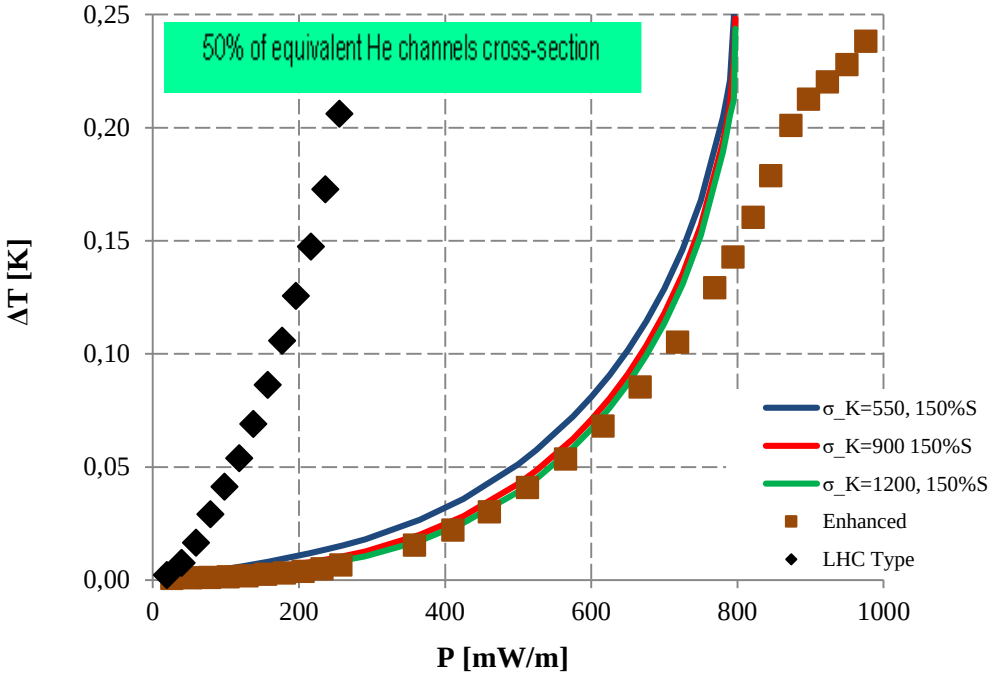

Fig. 7.11 Numerical calculation of heat flow in EI#1 with *Network Model* for heat transfer through helium only assuming that the helium channels in insulation layer 2 are 50 % open (reduced helium channels cross-section) and its comparison with experimental data published in [130]. The simulations were performed for three values of Kapitza coefficient and for contact surface equal 150% of surface calculated from cable dimensions (150 % S).

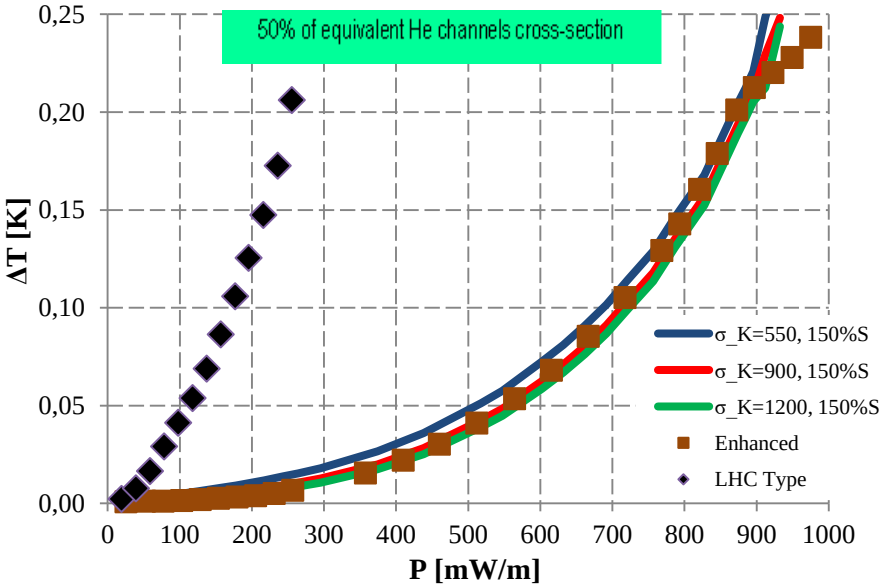

Fig. 7.12 The *Network Model* simulation results and its comparison with experimental data published in [130]. The simulations were performed for three values of Kapitza coefficient and for contact surface equal 150 % of surface calculated from cable dimensions (150 % S). In this figure both heat extraction through helium channels with 50% channel cross-section opening in insulation layer 2 and through insulation implemented in model is shown. This plot shows that there is a not negligible contribution to the heat extraction from heat transfer through insulation, and that when both mechanisms are taken into account there is a very good agreement between simulations and measurements.

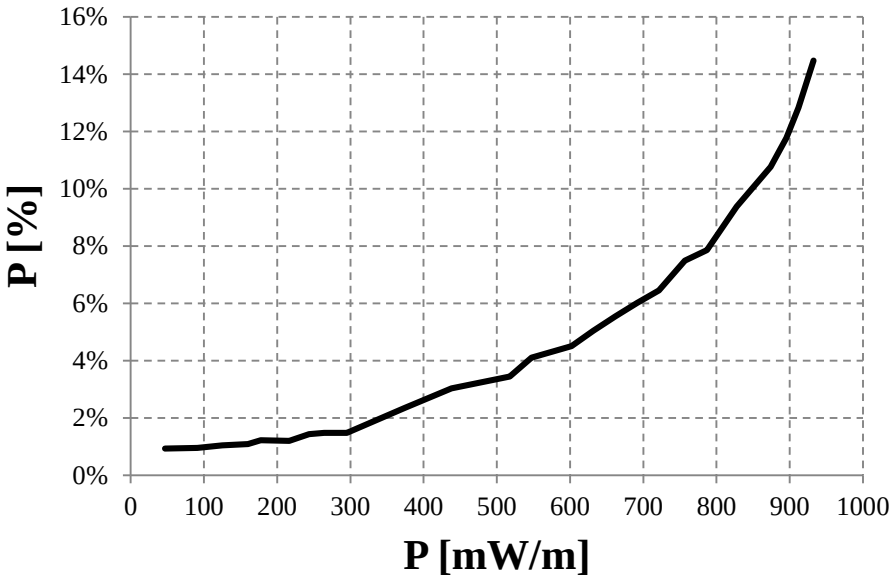

Fig. 7.13 The *Network Model* simulation result of heat extraction through the only solid part of cable insulation. The contribution to the heat extraction through the electrical insulation path increases from ~1 % for 0.1 W/m up to 15 % for 1 W/m.

VII.2 Nb_3Sn Technological Quadrupole magnets

The Nb_3Sn superconducting magnets were selected to be developed for the LHC luminosity upgrade. The USA LHC Accelerator Research Program (US LARP) was involved in the development of Nb_3Sn technology for accelerator magnets. This was a complex program, which included basic studies on superconducting strands and thermo-mechanical behaviors of the coil (for example [14] and [15]) as well as thermal optimization of superconducting magnets [13]. The Nb_3Sn coils production process is different compared to Nb-Ti based, currently used in the LHC. Since Nb_3Sn is a brittle material and requires a long-duration reaction process at high temperatures (up to ~700°C), the coil is winded from strand precursors, reacted over 7 days [14] and then impregnated to increase its stiffness. This coil production process means that there is no helium inside the cable and the whole coil cooling process must be done by heat transfer to the helium around the coil.

The *Network Model* of the Nb_3Sn magnet was prepared in order to optimize the heat transfer in developed magnets, especially to study inner coil insulation thickness. At first the *Network Model* of the so-called Technological Quadrupole (TQC02b) was prepared to compare the results from the numerical simulation and the data from measurements collected in Fermilab and presented in [131]. The *Network Model* of TQC02b was developed on base of the TQ magnet scheme showed in

Fig. 7.15. The main issue with this model was the heat conductivity of the epoxy-impregnated S-2 glass insulation. The thermal conductivity was approximated by the properties of the G10 fiberglass composite and data from [80] were used. The heat

reservoir was placed on the inner coil surface and the outer yoke surface because both are in direct contact with liquid helium. The contribution from the thermal contact resistance between different materials and between the coil insulation and liquid helium was assumed to be negligible with respect to the thermal resistances of coil insulation. The TQC02b was tested at 1.9 K and 4.5 K.

The Technological Quadrupole coils were built with the two-layers of cables made of 27 strands, 0.7 mm in diameter, with a nominal width of 10.05 mm, mid-thickness of 1.26 mm and keystone angle of 1.0 degree. The inner radius of the coil was 90 mm and one copper wedge was placed in the inner and outer cable layer (Fig. 7.14). The coils were surrounded by stainless steel collars and an iron yoke with the outer radius of 200 mm. The measurements of the TQC02b was performed with a dedicated 1-meter-long, 25.4 μm thick and 9.5-mm-wide stainless steel heating strip placed in the middle of the Kapton shim package at the coil inner layer, between adjacent coils (Fig. 7.14). It was expected that in this location the heat deposition from the beam would be a maximal one [131]. The TQC02b was also used as a demonstrator of technology and it was equipped with 2 types of coils: the coils TQ10 and TQ12 made from the Modified Jelly Roll (MJR) conductor and the coils TQ17 and TQ19 made from the Restacked Rod Process (RRP) conductor. The TQ10 and TQ12 (MJR) coils have an additional layer of 43 μm inner polyimide trace. The cables used to wind these coils (RRP and MJR) are insulated with S-2 glass sleeves. After high-temperature reaction, the coils were impregnated with epoxy resin. The thickness of the insulation and the epoxy of the reacted and impregnated coils may differ from the nominal thickness since it depends on the type of insulation and the pressures during reaction and impregnation. This might be source of uncertainties of the magnet quench limit determination. In order to set correct data in the model the actual insulation thickness of the RRP and MJR coils used in TQC02b were measured (Table 7.3).

The experimental setup was built from dedicated heating strips (indicated in Fig. 7.14) and the DC power supply, able to provoke quenches at a magnet current in the range from a few hundreds to ~9000 Amperes. The measurement procedure was the same as described in Chapter VI, namely each measurement involved setting the heater current to a chosen value, waiting for a few minutes to establish a steady-state heat flow. Then the magnet current was ramped with step of 20 A/s until the magnet quench. The 20 A/s ramp step allowing to avoid the additional coil heating by eddy currents.

Fig. 7.16 shows the results of numerical calculation and measurements of quench currents of the inner mid-plane cable. There is a good agreement between the calculated and measured values both at 1.9 K and 4.5 K and for both the RRP and MJR coils. The non-linear dependence of critical current density on a temperature of RRP 54/61 strands [132] explaining the discrepancy between the simulations and measurements for low quench current values. Unfortunately, J_c(T) parametrizations for the MJR conductor are not available, yet.

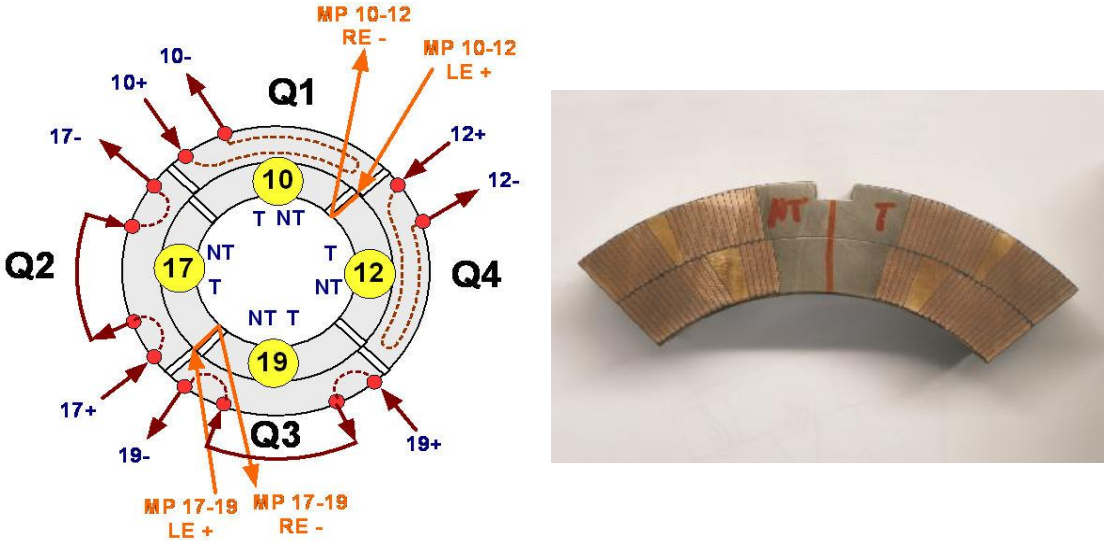

Fig. 7.14 The TQC02b electrical scheme (left) and photo of HQ03 coil (right). The TQ magnet was equipped with a dedicated stainless steel heating strip placed in the inner layer mid-plane, between the adjacent coils Q1-Q4 (TQ10-TQ12) and Q2-Q3 (TQ17-TQ19) [131] .

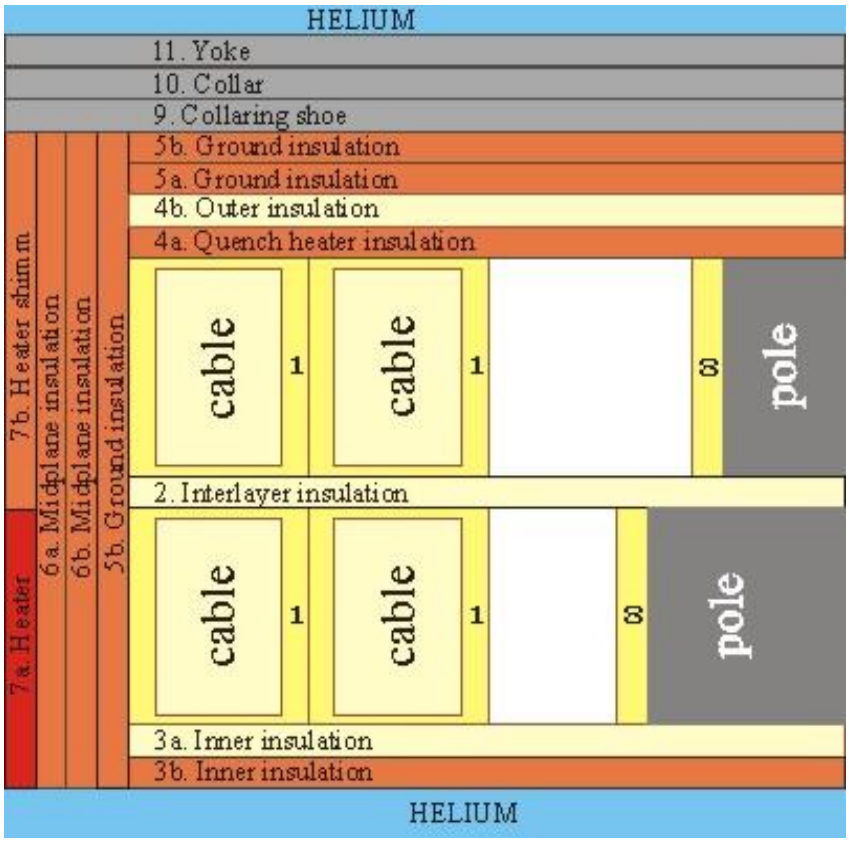

Fig. 7.15 The TQC02b coil model. The insulation scheme and heating strip are implemented in *Network Model.*

Table 7.3 The TQ and HQ coils insulation scheme implemented in the *Network Model*. The difference of TQ cable and coil insulation thickness is indicated for MJR and RRP type coils. A nominal insulation scheme was implemented in the HQ *Network Model* .

Item	Material	MJR (TQ 10-12)	RRP (TQ 17-19)	RRP HQ coil
		thickness [μm]	thickness [μm]	thickness [μm]
1	S-2+epoxy	99	95	127
2	S-2+epoxy	327	165	254
3a	S-2+epoxy	299	208	127
3b	Kapton	43	0	76
4a	Kapton	43	43	76
4b	S-2 +epoxy	273	165	381
5a	Kapton	127	127	127
5b	Kapton	127	127	127
6a	Kapton	76.2	76.2	127
6b	Kapton	50.8	50.8	-
7a	Stainless steel	25.4	25.4	-
7b	Kapton	25.4	25.4	-
8	S-2+epoxy	76.2	76.2	127
9	Stainless steel	787.4	787.4	787.4

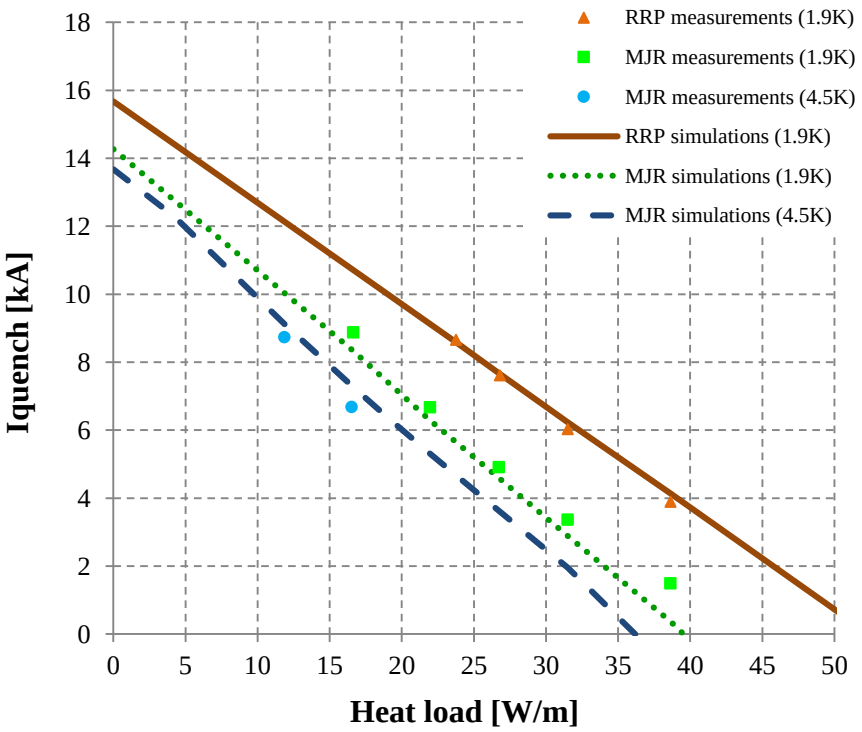

Fig. 7.16 The TQC02b *Network Model* validation with measurements [131]. Solid line and triangle markers show results of simulation and measurements at 1.9 K for TQ RRP coils. Dotted line and square markers corresponds to measurements taken at 1.9 K with TQ MJR coils. Dashed line and round makers corresponds to measurements taken at 4.5 K with TQ MJR coils.

VII.3 Nb_3Sn High-gradient quadrupole for the LHC upgrade

The *Network Model* developed for the US LARP Nb_3Sn Technological Quadrupole was used for thermal analysis and design optimization of the Nb_3Sn High-gradient quadrupole (HQ). The HQ was the third generation of the US LARP Nb_3Sn quadrupole magnets and it was developed as a demonstrator of the large aperture quadrupole magnet for an upgrade of the LHC inner triplet. The HQ coils design consists of 2-layer of superconducting cables with 120 mm bore, one wedge in the inner and one wedge in the outer cable layer. The HQ coil *Network Model* was based on the first-generation of the HQ cable, which was made of 35 strands, of 0.8 mm in diameter, a nominal width of 15.15 mm, mid-thickness of 1.44 mm and a keystone angle of 0.75 degree.

The objective of the simulations was the study of different inner coil insulation schemes to understand their impact on the thermal HQ coil behavior. In addition the dimensions of the annular helium channel between the coil and the cold bore, and the helium channels through coil poles were studied with the aim to optimize them in order to efficiently evacuate heat from the HQ coils. It was important to optimize the channels in the way to keep the helium in the channels in superfluid regime. The proposed helium channel pattern in the poles was 5 mm diameter hole drilled every 100 mm along the coil. The diameter and number of the holed was selected in order to have them equal or larger comparing to the annular channel cross-section. This assumption should allow to avoid helium quench in the pole channels.

The simulations were performed for the typical beam induced heat load and simulated with the MARS code [133]-[134]. The MARS model included a beam screen, a beam tube and a cooling channel around the cold bore. In simulation an additional 3 mm tungsten absorber in the horizontal and vertical planes were added in the magnet mid-plane in order to reduce the heat loads. Also the heat load to the cold bore was implemented into the MARS model. The heat load profile was simulated for the LHC luminosity upgrade target, namely $L = 5*10^{34}$ $cm^{-2}s^{-1}$ (Fig. 7.17). This profile has been used in order to qualitatively study of different inner coil insulation schemes as well as the coil cooling channels.

The results of the *Network Model* simulations are shown in Fig. 7.18 and Fig. 7.19 for the inner and outer cable layer respectively. The magnet mid-plane in the plots is indicated as 0, positive and negative x-values indicate cables in the coils part adjacent to the mid-plane and vertical values indicate the temperature increase in the cables above the bath temperature $T_b = 1.9$ K. Three scenarios were studied and shown in this figure: 1) only cable insulation in the coil inner diameter (ID), 2) cable insulation + an additional 127 μm G10 insulation layer in ID, 3) cable insulation + an additional 127 μm G10 and 43 μm polyimide insulation layer in ID. The non-symmetric temperatures distributions come from the fact that the heat load is not symmetric.

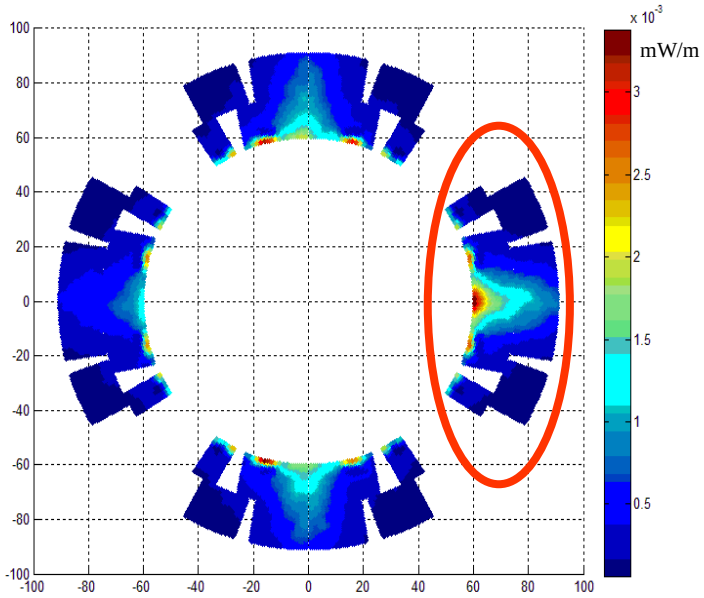

Fig. 7.17 The transverse heat deposition profiles in HQ magnet, obtained from the MARS simulation performed for an upgraded LHC IP5 optics layout, for luminosity $L=2.5*10^{34}$ $cm^{-2}s^{-1}$. In the *Network Model* simulation this distribution was multiplied by a factor 2 in order to approach the nominal LHC upgrade luminosity ($L=5.0*10^{34}$ $cm^{-2}s^{-1}$).

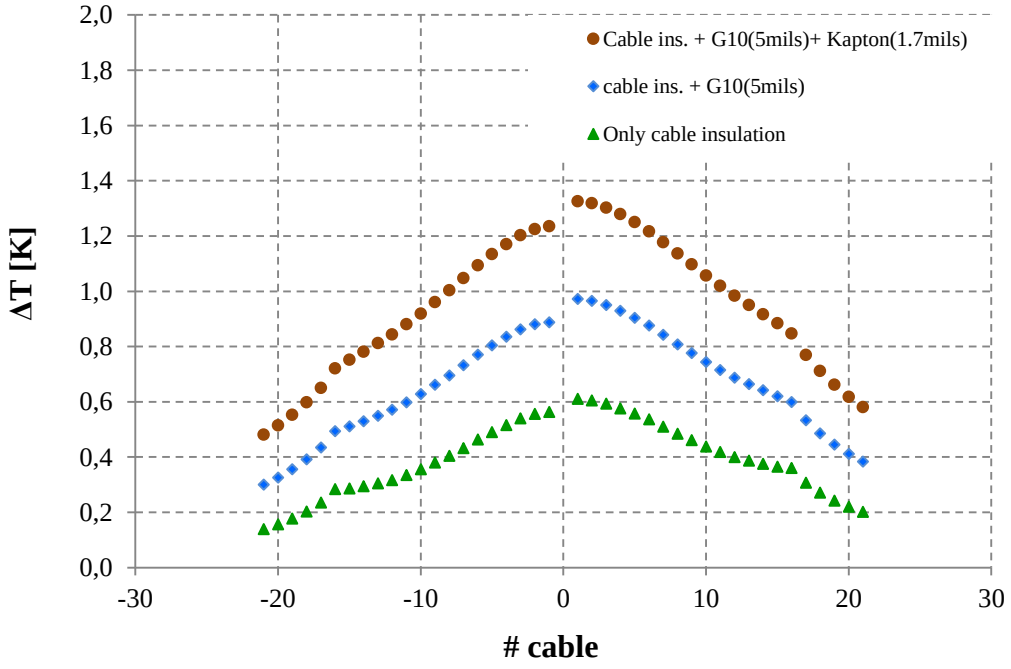

Fig. 7.18 The results of the numeric simulation with *Network Model* – HQ magnet inner cable layer. The zero on x-axis indicates the magnet mid-plane, the positive and negative values indicate the cables in the coils adjacent to the mid-plane. The values on y-axis indicate the temperature

increase in the cables above the bath temperature T_b=1.9 K. the *Network Model* simulations were performed for the heat load showed in Fig. 7.17.

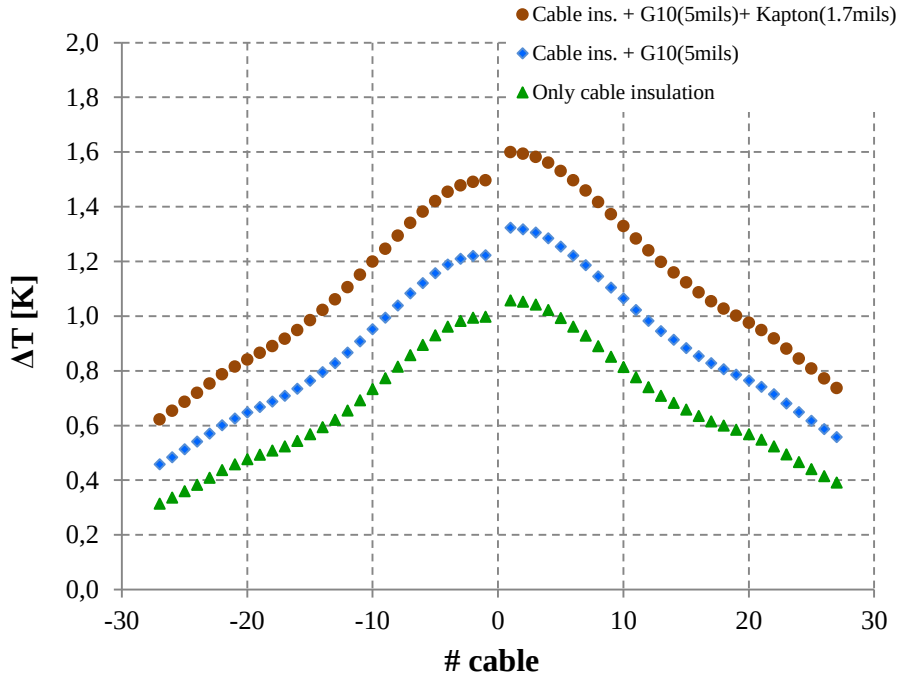

Fig. 7.19 The results of the numeric simulation with *Network Model* – HQ magnet outer cable layer.

The *Network Model* was used to simulate the thermal behavior of the Nb_3Sn quadrupole magnets. The TQ model was successfully validated with experimental data. The calculated and measured data are in good agreement and validate the model's accuracy, the material properties used in the simulations and also verify the choice of boundary conditions.

A 120 mm US LARP Nb_3Sn magnet was analyzed with this model. An estimated heat load distribution at a luminosity of $L = 5.0 \cdot 10^{34}$ $cm^{-2}s^{-1}$ was implemented in order to qualitatively study the coil insulation as well as the magnet helium channels cooling efficiency. The results show the significant temperature increase in the coil due to the increase of the inner coil insulation thickness. In order to efficiently evacuate heat from the coil the polyimide insulation should be minimized. The proposed helium channel dimensions ensure the helium to keep at superfluid regime.

Chapter VIII
Summary and outlook

This monograph discusses the results of studies on heat transfer in high-field superconducting accelerator magnets at cryogenic temperatures. The operation of the large accelerators constructed with the use of the superconducting magnets requires a careful control of the beam losses around the accelerator ring. The typical beam loss duration in case of the LHC varies between 10^{-9} and 10^{-6} second. The particles lost from the high energy and high intensity beams affect the operation of the superconducting accelerators magnets by inducing the quenches in the magnets coils. In order to protect the accelerator equipment several safety systems were designed to ensure a safe accelerator operation such as collimators, beam loss monitors, beam absorbers, beam dumps as well as the internal magnet quench protection systems.

The primary objective of the presented studies was the development of the thermal model which would allow to determine the limits of the energy which can be safely deposited to the magnet coils by the particles lost from the beam (the *quench limits*) during the Large Hadron Collider runs. The determination of the quench limits is essential for the accelerator's operation, especially during the collection of data during physics runs of accelerator, since the integrated luminosity depends on the time of the data collection. The reducing of the integrated luminosity affects the discovery potential of the accelerator, especially the physics analyses of rare events. In addition, the recovery of the LHC accelerator after the quench takes about 48 hours when more than 14 magnet cells quench and it involves a significant amount of money (the cost of one hour of only the LHC operation is estimated to be of order of ~10 kCHF).

The secondary objective, which was added at the later stage of the presented studies, was the implementation of the developed and validated model to the thermal optimization of the superconducting magnets designed for the LHC upgrade as well as the verification of a new technologies proposed for magnets enhancement. Following this objective, the *Network Model* was implemented to study the enhanced electrical insulation scheme proposed for the Nb-Ti cables , and the thermal optimization of the newly developed superconducting magnets based on the Nb_3Sn conductor.

The work presented in this monograph was organized in the form of dedicated experiments with a material data collection phase, construction of a model and model validation with measurements performed at CERN and FERMILAB test facilities. The complete experiments consisted of: (1) the theoretical background for development of *Network Model*, (2) the selection of tools for the numerical model development, (3) the selection of superconducting magnets to be studied, (4) the collection of material data required by the model, (5) the preparation of input values and distributions – heat load, (6) the numerical simulations, (7) the validation of the models with measurements, also with use of a dedicated equipment developed for this purpose, (8) the implementation of the model: the thermal optimization of the novel magnets and the thermal study of novel

magnets technologies. The important parts of this project were the mini-experiments performed for data collection, such as free void volume determination or the model validation, such as design, construction and using the Internal Heating Apparatus.

- The general conclusions on *Network Model* and its implementation are:
  - The *Network Model* is a fast, effective and flexible tool for modeling heat transfer in superconducting accelerator magnets, for different boundary conditions as well as for sub-components of superconducting magnets,
  - The *Network Model* was successfully validated with existing and newly developed heating sources, such as magnet Quench Heaters installed on top of the magnets coil or the Internal Heating Apparatus installed inside the magnet cold bore,
  - The *Network Model* supported the determination of the initial quench limit levels for first runs of the LHC main magnets, namely the main dipole (MB), the main lattice quadrupole (MQ) and the long straight section quadrupoles (MQM and MQY),
  - The *Network Model* allowed to understand the limitation for ion beam runs at the LHC. The initial modeling showed an insufficient temperature margin in a few of the main LHC dipole magnets,
  - The *Network Model* helped in the understanding of Enhanced Insulation limitations and triggered the additional ANSYS studies which confirmed the model results,
  - The *Network Model* helped in the thermal optimization of the newly developed Nb_3Sn superconducting magnets. The heat extraction from fully impregnated coils poses new challenges to the magnet design and the *Network Model* is a tool which can be really useful for initial optimization of the magnet cooling channels scheme, namely the dimensions and location of the cooling channels in the coils pole regions and thickness of the cooling channel between the cold bore and coil.

- During the course of the work presented in this monography some general observations on superconducting magnets thermal modeling came into being:
  - The geometry of the magnets requires careful implementation to the model since the geometry is the most important components of the thermal model. Even a tiny change of geometry can significantly change the thermal characteristic of designed magnet.
  - The materials properties at cryogenic temperatures are not always available. The use of the parameters for similar materials introduces uncertainty . This affects the model reliability and precision, or the results. Dedicated measurements, especially of the thermal conductivity of the used electrical insulation are mandatory.
  - The temperature margin of the superconductor is determined by the short sample measurements and the parametrization based on these numbers. The parametrization is optimized for the nominal operation current of the designed magnet. Since parametrization is not linear, at a low current the discrepancy

between measurements and simulations increases significantly, even by one order of magnitude. This is the main source of modeling uncertainty.

- The experimental validation of the *Network Model* has become more effective thanks to the development of dedicated hardware and measurement procedures.

- The future development of the model and experimental methods of model validation:
  - In presented work the *Network Model* was used for steady-state heat transfer modeling but in reality accelerators are much more complicated. At the LHC the beam consists of 2808 bunches and the beam has its own structure. The implementation of the beam pattern will be one of the major upgrades of the *Network Model*. But implementing the beam pattern means a mixture of steady-state and transient conditions, so the model has to be developed for transient cases, as well.
  - The heat load scenario is another vital component of modeling. The realistic 3-dimensional distributions of the energy depositions are required in order to precisely determine the quench level. For example, the energy deposits to the cold bore significantly reduce the quench level of the magnet due to common heat extraction from the coil and the cold bore through helium channel around the cold bore. The *Network Model* simulations for the main dipole magnet show that the quench limit for the nominal current I_{MB} = 11850 A is 14 mW/cm^3 whereas without heating the cold bore quench limit is 100 mW/cm^3.
  - The cable and the coil electrical insulation constitutes the most severe barrier for the heat extraction from the magnets coil to the helium bath. The optimization of the thickness of the electrical insulation is the way to increase the heat extraction from the magnet. In addition it is vital to understand heat transfer characteristics from the superconductor to the helium bath through the electrical insulation.

The objectives of the *Network Model* simulations were accomplished. The simulations provided initial quench limits for the LHC main magnets as well as helped in the understanding of enhanced insulation limitations for the Nb-Ti based magnet technology as reported in chapter VI and chapter VII. For the Nb_3Sn based magnet technology the *Network Model* simulations provided information on the impact of different electrical insulation schemes on the thermal stability of the Nb_3Sn superconducting magnets as reported in chapter VII.

ACKNOWLEDGEMENTS

The work presented in this monograph is a result of many years of research in the field of superconducting magnets. I was fortunate to come across and get to know many outstanding people. It is impossible to mention all of them here to express my thanks.

I am indebted to Prof. Piotr Malecki for guiding me through my scientific career, starting from 1995, during the preparation of my master thesis, through my PhD thesis and finally through the habilitation monography. During these 24 years we have had a lot of interesting and stimulating discussions and we performed many scientific activities.

I wish to thank Prof. Marek Jeżabek for trust and guidance and especially for motivating to complete this monograph

I would like to express my sincere gratitude to Andrzej Siemko and Bernd Dehning for supervising my first years of this work at CERN. They shared with me their experience and know-how as well as strongly supported both my theoretical and experimental parts of this work. They devoted a lot of valuable time to me, giving advice and offering never ending support.

I wish to thank Lucio Rossi and Luca Bottura for providing me with the best possible conditions to complete my work.

During the course of this work I received significant help from Ezio Todesco, Davide Tomassini, Glyn Kirby, David Richter, Christian Scheurlein, Marco Calvi, Pier Paolo Granieri, Clement Lorin, Angelo Bonasia, Rob van Weelderen, Francesco Cerutti, Luigi Esposito, Roderick Bruce, Giorio D'Angelo, Angelo Bonasia, J. Kotuła, J. Halik and many many others.

Starting from 2008 I continued this work in Fermilab as the Toohig Fellow of the USA LHC Accelerator Research Project (US-LARP) under supervision of Giorgio Ambrosio and Mike Lamm. I worked in the USA with many amazing people who shared with me their experience on the experimental measurements: Sandor Feher, Alexander Zlobin, Vladimir Kashikhin, Vadim Kashikhin, Mike Tartaglia, Guram Chlachidze, Vito Lombardo, Emmanuela Barzi, Daniele Turrioni, Luciano Elementi, Joe Dimarco, Roger Bossert, Fred Nobrega, Mike Whitson, Helene Felice, Paolo Feracin, GianLuca Sabbi, Peter Wanderer, Arup Ghosh, and many others.

I wish to show my gratitude to my most important supporters – to my family: my wife Małgosia and my children Karolina and Kajetan for their endless support and inspiration. Without it I am not sure I would have been able to complete my work. Thank you for always listening to me and for incessantly encouraging me. - To my parents and siblings, for their permanent motivation and support. - To my friends and all those who listened patiently to the endless talks about my work.

Bibliography

[1] Bocian D., Dehning B., Siemko A., "Modelling of quench limit for steady state heat deposits in LHC magnets", IEEE Appl. Trans. Supercond. **18**:112-115, (2008); doi: 10.1109/TASC.2008.921338;

[2] Granieri P.P., (D. Bocian) et al., "Stability Analysis of the LHC Cables for Transient Heat Depositions", IEEE Trans. Appl. Supercond. **18**:1257-1262, (2008); doi: 10.1109/TASC.2008.922543;

[3] Holzer E.B., (D. Bocian), et al., "Generation of 1.5 Million Beam Loss Threshold Values", LHC-PROJECT-Report-1158, CERN, (2008); https://accelconf.web.cern.ch/accelconf/e08/papers/thpc147.pdf;

[4] Bocian D., Dehning B., Siemko A., "Quench Limit Model and Measurements for Steady State Heat Deposits in LHC Magnets", IEEE Trans. Appl. Supercond. **19**:2446-2449, (2009); doi: 10.1109/TASC.2009.2019060;

[5] Böhlen T., (D. Bocian), et al., "First Experience with the LHC Beam Loss Monitoring System", CERN-ATS-2009-025. (2009); http://cds.cern.ch/record/1206505?ln=en#;

[6] Bruce R., Bocian D., Gilardoni S., Jowett J.M., "Beam losses from ultraperipheral nuclear collisions between $^{208}Pb^{82+}$ ions in the Large Hadron Collider and their alleviation", Phys. Rev. ST Accel. Beams **12**, 071002 (2009); doi: 10.1103/PhysRevSTAB.12.071002;

[7] Bocian D., Cerutti F., Dehning B., Esposito L.S., Siemko A., "Quench Limit Calculation for Steady State Heat Deposits in LHC Inner Triplet Quadrupole Magnets", Proceedings of IPAC2012, New Orleans, Louisiana, USA,(2012); http://accelconf.web.cern.ch/accelconf/ipac2012/papers/thppr036.pdf

[8] Bocian D., "Thermodynamic modeling of enhanced superconducting cable insulation for the proposed upgrade of the LHC inner triplet Nb-Ti quadrupole magnets", Proc. SPIE **8903** (2013); doi: 10.1117/12.2042140;

[9] Lorin C., Bocian D., Todesco E., "Numerical simulation of microchannel deformation in enhanced insulation for Nb-Ti superconducting accelerator magnets", IEEE Trans. Appl. Supercond. **25**, (2014); doi: 10.1109/TASC.2014.2341247;

[10] Ambrosio G., (Bocian D.) et al., "Final Development and test preparation of the first 3.7m long Nb3Sn quadrupole by LARP", LARP Collaboration, IEEE Trans. Appl. Supercond. **20**:283-287, (2010); doi: 10.1109/TASC.2010.2040471;

[11] Ambrosio G., (Bocian D.), et al., "Test results of the first 3.7 m long Nb3Sn quadrupole by LARP and future plans", LARP Collaboration, IEEE Trans. Appl. Supercond. **21**(3):1858-1862, (2011); doi: 10.1109/TASC.2010.2089586;

[12] Ambrosio G., (Bocian D.), et al., "Progress in the Long Nb_3Sn Quadrupole R&D by LARP", LARP Collaboration, IEEE Trans. Appl. Supercond. **22**, (2012); doi: 10.1109/TASC.2011.2175894;

[13] Bocian D. et al., "Steady State Heat Deposits Modeling in the Nb3Sn Quadrupole Magnets for the Upgrade of the LHC Inner Triplet", IEEE Trans. Appl. Supercond. **22**, (2012); doi: 10.1109/TASC.2011.2174591;

[14] Bocian D., Ambrosio G., Whitson G., "Measurement of Nb_3Sn conductor dimension changes during heat treatment", LARP Collaboration, Adv. Cryo. Eng. – Materials **58**, (2012); FERMILAB-CONF-11-272-TD; doi: 10.1063/1.4712096;

[15] Felice H., (Bocian D.) et al., "Impact of Coil Compaction on Nb_3Sn LARP HQ Magnet", LARP Collaboration, IEEE Trans. Appl. Supercond. **22,** (2012); doi: 10.1109/TASC.2012.2183843;

[16] Maingi L.S. "Numerical Study of Energy Deposits in Superconducting Magnet Coils", Lee Teng Internship Report, (2010); https://www.illinoisacceleratorinstitute.org/2010%20Program/student_papers/Logan_Maingi.pdf;

[17] Davies A., "Material properties data for heat transfer modeling in Nb3Sn magnets", Lee Teng Internship Report, (2011); https://www.illinoisacceleratorinstitute.org/2011%20Program/student_papers/Andrew_Davies.pdf;

[18] Wilson M.N., *Superconducting Magnets*, Oxford University Press, (1983);

[19] Bottura L., Rossi L., "Magnets for Particle Accelerators and Colliders", Encyclopedia of Applied Physics: Superconductivity, Wiley-VCH, (2016); doi: 10.1002/3527600434.eap793.

[20] Rossi L., Bottura L., "Superconducting magnets for particle accelerators", *Rev. Accel. Sci. Tech.* **5**(51):51-89, (2012); doi: 10.1142/S1793626812300034;

[21] van Delft D., Kes P., "The discovery of superconductivity", https://www.lorentz.leidenuniv.nl/history/cold/DelftKes_HKO_PT.pdf; "The resistance of pure mercury at helium temperatures", Comm. Leiden. April 28, (1911); "The disappearance of the resistivity of mercury". Comm. Leiden. May 27, (1911); "On the sudden change in the rate at which the resistance of mercury disappears". Comm. Leiden. November 25, (1911).

[22] Bardeen J., Cooper L.N., Schrieffer J.R., "Theory of Superconductivity", Phys. Rev.**108**(5), (1957): doi: 10.1103/PhysRev.108.1175

[23] Cooper L.N., "Bound electron pairs in a degenerate Fermi gas", Phys. Rev. **104**(4):1189-1190 (1956): doi: 10.1103/PhysRev.104.1189;

[24] Tinkham, M., *Introduction to Superconductivity*, Second Edition, New York, NY: McGraw-Hill, (1996).

[25] Patterson J., Bailey B., *Solid-State Physics, Introduction to the Theory: Superconductivity*, Springer Science & Business Media, pp. 463-512, (2010); doi: 10.1007/978-3-642-02589-1.

[26] Iwasa Y., *Case Studies in Superconducting Magnets*, Plenum Press. N. Y., (1994);

[27] Turner S., *Superconductivity in Particle Accelerators*, Proceedings of the CAS - CERN Accelerator School, Hamburg, Germany, 17-24 May 1995, (1996); doi:10.5170/CERN-1996-003.

[28] Bailey, R., *Superconductivity for Accelerators*, Proceedings of the CAS - CERN Accelerator School, Erice, Italy, 24.04 – 04.05 2013, (2015); doi:10.5170/CERN-2014-005;

[29] https://www.revolvy.com/page/List-of-superconductors; http://superconductors.org/;

[30] van Sciver S.W., *Helium cryogenics*, Plenum Press, New York and London, (1986);

[31] Meissner W., Ochsenfeld, R., "Ein neuer Effekt bei Eintritt der Supraleitfähigkeit", Naturwissenschaften **21**:787-788, (1933); doi: 10.1007/BF01504252.

[32] Nagamatsu J.et al., "Superconductivity at 39 K in magnesium diboride", Nature **410**,(6824):63-64, (2001); doi: 10.1038/35065039;

[33] https://csabg.org/low_temperature_superconductors/.

[34] Chao A.W., Chou W., *Reviews of Accelerator Science and Technology: Applications of superconducting technology to accelerators* **5**, World Scientific Pub., (2013);
[35] Bednorz J.G., Müller K.A., "Possible high T_c superconductivity in the Ba-La-Cu-O system", Z. Phys, B **64**(1):189-193, (1986); doi: 10.1007/BF01303701;
[36] Maeda H., Tanaka Y., Fukutumi M., Asano T., "A New High-T_c Oxide Superconductor without a Rare Earth Element", Jpn J. Appl. Phys. **27**(2):209-210, (1988); doi: 10.1143/JJAP.27.L209
[37] Wu M.K. et al., "Superconductivity at 93 K in a New Mixed-Phase Y-Ba-Cu-O Compound System at Ambient Pressure", Phys. Rev. Lett. **58**(9):908-910, (1987); doi: 10.1103/PhysRevLett.58.908;
[38] Sheng Z.Z., Hermann A.M., "Bulk superconductivity at 120 K in the Tl–Ca/Ba–Cu–O system", Nature vol. 332, Issue 6160, pp. 138-139, (1988); doi: 10.1038/332138a0;
[39] Ott H.R. et al., "Ube_{13}: An Unconventional Actinide Superconductor", Phys. Rev. Lett., vol. 50, Issue 20, pp. 1595-1598, (1983); doi: 10.1103/PhysRevLett.50.1595;
[40] Steglich F. et al., "Superconductivity in the presence of strong Pauli paramagnetism: $CeCu_2Si_2$", Phys. Rev. Lett., vol. 43, Issue 25, pp. 1892-1896, (1979); doi: 10.1103/PhysRevLett.43.1892;
[41] Steward G. R. et al., "Possibility of Coexistence of Bulk Superconductivity and Spin Fluctuations in UPt_3", Phys. Rev. Lett., vol. 52, Issue 8, pp. 679-682, (1984); doi: 10.1103/PhysRevLett.52.679;
[42] Takahashi H. et al., "Superconductivity at 43 K in an iron-based layered compound $LaO_{1-x}F_xFeAs$", Nature 453, pp. 376-378, (2008); doi: 10.1038/nature06972
[43] Drozdov A.P. et al., "Conventional superconductivity at 203 kelvin at high pressures in the sulfur hydride system", Nature 525, pp. 73-76, (2015); doi: 10.1038/nature14964;
[44] https://www.nextbigfuture.com/2018/03/graphene-superlattices-could-be-used-for-superconducting-transistors.html;
[45] Kamerlingh Onnes H., "Report on the researches made in the Leiden cryogenics laboratory between the second and third international congress of refrigeration: Superconductivity", Comm. Physical Lab. Leiden Suppl. **34b**:55-70, (1913); https://www.lorentz.leidenuniv.nl/history/cold/DelftKes_HKO_PT.pdf
[46] Miller J.R. et al., "A design for the superconducting outsert of a 45-T hybrid magnet system using cable-in-conduit conductors", IEEE Trans. Appl. Supercond. **3**:71-77, (1993); doi: 10.1109/77.233675;
[47] Rossi L., "Manufacturing and testing of accelerator superconducting magnets", CERN Yellow Report, CERN-2014-005, pp. 517-546, (2014); doi: 10.5170/CERN-2014-005.517;
[48] Rummel T. et al., "The Superconducting Magnet System of the Stellarator Wendelstein 7-X", IEEE Trans. Plasma Science **40**(3):769-776, (2012); doi: 10.1109/TPS.2012.2184774;
[49] Huguet M. *et al.*, "The ITER magnet system program-design and R&D", Proceedings of 16th International Symposium on Fusion Engineering **1**:138-143, Champaign, IL, USA, (1995); doi: 10.1109/FUSION.1995.534190;
[50] N. Mitchell *et al.*, "The ITER Magnet System", IEEE Trans. Appl. Supercond. **18**(2):435-440, (2008); doi: 10.1109/TASC.2008.921232;

[51] Seidel P. (Ed.), *Applied Superconductivity: Handbook on Devices and Applications* **1**:1233, 126, Wiley-VCH; Weinheim (Germany), 2015; doi: 10.1002/9783527670635;
[52] Abrikosov A.A.. "The magnetic properties of superconducting alloys", Journal of Physics and Chemistry of Solids **2**(3):199–208 (1957); https://www.sciencedirect.com/science/article/abs/pii/0022369757900835;
[53] Ginzburg V.L., Landau L.D., "On the theory of superconductivity", Zh. Eksp. Teor. Fiz. **20**:1064-1082, (1950); (English translation in: L. D. Landau, Collected papers, Oxford: Pergamon Press, p. 546, (1965)); https://cds.cern.ch/record/104093?ln=pl;
[54] Ketterson J.B., "The Physics of Solids: A Phenomenological Theory of Superconductivity: The Ginzburg–Landau Theory and the Josephson Effects", Oxford Scholarship online, (2016); doi: 10.1093/acprof:oso/9780198742906.003.0033;
[55] Bitter F.: Rev. Sci. Instrum. **7**:479, (1936); Rev. Sci. Instrum. **7**:482, (1936); Rev. Sci. Instrum. **8**:318, (1937); Rev. Sci. Instrum. **10**:489, (1939);
[56] Toth J., Bole S., "Design, Construction and First Testing of a 41.5 T All-Resistive Magnet at the NHMFL in Tallahassee", IEEE Trans. Appl. Supercond. **28**(3), (2018); doi: 10.1109/TASC.2017.2775578; https://nationalmaglab.org/magnet-development/magnet-science-technology/magnet-projects/28-mw-magnet;
[57] Collins S.C., Rev. Sci. Instrum. **18**:157, (1947);
[58] Yntema G.B., "Superconducting winding for magnets", Phys. Rev. APS **98**:1197, (1955);
[59] Kunzler J.E.; Buehler E.; Hsu F.S.L.; Wernick J.H. "Superconductivity in Nb_3Sn at High Current Density in a Magnetic Field of 88 kilogauss", Phys. Rev. Lett. APS **6**(3):89-91, (1961); doi: 10.1103/PhysRevLett.6.89;
[60] Fraser M.J., Hulm J.K., Riemersa H., Venturino A.J., Wein R.E., "A 43 kgauss superconducting solenoid", Cryogenics **2**, (1961); doi: 10.1016/0011-2275(61)90034-0;
[61] Berlincourt T.G., Hake R.R., "Upper Critical Fields of Transition Metal Alloy Superconductor", Phys. Rev. Lett. **9**(7):293-295, (1962); doi: 10.1103/PhysRevLett.9.293;
[62] Stekly Z.J.J, Thome R., Strauss B.P., "Principles of Stability in Cooled Superconducting Magnets", J. Appl. Phys. **40**(5):2238–2245, (1969); doi: 10.1063/1.1657964;
[63] Subramanian M.A. et al., "A new high-temperature superconductor: $Bi_2Sr_{3-x}Ca_xCu_2O_{8+y}$", Science **239**(4843):1015-1017, (1988); doi: 10.1126/science.239.4843.1015;
[64] Cava R.J. et al., "Structure and physical properties of single crystals of the 84 K superconductor $Bi_{2.2}Sr_2Ca_{0.8}Cu_2O_{8+\delta}$", Phys. Rev. B **38**(1):893-896 (1988); doi: 10.1103/PhysRevB.38.893;
[65] Schilling A., Cantoni M., Guo J.D., Ott H.R., "Superconductivity above 130 K in the Hg–Ba–Ca–Cu–O system", Nature **363**(6424):56-58, (1993); doi: 10.1038/363056a0;
[66] Chu C.W. et al., "Superconductivity above 150 K in $HgBa_2Ca_2Cu_3O_8+\delta$ at high pressures", Nature **365**(6444):323, (1993); doi: 10.1038/365323a0;
[67] Hazelton D.W. et al., "Recent Developments in 2G HTS Coil Technology", IEEE Trans. Appl. Supercond. **19**(3):2218-2222, (2009); doi: 10.1109/TASC.2009.2018791;

[68] https://www.researchgate.net/project/The-NHMFL-32T-all-superconducting-magnet-system;
https://nationalmaglab.org/magnet-development/magnet-science-technology/magnet-projects/32-tesla-scm;
[69] Braccini V. et al., "Development of Ex Situ Processed MgB_2 Wires and Their Applications to Magnets", Phys. C Supercond. **456**(1):209-217, (2007); doi: http://doi.org/10.1016/j.physc.2007.01.030;
[70] Ballarino A., "Design of an MgB_2 feeder system to connect groups of superconducting magnets to remote power converters", J. Phys. **234**, (2010); doi: http://doi.org/10.1088/1742-6596/234/3/032003;
[71] see: https://homelasa.mi.infn.it/en/events-outreach/newsing/538-test-of-superconducting-mgb2-coil-at-lasa.html;
http://eng.fisica.unimi.it/ecm/home/archives/news/content/success-in-the-test-at-lasa-of-an-innovative-superconducting-coil-in-mgb2.0000.UNIMIDIRE-63632;
[72] Billan J. et al., "A Superconducting High-Luminosity Insertion in the Intersecting Storage Rings (ISR)", IEEE Trans. Nucl. Sci. **26**(3), (1979); doi: 10.1109/TNS.1979.4329976;
[73] Edwards H. T, "The Tevatron Energy Doubler: A Superconducting Accelerator", Ann. Rev. Nucl. Part. Sci. **35**:605-660, (1983); doi: 10.1146/annurev.ns.35.120185.003133;
[74] Wolff S., "Superconducting HERA magnets", IEEE Trans. Magn. **24**:719-722, (1988); doi: 10.1109/20.11326;
[75] Bruning O. et al., "LHC Design Report: the LHC main ring", CERN-2004-003-V-1, (2004); doi: 10.5170/CERN-2004-003-V-1;
[76] http://www.uslarp.org/;
[77] http://www.fnal.gov/directorate/HEPAP_AARD0206/AARD_Gourlay.ppt
[78] Bejan A., Kraus A. D. *Heat Transfer*, J. Wiley and Sons, New York, (1993);
[79] Frost W., Heat transfer at Low Temperature, Plenum Press, New York, (1975); doi: 10.1007/978-1-4899-1998-4;
[80] Cryosoft, France, (2001);
[81] NIST database, www.nist.gov;
[82] Baudouy B., "Kapitza resistance and thermal conductivity of Kapton in superfluid helium", Cryogenics **43**:667-672 (2003); doi: 10.1016/S0011-2275(03)00178-4;
[83] Lawrence J. et al., "The thermal conductivity of Kapton HN between 0.5 and 5K", Cryogenics **40**(3):203-207, (2000); doi: 10.1016/S0011-2275(00)00028-X;
[84] Barucci et al, „Low temperature thermal conductivity of Kapton and Upilex", Cryogenics **40**:145-147 (2000); doi: 10.1016/S0011-2275(00)00013-8;
[85] Baudouy B., Polinski J., "Thermal conductivity and Kapitza resistance of epoxy resin fiberglass tape at superfluid helium temperature", Cryogenics **49**, (2009); doi: 10.1016/j.cryogenics.2008.11.004
[86] Kapitza P.L., Zh. Eksp. Teor. Fiz. 11, 1; [English: J. Phys. U.S.S.R. 4, 181] (1941); Kapitza P.L. Collected Papers of P. L. Kapitza, D. ter Haar, Ed. (Pergamon Press Ltd., Oxford, England, vol. **II**, (1967).
[87] Nacher PJ et al.," Heat exchange in liquid helium through thin plastic foils", Cryogenics **32**, (1992); doi: https://doi.org/10.1016/0011-2275(92)90053-D;

[88] Kashani A., Van Sciver S.W., "High heat flux Kapitza conductance of technical copper with several different surface preparations", Cryogenics **25**, (1985); doi: https://doi.org/10.1016/0011-2275(85)90202-4;
[89] Camacho D. *et al.,"*Thermal characterization of the He II LHC heat exchanger tube*",* LHC Project Report **232**, (1998); http://cds.cern.ch/record/365293?ln=de;
[90] Van Weeldereen R., private communication, Rob.van.Weelderen@cern.ch
[91] Charifoulline Z., "Residual Resistivity Ratio (RRR) measurement of LHC superconducting Nb-Ti cable", IEEE Trans. Appl. Supercond. **16**(2):188-1191, (2006); doi: 10.1109/TASC.2006.873322;
[92] Vasssighi A., Sachadev M., *Thermal and Power Management of Integrated Circuits*, Springer-Verlag, (2006); doi: 10.1007/0-387-29749-9;
[93] Kitamura T. et al., "A numerical model on transient, two-dimensional flow and heat transfer in He II", Cryogenics **37:**1-9 (1997); doi: 10.1016/S0011-2275(96)00096-3
[94] Weisend J.G., *Handbook of Cryogenic Engineering*, Taylor&Francis, Philadelphia, (1998);
[95] Jeanneret J.B. et al., "Quench levels and transient beam losses in LHC magnets", LHC Project Report **44**, CERN, (1996); https://cds.cern.ch/record/308241;
[96] Schmidt C., "Review of steady state and transient heat transfer in pool boiling helium I", Saclay, France: International Institute of Refrigeration: Commision A1/2-Saclay, pp. 17-31, (1981); https://inis.iaea.org/search/search.aspx?orig_q=RN:14781750;
[97] Nishi M. et all, "Boiling helium heat transfer characteristics in narrow cooling channel", IEEE Trans. Magn. **19**(3):390-393, (1983); doi: 10.1109/TMAG.1983.1062552;
[98] C. Meuris, B. Baudouy, D. Leroy, and B. Szeless, "Heat transfer in electrical insulation of LHC cables cooled with superfluid helium" Cryogenics **39**:921-931, (1999); doi: 10.1016/S0011-2275(99)00115-0;
[99] La China M. and Tommasini D., "Cable insulation scheme to improve heat transfer to superfluid helium in Nb-Ti superconducting accelerator magnets", IEEE Trans. Appl. Supercond. **18**(2):1285-1288, (2008); doi: 10.1109/TASC.2008.920574;
[100] Tommasini D. and Richter D. "A new cable insulation scheme improving heat transfer to superfluid helium in Nb-Ti superconducting accelerator magnets", proceedings of EPAC08, pp. 2467-2469, (2008); CERN/AT 2008-12;
[101] Russenschuck S. et al, "Design challenges for a wide-aperture insertion quadrupole magnet", IEEE Trans. Appl. Supercond. **21**:1674-1678, (2011);
[102] Sitko M., Skoczen B., "Modelling He I–He II phase transformation in long channels containing superconductors", Int. J. Heat and Mass Transfer. **52**:9-16, (2009); doi: 10.1016/j.ijheatmasstransfer.2008.06.0099;
[103] Bielert E.R. et al., "Implementation of the superfluid helium phase transition using finite element modelling: Simulation of transient heat transfer and He-I/He-II phase front movement in cooling channels of superconducting magnets", Cryogenics **53**:78-85, (2013); doi: 10.1016/j.cryogenics.2012.06.002
[104] Pietrowicz S., Baudouy B., "Numerical study of the thermal behavior of an Nb_3Sn high field magnet in He II", Cryogenics, **53**:72-77, (2013); doi: 10.1016/j.cryogenics.2012.09.007;

[105] Yamada R. et al., "2-D/3-D quench simulation using ANSYS for epoxy impregnated Nb3Sn high field magnets", IEEE Trans. Appl. Supercond. **13**:1696 – 1699, (2003); doi: 10.1109/TASC.2003.812870;
[106] Caspi S. et al., "Calculating quench propagation with ANSYS", IEEE Trans. Appl. Supercond., **13**:1714–1717, (2003); doi: 10.1109/TASC.2003.812867;
[107] Bielert E.R.,Verweij A.P., Kate H., "Implementation of the superfluid helium phase transition using finite element modeling: Simulation of transient heat transfer and He-I/He-II phase front movement in cooling channels of superconducting magnets", Cryogenics, **53**:78–85, (2013); doi: 10.1016/j.cryogenics.2012.06.002
[108] Volpini G., "Quench propagation in 1-d and 2-d models of high current superconductors", Proceedings of the COMSOL Conference Milan, (2009);
[109] Schwerg N. et al., "Quench Simulation in an Integrated Design Environment for Superconducting Magnets", IEEE Trans. Magnetics, **44**:934 – 937, (2008); doi: https://www.doi.org/10.1109/TMAG.2007.916304;
[110] Bermudez S., Bajas H., Bottura L. "Quench Modeling in High-field Nb_3Sn Accelerator Magnets", Physics Procedia, **67**:840-846, (2015); doi: 10.1016/j.phpro.2015.06.141;
[111] Sonnemann F., Schmidt, R., "Quench simulations for superconducting elements in the LHC accelerator" Cryogenics **40**:519-529, (2000); doi: 10.1016/S0011-2275(01)00008-X;
[112] L. Bottura et al., "THEA Thermal, Hydraulic and Electric Analysis of Superconducting Cable", CryoSoft, Geneva, (2003);
[113] K.B. Kumar et al., "Novel techniques to solve sets of coupled differential equations with SPICE", IEEE Trans. Circ. Dev. Mag. **7**:11-14, (1991); doi: 10.1109/101.63289;
[114] A. Verweij, QP3 User's Manual, CERN EDMS: 1150045, 2008.
[115] ZERODEE Software. CryoSoft, France, (2001);
[116] Bottura L., Calvi M., Siemko A., "Stability Analysis of the LHC Cables", Cryogenics **46**: 481-493, (2006); doi: 10.1016/j.cryogenics.2006.01.012;
[117] Picaud V., Hiebel P. Kauffmann J.-M., "Superconducting coils quench simulation, the Wilson's method revisited", IEEE Trans. Magn. **38**:1253-1256, (2002); doi: https://www.doi.org/10.1109/20.996320;
[118] Bordry F. et al., Machine protection for the LHC: Architecture of the beam and powering interlock systems, LHC Project Report **521**, (2001);
[119] Schmidt R.et al., "Beam loss scenarios and strategies for machine protection at the LHC", LHC Project Report **665**, CERN, (2003);
[120] Jeanneret J.B., "On the measurements of the beam losses in the LHC rings", LHC-BLM-ES-0001, CERN, (2004);
[121] Russenschuck S., "ROXIE: A Computer Code for the Integrated Design of Accelerator Magnets", (1999);
[122] ROXIE, CERN field computation software, http://cern.ch/roxie;
[123] Ferrari A., Sala P.R., Fasso A., and Ranft J., "FLUKA: a multi-particle transport code" CERN-2005-10 (2005), INFN/TC_05/11, SLAC-R-773, (2005);

[124] Böhlen T.T., Cerutti F., Chin M.P.W., Fassò A., Ferrari A., Ortega P.G., Mairani A., Sala P.R., Smirnov G. and Vlachoudis V., "The FLUKA Code: Developments and Challenges for High Energy and Medical Applications**",** Nuclear Data Sheets **120**:211-214 (2014);
[125] Verweij A.P., "Electrodynamics of Superconducting Cables in Accelerator Magnets", PhD thesis, Uniwersity of Twente, The Niderlands, (1995);
[126] Claudet et al., CRYOGENIE et ses applications en supraconductivite, IIF/IIR
[127] Gorter C.J. and Mellink J.H., "On the irreversible processes in the liquid helium II", Physics **15**:285, (1949);
[128] Rodriguez-Mateos F., Sonnemann F., "Quench Heater Studies for the LHC Magnets", Proc. IEEE Particle Accelerator Conference **5**:3451–3453, (2001); doi: 10.1109/PAC.2001.988141;
[129] Ravaioli E. et al., "New Coupling Loss Induced Quench Protection System for Superconducting Accelerator Magnets", IEEE Trans. Appl. Supercond. **24**, (2014); doi: 10.1109/TASC.2013.2281223;
[130] Granieri P.P. et al., "Heat transfer in an enhanced cable insulation scheme for the superconducting magnets of the LHC luminosity upgrade," IEEE Trans. Appl. Supercond. **20**(3):168-171, (2010); doi: 10.1109/TASC.2010.2040377;
[131] Kashikhin V.V. et al., "Quench margin measurement in Nb_3Sn quadrupole magnet", *IEEE Trans. Appl. Supercond.* **19**(3), (2009); doi: 10.1109/TASC.2009.2019290
[132] Cheggour N. (najib.cheggour@nist.gov), Goodrich F.L. (loren.goodrich@nist.gov): private communication;
[133] Mokhov N.V., http://www-ap.fnal.gov/MARS/;
[134] Mokhov N.V., et al., "Protecting LHC IP1/IP5 Components against Radiation Resulting from Colliding Beam Interactions", Fermilab-FN-732, LHC Project Report **633**, (2003); https://cds.cern.ch/record/613167?ln=pl;
[135] LHC Design Report, vol.1, CERN-2004-003; https://cds.cern.ch/record/782076?ln=pl
[136] G. Frei, S. Hartmann, G. Kühne, C. Scheuerlein, G. Willering, "Neutron micro-tomography: examination of a LHC Rutherford cable", PSI Scientific Report, (2007);
[137] P. Stallknecht, C. Scheuerlein, "Überprüfung von Supraleitern mit digitaler Bildanalyse", analySIS® Anwendungsbericht, Imaging & Microscopy, (2005);
[138] "Copper to Superconductor Volume Ratio Formula", in Clarification of the Technical specification for Superconducting Cable for LHC, Annex IV, CERN, (2002);
[139] APICAL Polyimide 100 AV, KANEKA High-Tech Materials, http://www.kanekahightech.com;

Appendix 1

Superconducting cable characteristic

Tab A1.1 The characteristic of the LHC superconducting cables developed at CERN [135].

		MB	MB	MQ	MQM	MQY	MQY
	Units	Type 1	Type 2	Type 3	Type 4&7	Type 5	Type 6
Strand diameter	mm	1.065	0.825	0.825	0.48	0.48	0.74
Number of strands		28	36	36	36	34	22
Average r = Cu/NbTi		1.65	1.95	1.95	1.75	1.75	1.25
Keystone angle	deg	1.25	0.9	0.9	0.91	0.9	1.72
Cable width (bare)	mm	15.1	15.1	15.1	8.8	8.3	8.3
Cable mid-thickness (bare)	mm	1.9	1.48	1.48	0.84	0.845	1.275
Cable inner thickness (bare)	mm	1.7353	1.3614	1.3614	0.7701	0.7798	1.1504
Cable outer thickness (bare)	mm	2.0647	1.5986	1.5986	0.9099	0.9102	1.3996
Transposition pitch	mm	115.00	100.00	100.00	66.00	66.00	66.00
Radial insulation thickness	mm	0.15	0.15	0.13	0.08	0.08	0.08
Azimuthal insulation thickness	mm	0.12	0.13	0.11	0.08	0.08	0.08
Cable width (ins.)	mm	15.4	15.4	15.36	8.96	8.46	8.46
Cable mid-thickness (ins.)	mm	2.14	1.74	1.70	1.00	1.005	1.435
Cable inner thickness (ins.)	mm	1.9720	1.6190	1.5794	0.9288	0.9386	1.3080
Cable outer thickness (ins.)	mm	2.3080	1.8610	1.8206	1.0712	1.0714	1.5620

Appendix 2

Free void volume

The Rutherford type LHC superconducting cables (see Appendix 1) contain voids, which can be filled up with liquid helium. In the following, the void volume inside the insulated superconducting LHC cables that can be occupied by helium is defined as the *free void volume.* The results of measurements and calculations of the free void volume in all of the LHC superconducting magnet cables are summarized below. The free void volume calculations were confirmed by micro-tomography measurements of the helium distribution inside an insulated LHC cable stack. Neutron miro-tomography measurements were performed at the ICON imaging facility of the SINQ spallation neutron source of the Paul Scherrer Institut in Switzerland [136]-[137].

The main LHC superconducting magnet coils are built from the Rutherford type superconducting cables (Fig. 5.2). A schematic view of an insulated superconducting cable cross-section is shown in Fig. 5.3. The strands are composed of Nb-Ti filaments within a copper matrix. The helium occupies the space between the strands and between the strands and the cable insulation (Fig. 5.4)). Table A1.1 in the Appendix 1 summarizes the nominal LHC cable parameters. The data presented in this table has been used for the free void volume calculations. A rough estimation of the free void volume, calculated for ideal, plastically non-deformed strands, can be obtained from the cable geometry (Tab A1.1).

CABLE CROSS SECTIONS CALCULATION FROM CABLE GEOMETRY

$$A_{cable} = \pi \cdot \left(\frac{1}{2} \cdot \frac{d_{strand}}{\cos\left(arctg\left(h / T_p \right) \right)} \right) \cdot \left(\frac{d_{strand}}{2} \right) = \pi \cdot \left(\frac{d_{strand}}{2} \sqrt{1 + \frac{h^2}{T_p^2}} \right) \cdot \left(\frac{d_{strand}}{2} \right) \qquad \text{Eq. A2.1}$$

$$\Delta A_{cable} = \left(\pi \cdot d_{strand} \cdot \sqrt{1 + \frac{h^2}{T_p^2}} \right) \cdot \Delta d_{strand} + \left(\pi \cdot \frac{d_{strand}^2}{2} \cdot \frac{h}{\sqrt{1 + \frac{h^2}{T_p^2}} \cdot T_p^2} \right) \cdot \Delta h - \left(\pi \cdot \frac{d_{strand}^2}{2} \cdot \frac{h^2}{\sqrt{1 + \frac{h^2}{T_p^2}} \cdot T_p^3} \right) \cdot \Delta T_p^2 \qquad \text{Eq. A2.2}$$

where: d_{strand} – is the strand diameter,
h – is the cable width,
T_p – is the cable transposition pitch,

$$A_{Cu} = A_{cable} \cdot \frac{r}{r+1} \qquad \text{Eq. A2.3}$$

$$\Delta A_{Cu} = \frac{r}{r+1} \cdot \Delta A_{cable} + A_{cable} \cdot \frac{1}{(r+1)^2} \cdot \Delta r \qquad \text{Eq. A2.4}$$

$$A_{NbTi} = A_{cable} \cdot \frac{1}{r+1} \qquad \text{Eq. A2.5}$$

$$\Delta A_{NbTi} = \frac{1}{r+1} \cdot \Delta A_{cable} - A_{cable} \cdot \frac{1}{(r+1)^2} \cdot \Delta r \qquad \text{Eq. A2.6}$$

where: r – is the copper to Nb-Ti ratio.

The strands in the LHC superconducting magnet cables are deformed during the cable production. Therefore, a more adequate method of the free void volume determination is based on measurements of the cable mass and volume. The collected samples of all six LHC superconducting main magnet cables were measured at room temperature with the slide clipper and weigh with a precise (four digits) laboratory weight. Cable samples with the following reference numbers have been prepared in the CERN cable testing area: cable 1 – 01B10951AF, cable 2 – 02B81441AD, cable 4 – 04E40101CR, cable5 – 05E50053GF, cable6 – 06E60029AD. Cable 2 and cable 3 are the same, cable 2 is used for main dipole (MB),whereas cable 2 is used in main quadrupole (MQ) magnets. The mass of the copper (m_{Cu}) and Nb-Ti alloy (m_{NbTi}) in the cable has been determined according to the following formulas. The error on the mass determination is shown as well.

$$m_{NbTi} = \frac{m_{tot}}{1 + r \cdot \frac{\rho_{Cu}}{\rho_{NbTi}}} \qquad \text{Eq. A2.7}$$

$$\Delta m_{NbTi} = \frac{1}{r \cdot \frac{\rho_{Cu}}{\rho_{NbTi}} + 1} \cdot \Delta m_{tot} - \frac{m_{tot}}{r^2 \cdot \frac{\rho_{Cu}}{\rho_{NbTi}} + 1} \cdot \Delta r \qquad \text{Eq. A2.8}$$

$$m_{Cu} = \frac{m_{tot}}{1 + \frac{1}{r} \cdot \frac{\rho_{Cu}}{\rho_{NbTi}}} \qquad \text{Eq. A2.9}$$

$$\Delta m_{Cu} = \frac{1}{1 + \frac{1}{r} \cdot \frac{\rho_{Cu}}{\rho_{NbTi}}} \cdot \Delta m_{tot} + \frac{m_{tot} \cdot \frac{\rho_{Cu}}{\rho_{NbTi}}}{\left(\frac{\rho_{Cu}}{\rho_{NbTi}} + r \right)^2} \Delta r \qquad \text{Eq. A2.10}$$

The reference density values for Cu and the Nb-47wt.%Ti alloy are 8930 kg/m^3, and 6022 kg/m^3 , respectively [138]. The density of the Polyimide insulation is 1420 kg/m^3 [139]. An acid test[11] had been performed as a complementary measurement to validate of the Nb-Ti alloy mass calculation. The relative differences between calculated and "acid test" values of m_{NbTi} are less than 0.3%. The results of measurements and calculations are shown in the Table A2.1.

Table A2.1 Length and mass of the different LHC cable samples. The measured samples data of LHC superconducting cables developed at CERN. The measurements were performed on bare cables at room temperature with laboratory weigh and the slide clipper.

	Units	Type-1	Type-2 & 3	Type-4 & 7	Type-5	Type-6
Sample length, *d*	mm	69.3	67.3	68.9	61.9	60.8
Sample weight (bare), m_{tot}	g	13.9128	10.7318	3.6242	3.0816	4.4095
m_{NbTi} (acid test)	g	4.0794	2.8033	1.0212	0.8751	1.5492
m_{NbTi} (m,ρ)	g	4.0914	2.7969	1.0220	0.8690	1.5644
m_{Cu} (m,ρ)	g	9.8214	7.9349	2.6022	2.2126	2.8451
m_{ins} (m,ρ)	g	0.537	0.509	0.184	0.157	0.162

Tab A2.2 The LHC cables electrical insulation. Layer 1 and layer 2 overlaps by 50%, layer 3 is a strip layer with a 2 mm space.

		Cable type					
Insulation	Units	Type-1	Type-2	Type-3	Type-4 & 7	Type-5	Type-6
layer 1	mm	0.0508	0.0508	0.0508	0.025	0.025	0.025
layer 2	mm	0.0508	0.0508	0.0375	0.025	0.025	0.025
layer 3	mm	0.0686	0.0686	0.0558	0.056	0.056	0.056

The volume of the bare cable sample has calculated as follows:

$$V_1(m,\rho) = \frac{m_{NbTi}}{\rho_{NbTi}} + \frac{m_{Cu}}{\rho_{Cu}} \qquad \text{Eq. A2.11}$$

where m_{NbTi} – is the NbTi alloy mass,
ρ_{NbTi} – is the NbTi alloy density,
m_{Cu} – is the copper mass,
ρ_{Cu} – is the copper density,

[11] Acid test means the procedure of removal of all non-superconducting material from the cable with acid.

The volume of the insulated cable sample has calculated as follows:

$$V_2(m,\rho) = \frac{m_{NbTi}}{\rho_{NbTi}} + \frac{m_{Cu}}{\rho_{Cu}} + \frac{m_{ins}}{\rho_{ins}} \qquad \text{Eq. A2.12}$$

where m_{ins} and ρ_{ins} are the insulation mass and density respectively.

The volume of the cable in the coil (at the working conditions i.e. prestress and stress from Lorentz forces) can be calculated from the nominal cable geometry:

$$V_3(\alpha,a,b,h,d) = \frac{a+b}{2}\cdot h \cdot d \qquad \text{Eq. A2.13}$$

where a – is the cable inner thickness,
b – is the cable outer thickness,
$h = l \cdot cos(\alpha/2)$ – is the cable width,
α – is the keystone angle,
d – is the cable (sample) length,

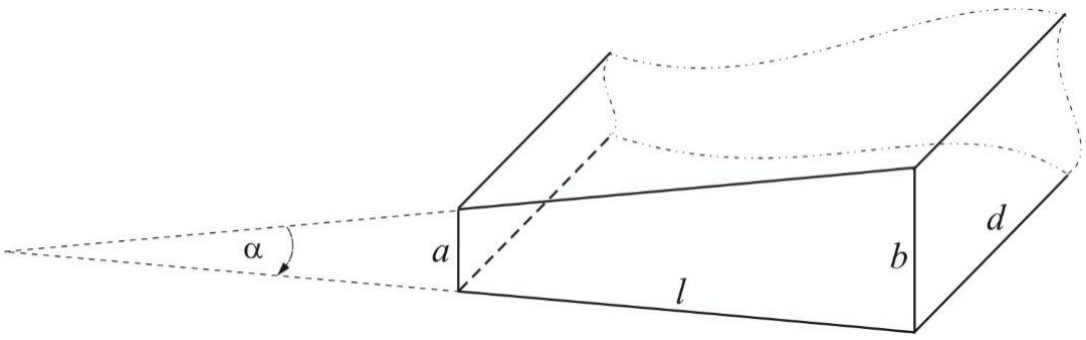

Fig. A2.1 Superconducting cable sketch. α – is the keystone angle, a – is the cable inner thickness, b – is the cable outer thickness, l – is the cable width, d – is the cable (sample) length,

The volume V_3 (α, a, b, h, d) was calculated both for bare and insulated cables. To distinguish these two volumes an additional subscript was introduced as follows: V_{3_bare}(α, a, b, h, d) for bare cables and $V_{3\_ins.}$(α, a, b, h, d) for insulated cables. The formulae for the free void volume calculations are:

$$V_{free\_void} = V_{3\_bare}(\alpha,a,b,h,d) - V_2(m,\rho) \qquad \text{Eq. A2.14}$$

$$V_{free\_void} = V_{3\_ins.}(\alpha,a,b,h,d) - V_2(m,\rho) - V_{\mu-channels} \qquad \text{Eq. A2.15}$$

Table A2.3 The free void volume calculation of CERN cables . Volume is normalized to 1 m of cable length and the results are presented as a cross section in mm^2. The table summarizes calculations, which assumes that the total μ-channels volume is occupied by the glue from the last layer of cable insulation (fifth column) and ideal case when μ-channels are fully active i.e. volume is occupied by the helium only.

	Free void volume (bare cable)		Free void volume (insulated cable & 0% of μ-channel efficiency)		$S_{\mu\text{-channel}}$	Free void volume (insulated cable & 100% of μ-channel efficiency)	
	mm^2	**%**	mm^2	**%**	mm^2	mm^2	**%**
Type-1	3.20	**11.15**	2.01	**6.09**	0.36	1.65	**5.00**
Type-2	2.37	**10.62**	1.49	**5.58**	0.35	1.15	**4.27**
Type-3	2.37	**10.62**	1.63	**6.23**	0.28	1.34	**5.15**
Type-4 & 7	0.75	**10.09**	0.43	**4.79**	0.17	0.26	**2.94**
Type-5	0.72	**10.31**	0.42	**4.97**	0.16	0.26	**3.12**
Type-6	1.15	**10.86**	0.84	**6.88**	0.16	0.67	**5.53**

The free void volume was normalized to 1 m of cable length and the results are presented as a cross section in mm^2. It is assumed that the cable insulation is not plastically deformed due to the pre-stress applied to the magnet coil and stress from the Lorentz force. The Young modulus of the polyimide insulation is of the order of 30 GPa [139] and from Hooke's law one could calculate the insulation relative compression under the nominal stress of 70 MPa. The insulation is changing its thickness by order of 0.25% only. This means that the insulation does not change its volume significantly and under compression is forced to fill the void between strands and insulation. In the calculations of free void volume the difference between two volumes is calculated. The volume calculated from the cable nominal geometry has to take into account the effectiveness of μ-channels. Assuming that μ-channels are effective i.e. are occupied by the liquid helium only, the calculated free void volume inside of the cable decrease by the volume of the μ-channels. On the other hand, under compression the glue from the last layer of insulation can flow out to the μ-channels and fulfil them in 100%. Both scenarios are calculated and the results are covered in the Table A2.3.